ΓΙΑΝΝΗΣ ΖΑΧΑΡΑΚΗΣ

Χρονικά Αναλυόμενες Μελέτες Διάδοσης Φωτός σε Ισχυρά Σκεδαστικά Μέσα Εφαρμογές στον Οπτικό Χαρακτηρισμό Ιστών (Οπτική Μαστογραφία) και Στην Ενίσχυση Φωτός

Διδακτορική Διατριβή

UNIVERSITY OF CRETE
SCHOOL OF MEDICAL SCIENCES
DEPARTMENT OF MEDICINE

Time-resolved Studies of Light Transport Through Highly Scattering Media
Applications in: Optical Characterization of Tissue (Optical Mammography) and Light Amplification

GIANNIS ZACHARAKIS

PhD Thesis

HERAKLION 2002

Supervising committee:

        Prof. E. Koumantakis
        Prof. C. Fotakis
        Dr.   T. G. Papazoglou

Examination committee:

E. Koumantakis (Professor of Medicine)

C. Fotakis (Professor of Physics)

E. Ekonomou (Professor of Physics)

D. Charalambidis (Associated Professor of Physics)

D. Tsiftsis (Professor of Medicine)

K. Relakis (Assistant Professor of Medicine)

E. Sanidas (Lecturer of Medicine)

FEBRUARY 2002
HERAKLION, CRETE

Στη μνήμη του πατέρα μου...

To the memory of my father…

Summary

In this thesis the time resolved studies of light propagation through highly scattering media in two extreme cases are reported. The first case concerns media where the dominating process is multiple scattering with negligible absorption, with the second regime being media, which both scatter and amplify light. Light propagation is diffusive in both cases however a very interesting phenomenon takes place in the latter. In this extreme case light emanating from a random, highly disordered medium can have highly ordered (lasing) properties. This phenomenon namely random lasing has raised an enormous research interest. The final goal of the study was the investigation of the possible use of light transport through and the light emission from such media for the improvement of optical biopsy and imaging techniques. In the introductory part of the thesis the most common benign and malignant abnormalities occurring in the female breast as well as a synopsis of the present status on imaging techniques are given. Then an introduction is also made for the propagation of light through highly scattering amplifying media and the vast number of applications that the phenomenon of random lasing brings into play.

After the introductory part the processes governing the interaction of light and matter are described theoretically and focused in the cases that are studied experimentally as well. Diffusive transport of light and lasing theory are the two key aspects in random amplifying media. The coherent properties of the light emitted from random lasers are also investigated. At the same time an overview of the current

state of theory describing such media is presented to give a complete picture to the reader.

For the time-resolved study of light propagation through turbid matter such as female breast tissue a mode-locked Ti:Sapphire laser emitting 200 fs pulses at 800 nm with an average power of ~1 W and a repetition rate of 82 MHz was used. The detection was performed with a streak camera with a temporal resolution of 2 ps. The tissue samples were excised from female breast during tumor extraction or biopsy operations and concerned normal adipose and fibrous tissue. The theoretical analysis of the temporal spread of the transmitted ultra-fast laser pulses provides the optical properties of the studied medium. Large samples can be studied based on the diffusion theory whereas small biopsy samples are studied based on the Laguerre expansion of the kernels technique. Recently cancer tissue was studied as well. Results are in complete agreement with the histological analysis and thus very promising for the implementation of these techniques in optical biopsy.

As far as the scattering gain media is concerned different types of laser systems were used depending on the excitation scheme combined with the same workstation employing a spectrograph - streak camera system for the simultaneous detection of both spectral and temporal information. The temporal resolution is 2 ps and the spectral resolution 1 nm. For one-photon excitation of random lasing materials a Lambda Physik distributed feedback dye laser (DFDL) emitting 500 fs pulses at 496 nm with output energy of 50 μJ pumped by a XeCl excimer laser emitting at 308 nm was used. For two-photon excitation the regeneratively amplified output of the mode-locked Ti:Sapphire laser system emitting 200 fsec pulses at 800 nm with a repetition rate of 1 KHz and an average power of 500 mW was used. The samples were prepared by mixing different lasing dyes with TiO_2 microparticles with average diameter of 400 nm in liquid or solid matrices thus providing multiple scattering and gain. As mentioned above light emanating from such media has the temporal and spectral properties of laser light. Pulses of few picoseconds long and few nanometers wide (down to the detection limits of the system) have been detected when the samples were excited above a well-determined energy threshold. This optical explosion provides a beacon like light source, which could be very valuable for detection modalities. Especially the excitation with two near-infrared photons consequently and most importantly provides the necessary penetration inside the strongly scattering media, as well as negligible photobleaching and phototoxication of

tissue due to the low energy of the photons. The non-linearity insures that the effect will be confined only on the focal region, thus improving the spatial resolution by minimizing the out of focus fluorescence.

The coherent properties of the laser-like emission were studied using the frequency doubled output of the above described laser system employing the regeneratively amplified output of the mode-locked Ti:Sapphire laser emitting at 800 nm. Single photon counting measurements were performed in order to obtain the photon count distributions of the emitted light. Coherent light is described by Poisson distribution whereas chaotic light by Bose-Einstein distribution. The experimental results suggested that depending on the scattering properties of the medium and on the excitation scheme, the emitted light comprised of different amounts of coherent and incoherent components since different modes are overlapping.

Similar studies are underway when various fluorophores are embedded in biological tissues. The final goal is to take advantage of this effect towards a more spatially and spectrally confined agent in Photodynamic Therapy of target tissue lesions on skin or other types of superficial lesions. Very promising in the field of skin PDT would be thin patches with various fluophores, which could be applied directly on the lesion and allow the selection of different irradiation wavelengths using the same laser as excitation source.

Some of the applications in addition to PDT are photonic marking for identification purposes (photonic codes, search and rescue missions, military applications, marking of hazardous material), substitution of ordinary lasing media in dye lasers and boosting the emission of LEDs and diode lasers in the blue region of the spectrum (if used with electro luminescent polymers). A lot of effort is also put in the study of dye infiltrated opal photonic crystals and the light emitted from such an ordered (crystal structure) and disordered (random photons' path) structure.

Περίληψη

Στη διατριβή αυτή παρουσιάζονται χρονικά αναλυόμενες μελέτες της διάδοσης του φωτός μέσα από ισχυρά σκεδαστικά υλικά. Δύο είναι οι περιπτώσεις οι οποίες μελετώνται. Στην πρώτη η κυρίαρχη διαδικασία είναι η σκέδαση, με αμελητέα απορρόφηση, ενώ η δεύτερη αφορά σε υλικά τα οποία ταυτόχρονα σκεδάζουν και ενισχύουν το φως. Η διάδοση του φωτός και στις δύο περιπτώσεις χαρακτηρίζεται από τη θεωρία διάχυσης. Παρόλα αυτά κάποια πολύ ενδιαφέροντα φαινόμενα συμβαίνουν στη δεύτερη. Το φως που εκπέμπεται από ένα ισχυρά σκεδαστικό μέσο μπορεί να έχει ιδιότητες που χαρακτηρίζουν το φως λέιζερ. Το φαινόμενο αυτό το οποίο ονομάζεται random laser έχει προκαλέσει μεγάλο ενδιαφέρον στην επιστημονική κοινότητα. Ο τελικός σκοπός της έρευνας είναι η μελέτη της πιθανής χρήσης της διάδοσης και της εκπομπής φωτός από τέτοια υλικά για την βελτίωση των τεχνικών οπτικής βιοψίας και απεικόνισης. Στο εισαγωγικό τμήμα της διατριβής παρουσιάζονται οι πιο κοινές καλοήθεις και κακοήθεις παθήσεις του γυναικείου μαστού, όπως και μια σύνοψη των τεχνικών απεικόνισης. Μετά γίνεται μια εισαγωγή για τη διάδοση του φωτός διαμέσου ισχυρά σκεδαστικών υλικών ενίσχυσης και τον τεράστιο αριθμό εφαρμογών τους.

Στη συνέχεια περιγράφονται θεωρητικά οι διαδικασίες που χαρακτηρίζουν την αλληλεπίδραση του φωτός με την ύλη. Τα υλικά με ιδιότητες σκέδασης και ενίσχυσης χαρακτηρίζονται από τη θεωρία διάχυσης και τη θεωρία της ακτινοβολίας λέιζερ. Οι ιδιότητες συμφωνίας του φωτός που εκπέμπεται από τα random laser εξετάζονται επίσης και ταυτόχρονα δίνεται μια σύνοψη των σύγχρονων θεωριών.

Για τη χρονικά αναλυόμενη μελέτη της διάδοσης του φωτός μέσα από σκεδαστικά υλικά όπως ο ιστός από γυναικείο μαστό, χρησιμοποιήθηκε ένα σύστημα λέιζερ Ti:Sapphire το οποίο εκπέμπει παλμούς με διάρκεια 200 fs στα 800 nm με μέση ισχύ ~1 W και με επαναληψιμότητα 82 MHz. Η ανίχνευση γίνεται με streak camera με χρονική διακριτική ικανότητα 2 ps. Τα δείγματα ιστού λαμβάνονται από εγχειρήσεις αφαίρεσης όγκου και από εγχειρήσεις βιοψίας και αφορούσαν φυσιολογικό λιπώδη και ινώδη ιστό. Η θεωρητική ανάλυση της χρονικής διασποράς του διαδιδόμενου παλμού λέιζερ παρέχει τις οπτικές ιδιότητες του υπό εξέταση υλικού. Η μελέτη των δειγμάτων με μεγάλες διαστάσεις βασίζεται στη θεωρία διάχυσης, ενώ αυτή των δειγμάτων με μικρές διαστάσεις όπως είναι τα δείγματα βιοψίας στη μέθοδο της ανάλυσης των πολυονύμων Laguerre. Τελευταία κατέστη δυνατόν να μελετηθεί και καρκινικός ιστός για την ολοκλήρωση της μελέτης. Τα αποτελέσματα είναι σε πλήρη συμφωνία με τα αντίστοιχα από την ιστολογική ανάλυση και γι' αυτό πολλά υποσχόμενα για την πιθανή χρήση της μεθόδου για οπτική βιοψία.

Όσων αφορά στα υλικά με ιδιότητες σκέδασης και ενίσχυσης του φωτός, χρησιμοποιήθηκαν διαφορετικά συστήματα λέιζερ ανάλογα με τον επιλεγμένο τρόπο διέγερσης, σε συνδυασμό με την ίδια ανιχνευτική διάταξη, η οποία περιλαμβάνει ένα σύστημα φασματογράφου - streak camera για την ταυτόχρονη καταγραφή της φασματικής και της χρονικής πληροφορίας. Η χρονική διακριτική ικανότητα είναι 2 ps, ενώ η αντίστοιχη φασματική 1 nm. Για την διέγερση των υλικών με ένα φωτόνιο χρησιμοποιήθηκε ένα λέιζερ χρωστικών κατανεμημένης ανάδρασης (distributed feedback dye laser) το οποίο εκπέμπει παλμούς 500 fs στα 496 nm με ενέργεια 50 μJ, το οποίο αντλούνταν από ένα λέιζερ διεγερμένων διμερών XeCl στα 308 nm. Για τη διέγερση με δύο φωτόνια χρησιμοποιήθηκε η διάταξη ενίσχυσης της εξόδου του συστήματος λέιζερ Ti:Sapphire το οποίο εκπέμπει πακμούς 200 fs στα 800 nm με επαναληψημότητα 1 KHz και μέση ισχύ 500 mW. Τα δείγματα παρασκευάστηκαν αναμιγνύοντας διάφορες χρωστικές με μικροσφαιρίδια TiO_2 διαστάσεων ~400 nm σε υγρά ή στερεά υποστρώματα, παρέχωντας έτσι τις απαραίτητες ιδιότητες σκέδασης και ενίσχυσης. Το φως που εκπέμπεται από τέτοια υλικά έχει τις χρονικές και φασματικές ιδιότητες της εκπομπής λέιζερ. Παλμοί με διάρκεια μερικών picosecond και πλάτους μερικών nanometers (στα διακριτικά όρια του ανιχνευτικού συστήματος) ανιχνεύονται όταν η ενέργεια διέγερσης των δειγμάτων είναι πάνω από ένα καλά καθορισμένο κατώφλι. Αυτή η οπτική έκρηξη παρέχει μια πηγή φωτός σαν φάρο, η

οποία θα μπορούσε να βελτιώσει τις τεχνικές ανίχνευσης και απεικόνισης. Ειδικά η διέγερση με δύο φωτόνια υπέρυθρου μήκους κύματος παρέχει το απαραίτητο βάθος διείσδυσης μέσα σε ισχυρά σκεδαστικά υλικά, ενώ ταυτόχρονα ελαχιστοποιεί τη φωτοδιάσπαση και τη φωτοτοξικότητα του ιστού εξαιτίας της χαμηλής ενέργειας των φωτονίων. Η μη γραμμική συμπεριφορά εξασφαλίζει ότι το φαινόμενο περιορίζεται στην περιοχή εστίασης με αποτέλεσμα τη βελτίωση της χωρικής διακριτικής ικανότητας.

Η πιθανή χρονική συμφωνία της εκπομπής λέιζερ μελετήθηκε χρησιμοποιώντας τη διάταξη ενίσχυσης της εξόδου του συστήματος λέιζερ Ti:Sapphire στα 800 nm αφού διπλασιαστεί η συχνότητά του. Στη συνέχεια πραγματοποιήθηκαν μετρήσεις single photon counting για τη δημιουργία των στατιστικών κατανομών οι οποίες χαρακτηρίζουν το εκπεμπόμενο φως. Το σύμφωνο φως υπακούει στην κατανομή Poisson ενώ το μη σύμφωνο φως υπακούει στην κατανομή Bose-Einstein. Τα πειραματικά δεδομένα υπέδειξαν ότι ανάλογα με τις ιδιότητες σκέδασης του υλικού και του τρόπου διέγερσης, το εκπεμπόμενο φως αποτελείται σε διαφορετικό βαθμό από σύμφωνες και μη σύμφωνες συνιστώσες.

Παρόμοιες μελέτες πραγματοποιούνται όταν διάφορες φωτοχρωστικές ουσίες εμβαπτίζονται σε βιολογικό ιστό. Ο τελικός στόχος είναι η εκμετάλλευση του φαινομένου random laser για μια πιο εντοπισμένη χωρικά και φασματικά δράση στη φωτοδυναμική θεραπεία επιφανειακών αλλοιώσεων. Πολλά υποσχόμενη είναι η κατασκευή λεπτών γαζών με διάφορες χρωστικές, οι οποίες θα εφαρμόζονται απ' ευθείας πάνω στην αλλοίωση και θα επιτρέπουν την επιλογή του κατάλληλου μήκους κύματος χρησιμοποιώντας την ίδια πηγή λέιζερ για διέγερση.

Μερικές από τις άλλες εφαρμογές είναι το μαρκάρισμα για ανιχνευτικούς σκοπούς (φωτονικοί κώδικες, αποστολές διάδοσης, μαρκάρισμα επικίνδυνων υλικών), αντικατάσταση των κοινών ενεργών υλικών στα λέιζερ χρωστικών και η ώθηση της εκπομπής των LEDs και των διοδικών λέιζερ στην μπλε περιοχή του φάσματος (σε συνδιασμό με electro-luminescent πολυμερή). Μεγάλη προσπάθεια καταβάλλεται επίσης για τη μελέτη φωτονικών κρυστάλλων που εμπεριέχουν χρωστικές και του φωτός που εκπέμπεται από ένα υλικό που συνδυάζει την τάξη (κρυσταλλική δομή) με την αταξία (τυχαίες πορείες φωτονίων).

Table of contents

1. Introduction

The most astonishing question that I was asked during my thesis was the following: "Why is a glass lens used for imaging objects while scattering media (e.g. a sheet of white paper) act detrimentally to any such attempt"? Why the direction of the propagating electromagnetic wave is altered in a lets say "controlled" way in one case and randomly in the other? Macroscopically both media look homogeneous and in both cases the mechanism behind the propagation change is scattering. What are the fundamental differences, which alter the properties of these materials? Why can't we take a look inside our body and why the Victorian doctors failed to do so using candlelight?

Outline of this thesis

Before proceeding to the reading of this thesis it would be useful to take a look at the different parts, which it comprises of. The effort during the writing of the text was concentrated, beyond the obvious need to present the results, on giving the potential reader the ability to get an overview of the current status of the research in both areas of optical imaging and random lasers. And of course, to give a theoretical background sufficiently profound and extensive, but not detailed that could tire the reader. At the end some of recent and future developments as well as the tendency of the current research will be presented.

The interaction of light with a highly scattering environment was studied in two extreme but very characteristic cases. In both occasions the "turbid" environment tends to alter the characteristics of light although the end result is reverse. In other

words, in the first case light looses its laser properties whereas in the second case it evolves from completely incoherent (fluorescence) to partially coherent laser light.

Firstly the "**damaging**" influence of scattering during the propagation of laser light in biological tissue was examined and an experimental methodology in order to extract useful information out of the "blurred" data was introduced. This methodology is tested on real human breast-tissue samples.

On the other hand the effect of optically turbid media on the fluorescence emission of organic dyes under intense laser pumping was analysed. In this case it has been observed that the scattering medium assists the emission of the dyes and in effect "**amplifies**" it efficiently.

Both studies aim towards the better understanding of the physics involved as well as the exploitation of their results in the field of Biomedical Optics.

Optical imaging

In this chapter a brief description of the female breast anatomy will be given. The most important breast diseases, both benign and malignant, will be reviewed. Thus, the need for a reliable, accurate and cost effective technique of detecting these diseases and screening of the female population will be justified. Later on a historical review of optical imaging is attempted and the recent developments on imaging and screening modalities are described.

Scattering and amplification. An introduction to random lasing

The second chapter deals with a phenomenon, which has attracted much interest among researchers and has raised much of the debate among them during the last decade. The phenomenon of laser action in highly scattering gain media. Or as it has prevailed: Random Lasing. A phenomenon where multiple scattering and lasing, two seemingly opposing natures, are combined. In this chapter after a brief historical review, the first introduction to the physics and mechanisms that govern these materials (namely random lasers) will be given. Finally, the remarkable applications that these materials could have in the near future, some of which could have a real impact on the every day life, are presented.

Theory

In this part of the thesis an overview of the theoretical aspects of the interaction of light and matter will be given. The processes of absorption, spontaneous emission, scattering and fluorescence, which take place when photons interact with matter, will be described. Then the interest will be concentrated on describing the processes that govern a medium (random laser), which combines all of the above and on explaining both the emanation and the properties of the emitted light. The current status of the theory on random lasing will be described both after one- and two- photon excitation. Finally, the coherent properties of the emitted light will be discussed both theoretically and experimentally.

Experimental

In this chapter the experimental arrangements, which were used during this thesis will be described. A detailed analysis of the sources of the ultra-short (femtosecond) pulses as well as the detecting device will be given, in an attempt to help the potential experimentalist to repeat the experiments based on the text of this chapter. The detection system used during the experiments (Streak Camera), as well as the details of the different laser systems used in the different experiments are described. The spectral calibration of the apparatus and the sample preparation procedures are also given.

In vitro optical characterization and discrimination of female breast tissue during near infrared femtosecond laser pulses propagation

Ultra-short infrared laser pulses were transmitted through excised female breast tissue. The resulted signal was recorded by a streak camera with a time resolution of the order of a few picoseconds. Experimental data of the temporal spread of the ultra-short pulse during the transmission through the tissue have been analyzed using the Patterson analytical expression derived from the diffusion theory. This resulted in the calculation of the absorption and reduced scattering coefficients, which are related to the optical characteristics of each type of tissue. The goal of the study was to use the theoretical values of the coefficients to discriminate different kinds of tissue.

The study concerned tissue from twenty cases in total. Twelve of them were macroscopically characterized as fat deposited and eight of them as fibrous. The results were then compared with the corresponding from the histological analysis to complete the study, aiming towards optical tomography.

Non-parametric characterization of human breast tissue by the Laguerre expansion of the kernels technique applied on propagating femtosecond laser pulses through biopsy samples

A different approach on the characterization of different types of tissue is the Laguerre expansion of kernels, which has been applied when the tissue samples are very small (< 4 mm, biopsy samples) where the diffusion theory fails to describe the photon propagation. This method treats the medium of propagation as a "black box system" and using data sets of incident – transmitted pulse it relates to this system a set of coefficients as well the first order system kernels. This analysis could present an alternative method of tissue characterization when, due to the limited optical thickness of small biopsy samples, the photon diffusion approximation cannot be used successfully. The Laguerre expansion technique was introduced in order to best describe nonlinear physiological systems stimulated with broadband random inputs. However, this technique can be used to study systems with either random or deterministic inputs. Samples were taken from 20 different breast biopsies at the department of Gynecology of the University Hospital. The experimental imaging system is the same as described in the above session.

Investigation of the laser-like behavior of polymeric scattering gain media under sub-picosecond laser excitation

The narrowing effects of scatterers on the lifetime and spectral width of laser-induced fluorescence of organic dyes hosted inside poly-methylmethacrylate (PMMA) polymer sheets were studied. The excitation source was a distributed feedback dye laser emitting 500 femtosecond pulses at 496 nm. Spectral and temporal features were simultaneously recorded on a spectrograph- streak camera detection system. The results were then compared with those obtained from dye solutions in methanol, recorded in previous experiments. The effects of the different host environment on the fluorescence characteristics of the dye were thus investigated.

These effects are currently studied when the dye is inserted in human tissue, in an attempt to boost tumor detection and Photodynamic Therapy (PDT) efficiency, and some initial results are presented.

Photon statistics of the laser-like emission from polymeric scattering gain media

The coherent properties of the temporally and spectrally narrowed emission of laser-induced fluorescence of organic dyes hosted inside artificial scattering matrices ("random lasers") were investigated. The excitation source was a frequency doubled 200 femtosecond pulsed laser emitting at 400 nm. Spectral and temporal features were simultaneously recorded using a spectrograph and a streak camera operating on the photon counting mode. Photon number distributions were thus created. The temporal coherence of the laser-like emission above and bellow the excitation energy threshold has been investigated from the photon number distribution obtained.

Coherent two-photon excited random lasing from highly scattering gain media

We present experimental evidence of laser-like emission following two-photon excitation of dye agents in solid random gain media of biological significance for the first time. The excitation was performed with sub-picosecond laser pulses at 800 nm and the emission, at 480 nm, was observed with a spectrograph streak camera detection system. Pumping with near-infrared lasers for random lasing in the visible would increase the efficiency of both the detection and photodynamic therapy of tumors, with the least effect on healthy tissue.

Recent developments - Conclusions - Future goals

This thesis is concluded by giving the developments that were achieved in the very last moment before starting the writing of the text and the generalized conclusions of the performed work as well as some indications for the future research on optical imaging and random lasers.

2. Optical Imaging

Breast cancer is the prime factor of women mortality in the developed countries. 75,000 women die every year of breast cancer in Europe alone. And many more have to suffer the procedure of screening and possible surgical biopsy. Thus, the need for a reliable, accurate and cost effective technique is imperative. In this chapter the most important breast diseases, both benign and malignant, will be reviewed. Later on a historical review of optical tomography is attempted and the recent developments on imaging and screening techniques are described.

2.1 Female Breast physiology and anatomy [1,2]

2.1.1 Breast composition

The breast is a mass of glandular, fatty and fibrous tissues positioned over the pectoral muscles of the chest wall and attached to the skin by fibrous strands called Cooper's ligaments. A layer of fatty tissue surrounds the breast glands and extends throughout the breast. The fatty tissue gives the breast a soft consistency. The glandular tissues of the breast house the lobules (milk producing glands at the ends of the lobes) and the ducts (milk passages). Towards the nipple, each duct widens to form a sac (ampulla). During lactation, the bulbs on the ends of the lobules produce milk. Once milk is produced, it is transferred through the ducts to the nipple.

The female breast, being dependent on a variety of hormones for its normal activity, exhibits considerable structural and functional variation through life. Apart from the overt changes occurring at puberty, pregnancy, lactation and menopause, more subtle changes also occur within the normal menstrual cycle; as a result of

hormonal disturbances, which probably underlie various disorders of the breast, especially *fibroadenosis*, but might also play some role in the pathogenesis of more serious conditions such as breast tumors. Likewise, the male breast normally remains rudimentary unless breast enlargement; which may also result from the use of certain drugs.
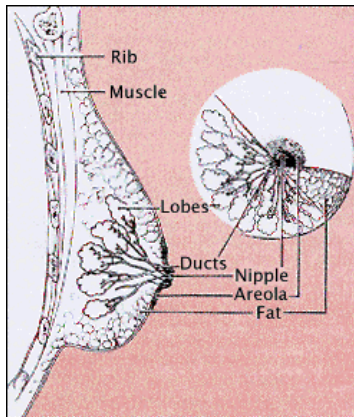
Fig. 2.1: *Schematic representation of the female breast structure [3].*

Most clinically significant breast disorders occur as lumps. It is thus of vital importance to identify those, which are malignant tumors so that the patient may be treated promptly. Several screening programs nowadays use radiological techniques (*mammography*) to identify early suspicious breast lesions, which are then subject to excision biopsy in the hope that removal of early-stage malignancy will prevent metastasis.

2.1.2 Inflammatory disorders of the breast

Infections of the breast are uncommon and mainly occur during lactation. The organisms (*usually Staphylococcus aureus*) gain access through cracks and fissures in the nipple and areola. Without early antibiotic therapy the resulting *bacterial mastitis* is often followed by the development of a *breast abscess*, which may require surgical drainage. More commonly, localized areas of the inflammation of the breast follow trauma, which may be of sufficient severity to produce necrosis of mammary adipose tissue, a condition known as *fat necrosis* (Figure 2.2). Following a typical initial acute inflammatory response, the continuing presence of necrotic adipose tissue **A** excites a chronic inflammatory cell infiltrate **In**, in which lipophages (macrophages containing lipid) and plasma cells may be present in large numbers. Fibrous proliferation at the

margins of the damaged area produces a hard, often irregular, breast lump, which may resemble a breast carcinoma on palpation.

Fig. 2.2: Fat necrosis

2.1.3 Hyperplastic lesions

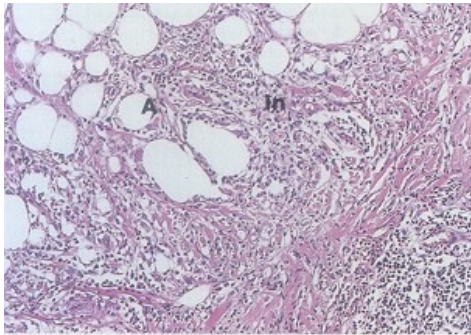The term hyperplastic lesion implies a benign condition of the breast and includes *adenosis, ductal and lobular hyperplasia, papillary lesions, radial scar and fibrous change (fibrosis).* These conditions are common in the breasts of mature women, increasing in frequency and severity towards the menopause. They are characterized by proliferative changes affecting components of the mammary unit (lobule, ducts and supporting stroma) probably in response to subtle disturbances of the hormone levels, particularly oestrogen. Unequal growth of epithelial and stromal elements gives rise to a variety of solid and cystic nodules within the breast, which are clinically important, as they must be distinguished from malignancy. The basic lesion is illustrated in Figure 2.3 and common variants shown in Figure 2.4.

In essence, the changes of fibroadenosis are the result of various different patterns of distortion and overgrowth of the functional breast unit, including ducts, lobules and supporting fibrous stroma. The epithelial components show hyperplastic overgrowth (*adenosis*) and the fibrous tissue increases (*fibrosis*).

The micrograph of Figure 2.3 shows the histological appearances of a typical lesion of fibroadenosis. There is hyperplasia of the breast acinar tissue in the lobules (*adenosis*) to produce islands of dark staining epithelium **A**. A prominent feature is fibrosis **F** surrounding the areas of adenosis. A frequent feature is marked dilatation of the ducts, to produce cystic lesions **C** lined by flattened ductular epithelium. The epithelium in areas of adenosis often develops strongly eosinophylic cytoplasm and comes to resemble the epithelium in apocrine sweat glands. This is termed *apocrine metaplasia* and is shown in the top of the micrograph **M**. Several variants of the

fibroadenosis, which are commonly encountered and produce histological patterns, which can be confused with carcinomas, are illustrated in Figure 2.4.
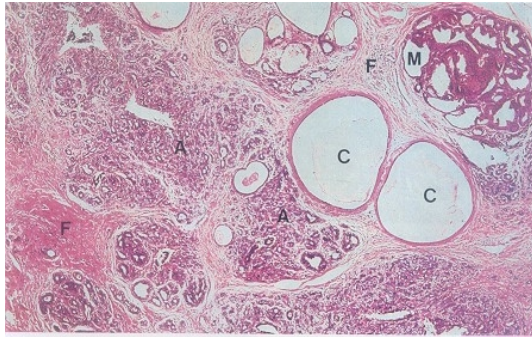

Fig 2.3: *Fibroadenosis-typical lesion*

The hyperplastic overgrowth of epithelium and stroma in fibroadenosis may preferentially affect one tissue component, giving rise to patterns, which can superficially resemble carcinoma. Two of the more common variants of fibroadenosis are illustrated in these micrographs. Sometimes marked epithelial overgrowth results in the cystically dilated ducts **C** being filled by papillary ingrowths from the wall, a condition known as *duct papillomatosis* shown in micrograph (a). Solitary duct papillomas of similar appearance may occlude the larger mammary and nipple ducts. Note the areas of adenosis **A** and fibrosis **F**, which continue more usual components of fibroadenosis.

The changes, which may occur in the mammary lobules in fibroadenosis, are essentially those of hyperplastic proliferation of lobular acini (*adenosis*) and of the terminal part of the mammary duct within the lobule (*terminal duct hyperplasia*). In some variants, there is proliferation of the specialized hormone responsive lobular stromal elements, splitting the acini apart and compressing them into elongated strips. The change, known as *sclerotic adenosis* **SA**, is seen in micrograph (b). The importance of this condition is that it may be difficult to distinguish histologically from some invasive patterns of carcinoma, particularly in frozen sections of breast biopsies. Sclerotic lesions smaller than 1 cm are called *radial scars.* They have lost the lobulocentric configuration of *sclerotic adenosis* and are characterized by a central fibro-elastic core with a stellate arrangement of radiant tubular structures. The cellular, connective tissue around the ducts causes much distortion, but careful examination will demonstrate the two-cell structure of benign lesions. Micrograph (b) also illustrates apocrine metaplasia **M**. Some areas of fibroadenosis occasionally contain ill-defined nodules, which are histologically identical to benign fibroadenoma.

At one extreme, fibroadenosis may show only replacement of mammary adipose tissue by dense fibrous tissue, with the only epithelial component being dilated mammary ducts. This is particularly seen in women after the menopause and is described as *mammary fibrosis with duct ectasia*.
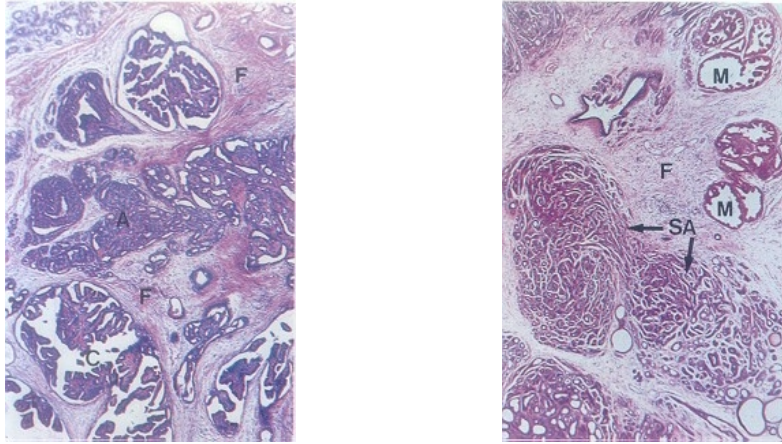
Fig. 2.4: Fibroadenosis variants: a) adenosis and duct papillomatosis, b) sclerotic adenosis

The only other benign tumor of much clinical significance is the benign *intraduct papilloma* (Figure 2.6), usually occurring as a solitary lesion in one of the larger mammary ducts. Histologically similar papillary lesions may also be multi-focal, occupying some of the ectatic (dilated) as a component of some patterns of fibroadenosis. Here the lesion is known as *duct papillomatosis* and probably represents hormone induced hyperplasia rather than a true neoplasm.
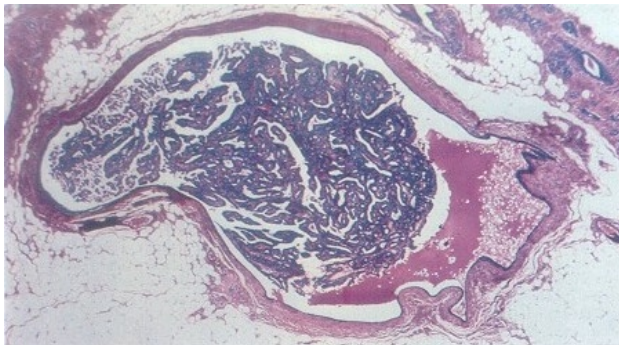
Fig. 2.6: Intraduct papilloma

Papillomas of mammary duct epithelium may arise as solitary or multiple lesions. Solitary lesions as those shown here are usually located in the larger lactiferous ducts near the nipple and present with blood stained discharge from the nipple. The lesions are usually small, consisting of a delicate pink stained supporting stroma covered by a single or double layer of cuboidal or low columnar epithelial

cells resembling those lining the mammary duct from which the papilloma has arisen. With larger lesions, the duct is often dilated. Multiple duct papillomas (florid duct papillomatosis) occur as a component of fibroadenosis. Malignant change is rare.

2.1.4 Breast lumps

The most common benign neoplasm of the breast is the *fibroadenoma* (Figure 2.5), a localized proliferation of breast ducts and stroma. Such lesions occur most frequently in isolated form in women aged 25-35 ('breast mice'), but nodules of histologically identical tissue may also be a component of fibroadenosis. Fibroadenoma may therefore be a form of hormone dependent nodular hyperplasia rather than a true benign tumor. It is usually considered to be a benign tumor but may well represent a nodular form of benign mammary hyperplasia (fibroadenosis). It is well circumscribed by a condensation of connective tissue and is composed of both epithelial and fibrous stromal components. The epithelial components form glandular structures lined by mammary duct type epithelium, whilst the stromal component is a loose, cellular form of fibrous tissue **F**. In very large masses, the stroma may be myxomatous.
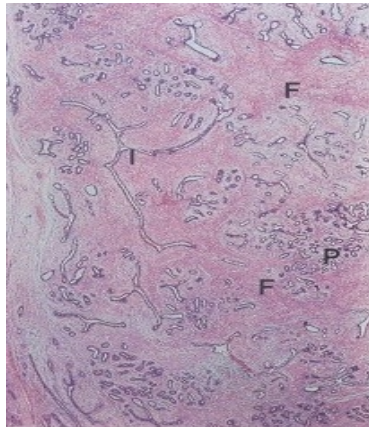
Fig. 2.5:*Fibroadenoma*

Two patterns of growth are seen, often in the same lesion. In the *pericanalicular pattern* **P**, the epithelial component takes the form of rounded ducts, which remain small and undistorted, with the stroma arranged round them in a roughly symmetrical and regular manner. By contrast, in the *intracanalicular pattern* **I**, The ducts appear elongated but actually represent sections cut through flattened spaces compressed by the stromal component, which appears to proliferate in an irregular nodular manner. In general, this latter pattern is more prominent in the larger fibroadenoma. In both

patterns of fibroadenoma, hormonal changes such as those occurring during pregnancy and lactation may induce marked proliferation of the epithelial component.

2.1.5 Breast cancer

Malignant tumors of the female breast are extremely common, with a peak incidence in the decade before the menopause. Most are adenocarcinomas arising from the epithelium of either the mammary lobules (*lobular carcinoma*) or the mammary ducts (*ductal carcinoma*). The range of histological appearances is illustrated in figure 2.7. In some cases the development of invasive breast cancer may be preceded by carcinoma in situ in which the malignant cells proliferate within the mammary ducts or lobules but do not breach the basement membrane (*intraduct or intralobular carcinoma*). In addition to the main groups of lobular and ductal carcinoma there is a small group of special breast carcinomas, which are associated with distinct clinical and pathological features, often with a good prognosis. Examples are *tubular carcinoma* and *medullary carcinoma*. Carcinoma of the breast does occur in males but is extremely uncommon.
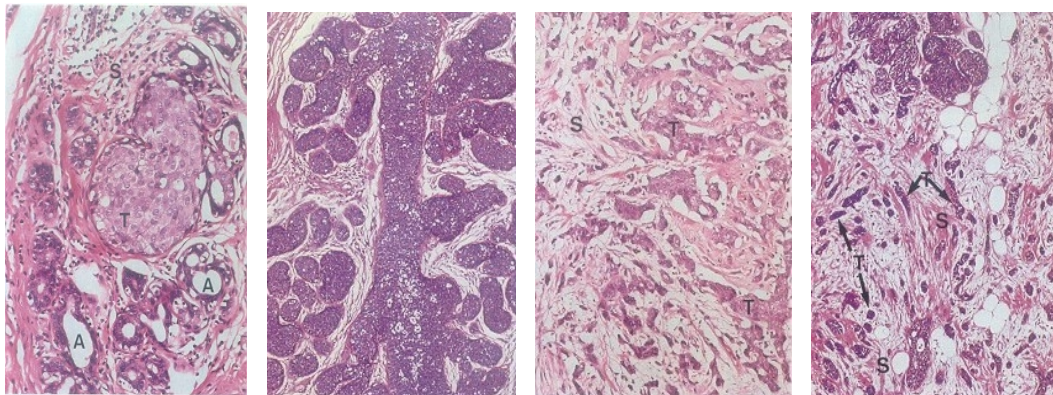
Fig. 2.7: *Carcinoma of the breast: a) intraduct carcinoma, b) lobular carcinoma in situ, c) invasive ductal carcinoma and d) invasive lobular carcinoma*

In non-invasive *intraduct carcinoma*, tumor cells fill and distend the ducts. In micrograph (a), note a small duct filled with tumor **T** surrounded by normal acini **A**. The tumor cells are large and pale staining with large nuclei. There may be evidence of increased mitotic activity. Sometimes, duct distension is marked and the tumor cells at the center undergo necrosis (*comedo pattern*). Note that there is no infiltration into surrounding stroma **S** and that the epithelial basement membrane is not breached. Infiltration eventually supervenes with development of an *invasive ductal carcinoma*.

As shown in micrograph (c), cords of tumor cells **T** then spread out from their ductal origin into the surrounding fibrous stroma **S**.

In non-invasive *lobular carcinoma in situ* as shown in micrograph (b), the normal lobular mammary architecture in maintained but the mammary lobules are increased in size as a result of proliferation of lobular epithelial cells with the cytological characteristics of malignancy. The cells fill and expand the acini of the mammary lobule, but the basement membrane remains intact and the general architecture of the lobule thus remains undisturbed.

In *invasive lobular carcinoma* as shown in micrograph (d), the tumor cells **T** breach the basement membranes of the acini and spill out into the surrounding stroma **S**, where they infiltrate into the fibro-adipose breast tissue, often in narrow cords and rows of cells described as 'Indian file' pattern of invasion. Lobular carcinoma has a high risk of bilateral breast involvement.

2.2 Historical review [4]

The idea of medical imaging appeared for the first time many years ago and has become one of the most important aspects for the development of medicine. Both in diagnosis and prognosis the contribution of tomography has been of catalytic importance. It has helped greatly to the understanding of the function of human organs and has given solutions to problems that used to demand surgical operations in order to assess both the disease and therapy processes.

The basic experimental setup consists of the source of radiation, the target and the detector. Since many years tomography is a separate scientific field exploiting many physical and computational methods in order to develop techniques suitable for non-invasive imaging. Nowadays the use of on-line imaging systems is possible, which monitor the function of vital organs and blood flow. However, the development of a system that could be used from the patient, such as a monitoring devise for the glucose level in the blood for diabetics, without blood extraction would have been a breakthrough. This has been the ultimate goal of scientific research.

Even from the 19th century medical doctors together with scientific groups tried to combine the function of internal organs with external visual symptoms. The goal

was the immediate diagnosis without invading the patient's body with an operation. The most successful method to date is histological analysis, even though it requires the excision of small biopsy tissue samples. The first to attempt an optical biopsy were the Victorian medical doctors, who tried to perform mammography with candlelight. Unfortunately the results were disappointing because of the excessive scattering that the light underwent so that any information useful for imaging the interior of the breast was lost.

2.3 Present status

2.3.1 X-rays Imaging

During the recent years however, many techniques have been developed and applied, whereas many more are in experimental stage. They are based on the exploitation of different radiations that can be transmitted through tissue and image the shadow of inner organs and bones. The most commonly used are X-rays, which are applied to the detection of bone fractions, dental lesions and breast tumor imaging (mammography). X-rays imaging is so clear because of the small wavelength (~ 0.01 nm) of the radiation, which cancels the extensive scattering [5]. The scattering of radiation becomes stronger as the wavelength approaches the dimensions of the components of tissue (typically in the range of nm – μm). Thus, X-rays penetrate deep into the tissue in contrast with highly scattered visible (400 – 800 nm) radiation. The produced image is the 2D projection of the attenuating properties of tissue along the path of the detected X-rays. The principal interactions that cause the attenuation are photoelectric absorption and inelastic scattering. The drawback however of the use of X-rays is introduced by the small wavelength, which is associated with very high energies (~100 KeV for X-rays), which can highly damage the tissue by ionization, breaking of DNA molecules and carcinogenecis. This limits the exposures a patient can undergo during his/her life. Moreover, these energies are much higher than the molecular energy levels, thus making impossible the determination of chemical composition. Finally, X-rays present many difficulties since they cannot be manipulated with conventional optics.

Conventional radiographic imaging provides no depth information, as the 3D body structure is projected onto a 2D image. Another limitation mentioned above is

the low soft tissue contrast, which is particularly important in many imaging schemes. X-rays computed tomography imaging is the development that gave the answer to these limitations. It produces thin 2D sections of the body, approximately 1 mm in thickness. Sub-millimeter spatial resolution with good discrimination between tissues (better than 1% attenuation change) can be achieved. The data acquisition is performed with a rotating fan beam X-ray source, which scans along the patient and a series of detectors. The image is then reconstructed from the 2D body slices.

2.3.2 X-rays Mammography

As far as mammography is concerned, the use of X-rays has become a necessity in recent years and has helped to reduce the mortality of breast cancer. However, the fact that 75,000 women die of breast cancer every year in Western Europe alone imposes that more effort should be directed towards a more reliable, more accurate and cost effective screening technique. The inability of this technique to differentiate between different types of soft tissue, introduces serious drawbacks since an interventional surgical biopsy would be required. This luck of specificity subjects a large number of women with benign breast diseases to unnecessary biopsy. And this is a very serious disadvantage taking into account that the cost of the performed biopsies is higher than the cost of the mammograms themselves. Furthermore, more effort should be directed towards an increasing compliance of the women to X-rays mammography, since even though inherently limited it is the only modality capable of decreasing mortality as much as 30%.

2.3.3 Diagnostic Ultrasound Imaging

Alternative methods that are already vastly in use are Ultrasound Imaging and Magnetic Resonance Imaging (MRI) [6]. In diagnostic ultrasound imaging, high frequency pulses of acoustic energy are emitted into the patients' body where they experience reflection at boundaries between tissues of different characteristic impedance. From the measurement of time delay and intensity of the reflected pulses (echoes), an image indicating tissue interfaces can be reconstructed. Ultrasound imaging is considered to involve negligible risk, provided that the incident intensities are sufficiently small. The comparable long wavelengths of ultrasounds (>cm) minimize scattering and on the same time are harmless for humans. Unfortunately this sets the limit of the resolution to the centimeter range. Moreover as for X-rays they

are not absorbed by the molecules, thus giving no information concerning the composition of tissue.

2.3.4 Triple Examination

X-Rays Mammography and Ultrasound Imaging comprise the second part of the triple assessment, which is the standard approach to diagnosis and assessment of breast diseases. The first part is the clinical examination, which includes history, inspection, palpation and Fine Needle Aspiration Cytology (FNAC). The third part is the pathology examination. The results are increasingly reported on a consistent grading scale from 1 to 5 as shown in the following table. FNAC has an accuracy of 99% when carried out by an experienced aspirator and read by an expert cytopathogist [2].

Table 2.1 Results of Fine Needle Aspiration Cytology		
C1	Inadequate	A cellular or sparsely cellular or poorly preserved smear
C2	Benign	Adequately cellular with unequivocal benign epithelial cells
C3	Probably benign	Adequately cellular with mainly benign cells present but some mild atypia present
C4	Suspicious/probably malignant	Some features of malignancy in a low cellularity sample or highly cellular with some atypical cells present
C5	Malignant	Frankly malignant cells present Cells showing lack of cohesion with large nuclear to cytoplasmic ratios and nuclear variability Severe nuclear pleomorphism

2.3.4 Magnetic Resonance Imaging

On the other hand Magnetic Resonance Imaging (MRI), also referred as Nuclear Magnetic Resonance Imaging (NMR), is utilized to obtain images as a function of proton spin density and relaxation times. The patient is placed inside a strong magnetic field, which is usually generated by large bore super conducting magnets. The resolution can go below the millimeter scale and many attempts are made to overcome that limit. Further advantages of MRI are the very low risk imposed to the

patient and the complete non-invasive nature of the technique [6]. However, some very important features for the diagnosis such as oxygenation of the tissue, are impossible to image. Only recently has it become possible to obtain functional information by using hemoglobin as a paramagnetic tracer. This method called functional MRI is capable of directly measuring the brain activation. The main drawback of MRI however is the extremely high cost of the devise and especially of the super conducting magnets that are necessary for the strong magnetic field, the large size of the equipment and the requirement for the patient to stay still in the magnet for up to about half an hour, as well as the problems associated with the presence of high magnetic fields.

2.3.5 Radioisotope Imaging

Radioisotope imaging is fundamentally different from the previously introduced imaging modalities in that the radiation originates from inside the body [6,7]. Radioisotope tagged compounds in tracer quantities are injected into the patients' body where they decay and produce detectable γ-photons. Hence it is possible to obtain images of the distribution of the radionuclide. Through the suitable choice of a labeled agent its distribution can be made representative of physiological function, such as blood flow, blood volume and various metabolic processes. Radioisotope imaging modalities are Single Photon Emission Computed Tomography (SPECT) and Positron Emission Tomography (PET).

In SPECT a single γ-ray is emitted per nuclear decay. A gamma camera, fitted with a parallel-hole collimator, rotates around the patient and records 1D projections of the radioactivity. A large number of such data sets allow the reconstruction (using a filtered back-projection similar to X-rays Computer Tomography) of a 2D cross-sectional image of the radiopharmaceutical distribution inside the body. Combining opposite projections helps to take into account the photon absorption within the body. SPECT provides functional images with improved contrast at the expense of spatial resolution, as compared to planar radioisotope imaging.

The question of a relatively cheap and fast imaging technique remains while the need for such a system becomes ever more essential.

2.3.6 Optical Tomography

Optical tomography (with the use of laser radiation) has a series of advantages over the previous methods. To begin with it is based on the use of non-ionizing radiation (wavelengths in the visible and near infrared-NIR region), thus minimizing the effects on the tissue and if the intensity delivered is limited to the maximum permissible exposure of 2 mW/mm^2, which corresponds to the solar constant, the only effects are restricted to only thermal heating. Furthermore, if the wavelength is chosen between 600 and 900 nm where the absorption is minimum, the thermal effects are also minimized. Moreover, since the energies in the visible range correspond to the energy gaps of the molecular transitions, spectroscopic information could also be obtained. This makes feasible the imaging of the blood content in the tissue, which is important for the monitoring of the function of vital organs. Moreover, optical imaging gives the potential of discriminating between different types of soft tissue (major advantage over X-ray imaging), as well as the possibility to derive functional information from quantitative measurements of chromophore concentrations [8-11].

However, the big disadvantage of the use of visible radiation is the extensive scattering that the photons undergo inside tissue since the dimensions of the typical scatterers are the same as the wavelength. To overcome this drawback various techniques have been used in order to detect objects hidden in turbid media. Enhancement of the early part of the propagating pulse via non-linear techniques or time gating imaging has been used in order to discriminate between the photons that can carry information from the diffusively scattered ones. These are the photons that are transmitted ballisticaly through the medium and arrive first on the detector. The temporal spreading of a short light pulse as it propagates through the scattering medium might provide further information about the optical coefficients of the medium. A different approach, namely "the inverse problem", which is based on the detection of the entire transmitted radiation and on the application of mathematical models in order to calculate characteristic parameters and reconstruct the medium that the photons have transmitted through, is used for imaging of discontinuities buried in turbid media. Something like reconstructing the cow from the hamburger!

2.3.7 Optical Coherence Tomography

In optical tomography the photons that would be detected could be either the transmitted or the diffuse reflected [12]. The latter has been applied in imaging onto

the dermis, quite extensively in the ocular cavity and especially in pediatrics for skull and chest imaging with Optical Coherence Tomography (OCT). OCT is an example of a successful clinical diagnostic application of near infrared light imaging technology, which overcomes the scattering problem of conventional optical tomography. It is based on the use of short coherence length light to record depth-resolved images using an interferometer. Depth information is obtained by optical ranging. Low coherence length light is directed into an interferometer (Michelson), one arm of which consists of a mirror on an adjustable stage and the other is used to direct the light onto the sample surface and collect the diffused reflected light. When the difference between the lengths of the two arms is less than the coherence length of the light, then a fringe pattern will be observed at the output. Thus by scanning the length of the reference arm and recording the mirror positions for which interference fringes are obtained, it is possible to determine the depth from which the light in the sample arm was reflected. The amplitude of the detected fringes depends on the amount of the absorption along the line-of-sight in the sample arm. By transversely scanning the line-of-sight of the sample arm through two dimensions, it is possible to build-up a depth-resolved absorption distribution. Thus a three dimensional image can be constructed. The depth resolution is limited to the coherence length. The time-of-flight or time gating technique may employ either broadband incoherent white light or ultra-short coherent optical pulses.

This thesis will be concentrated on the use of optical tomography for the calculation of the optical properties of breast tissue. In the following chapters the diffused optical method, which was used for the calculation of absorption and scattering coefficients will be described. Furthermore, a brief theoretical approach of the problem of light diffusion in turbid matter will be given.

References

1. P. R. Wheater, H. G. Burkitt, A. Stevens, J. S. Lowe, *"Basic Histopathology"*, Second Edition, Churchill Livingstone, New York (1991)

2. L. E. Hughes, R. E. Mansel, D. J. T. Webster, "*Benign Disorders and Diseases of the Breast: Concepts and Clinical Management*", Second Edition, W. B. Saunders, London, (2000)

3. **http://www.imaginis.com/breasthealth/breast_anatomy.asp?mode=1**

4. D. A. Benaron, G. Müller, B. Chance, *"Medical Optical Tomography: Functional Imaging and Monitoring"*: Medical perspectives at the threshold of clinical optical tomography, SPIE, Belingham, Washington (1993)

5. W. Kalender, *"Medical Optical Tomography: Functional Imaging and Monitoring"*: X-ray computed tomography: state of the art, SPIE, Belingham, Washington (1993)

6. Florian E. W. Schmidt PhD Thesis,
    http://www.medphys.ucl.ac.uk/research/borg/homepages/florian/thesis

7. B. Chance, *Optical tomography, photon migration and spectroscopy of tissue and model media: Theory, human studies and* instrumentation: Time resolved spectroscopy and imaging, SPIE, **2389**, 122 (1995)

8. J. C. Hebden and K. S. Wong, *"Time resolved optical tomography"*, Appl. Opt. **32**, 372 (1993)

9. K. A. Kang, B. Chance, S. Zhao, S. Srinivassan, E. Patterson and R. Troupin, "Breast tumor characterization using near-infrared spectroscopy", SPIE, **Vol. 1888**, 487-499 (1993)

10. J. Kölzer, G. Mitic, J. Otto and W. Zinth, "Measurements of the optical properties of breast tissue using time-resolved transillumination", SPIE **Vol. 2326**, 143-152 (1994)

11. V. G. Peters, D. R. Wyman, M.S. Patterson and G. L. Frank, "Optical properties of normal and diseased human breast tissues in the visible and near infrared", Phys. Med. Biol., **35**, 1317-1334 (1990)

12. D. Huang, E. A. Swanson, C. P. Lin, J. S. Schuman, W. G. Stinson, W. Chang, M. R. Hee, T. Flotte, K. Gregory, C. A. Puliafito, J. G. Fujimoto, *"Optical coherence tomography"* Science **254**, 1178 (1991)

3. Scattering and Amplification. An Introduction to Random Lasing

This chapter deals with a phenomenon, which has attracted much interest among researchers and has raised much of the debate among them during the last decade. Laser action in highly scattering gain media. Or as it has prevailed: Random Lasing. A phenomenon where multiple scattering and lasing two seemingly opposing natures are combined. In this chapter after a brief historical review, the first introduction to the physics and mechanisms that govern these materials (namely random lasers) will be given. A first attempt for an explanation, which is expected in the theoretical part, will also be undertaken. Finally, the remarkable applications that these materials could have in the near future, some of which could have a real impact on the every day life, are presented.

3.1 Laser and disorder

Nowadays lasers are well known to everyone. They are used in industry and in hospitals, in supermarket bar code scanners, compact disk players and laser light shows. The difference between light from a laser and that from a normal electric light bulb is that laser light has a well-defined color (wavelength) and direction, whereas light bulbs emit radiation with a wide range of colors and directions. A very attractive picture of what a coherent light resembles, is the marching of well-trained soldiers, which are completely synchronized (**coherent**), whereas light from a bulb resembles the marching of a crowd randomly distributed in a square (**incoherent**) (figure 3.1).
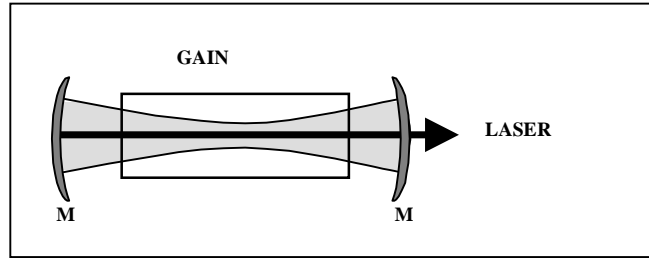
Fig. 3.1*: Schematic representation of a laser cavity, with the gain medium and the lasing output*

A laser comprises of a gain medium, which is responsible for the emission of photons after excitation (population inversion, see also section 4.1.4) and a mirror cavity, which amplifies the emitted light by the stimulated emission and the bouncing of photons between the mirrors. Laser action occurs when the amplification in each round trip exceeds the losses of the cavity. A laser is a highly spatially, temporally and spectrally coherent source of light. In other words, it is a highly ordered system. Great care is taken to ensure that the laser gain medium and cavity are homogeneous and non-scattering. Otherwise, the pump and emitted light would be scattered out of the cavity and the coherence would be lost. Even the presence of a small inhomogeneity in the cavity can cause mode-hopping, intensity fluctuations etc. and can be a major source of noise in an otherwise highly ordered output [1].

Disordered systems on the other hand are less well known, although they are common in our every day lives. For example clouds, fog, sugar, sand, white paint and human tissue are highly turbid media. On a macroscopic level, the propagation of light through these materials is simple. The incident light is attenuated according to Beer's law and a diffuse "glow" is formed. On a microscopic level, however, this problem is extremely complicated. White paint, for instance, consists of a large collection of microscopic particles (for example TiO_2 microparticles), which are distributed randomly. Light incident on white paint is randomly scattered thousands of times before leaving the paint again, thereby following a complicated random trajectory.

Two key processes in the interaction of light and matter are scattering and absorption. If an object strongly absorbs light at all wavelengths, it appears black. On the other hand, if it only scatters light, it looks white. The details of these processes are going to be described in the following section 4, where a connection between absorption, gain (laser action) and multiple scattering will be attempted. Multiple

scattering in all kinds of disordered systems is currently an active area in both fundamental and applied research.

But what would happen if a beautiful laser crystal were grounded into a fine powder (figure 3.2)? If the powder could be excited, it would still amplify. But the small grains would also multiply scatter the light! What would the output of such a powder look like? Would laser action still be possible in such a highly scattering gain material? And if laser action were possible, how coherent or incoherent would it be?

Fig. 3.2: *Model picture of a random lasing medium. The microparticles both scatter and amplify light [2].*

3.2 Lasing in random amplifying media

Could the seemingly opposing natures of disorder and lasing be combined and can lasing action be actually aided by the deliberate introduction of scattering into a lasing system? That is,

Can a random system have an ordered (laser) output?

This question has raised great scientific debate during the past decade.

The first theoretical prediction of the emission from a random scattering medium with negative resonance (gain) was made in 1968 by **V. Letokhov** [3]. He calculated the optical properties of a random medium, which both amplifies and scatters light. Amplifying media are thermodynamically unstable because there are more atoms or molecules in the excited state than in the ground state. In an amplifying medium the intensity of a light wave, which is traveling through it, increases. However, such a state can be maintained in a finite region of space. Normal materials that absorb light are thermodynamically stable because, over long distances, all the

energy eventually gets absorbed from the atoms or molecules that populate the ground state.

For a very long time, though, Letokhov's pioneering work was not followed up by experiments. It was 1993, however, that **Arnold Migus** and colleagues showed that a random amplifying medium could be made by grinding a laser crystal into a powder [4].

Even so, the great advancement in the research of these materials was given by the experiments performed by **A. Genack et al.** and especially by **Nabil Lawandy** and co-workers, where placing random scatterers in a gain medium could enhance the frequency stability of the laser emission [5,6]. In these experiments, it was found that the introduction of disorder (by suspending Titania microparticles) into a homogeneous Rhodamine laser dye solution caused a drastic spectral narrowing of the emission from the dye, above a well-defined threshold of pump light intensity. Undoubtedly, this is a well-known phenomenon, which occurs even in homogeneous amplifying media due to Amplified Spontaneous Emission (ASE). But the remarkable aspect in these experiments was that, the threshold of the pump laser intensity at which the fluorescence spectrum collapsed dramatically was almost two orders of magnitude smaller in the case of the microsphere-laser dye suspension, compared to the case of the ASE in the neat dye solution. Laser experiments showed that the emitted pulses from the random amplifying medium exhibited temporal shortening (much like in high gain lasers), and a bichromatic emission at some intermediate pumping levels. Lasing in these media occurs even at very small concentration of the scatterers, i.e. even when the mean free path of light in the medium is larger than the sample size.
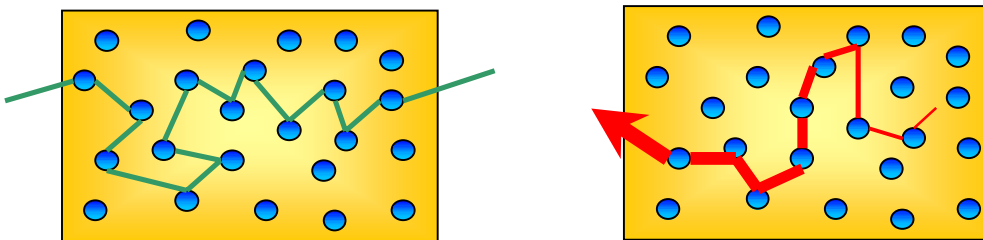

Fig. 3.3*: **a**) Scattering of pumping radiation. **b**) Scattering and amplification of emitted radiation*

In the recent experiment of **S. V. Frolov er al.** [7] and **Hui Cao et al**. [8], where the lasing from very strongly scattering semiconductor powder was studied in different conditions, a connection between lasing and Anderson localization of light has been claimed. Hui Cao and colleagues have created a random laser by grinding a ZnO crystal into a fine powder and excited with short pulse lasers and observed the temporal and spectral characteristics of distinct lasing modes at different geometries. They found that for different excitation and detection geometries the spectral peaks of the emission appear at different wavelengths. This observation suggests that due to the localization of light the emission originates from different micro-cavities inside the powder.
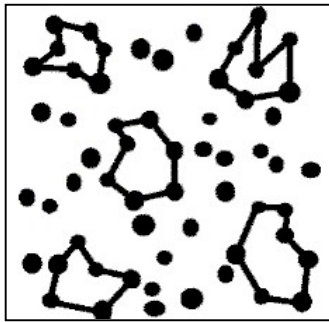

Fig. 3.4*: Schematic representation of the micro-cavities formed when light travels inside highly dense scatterers [2].*

Let us now investigate the experiment, which was mentioned above, of grounding a typical laser crystal into a fine powder (size ≤ 1µm) and exciting it in the absorption band with pulses from a powerful laser. Then spectral and temporal measurements of the emission in different directions could be carried out. Yet, optical excitation is difficult for a random material, because most of the excitation light is simply scattered out and very little is absorbed. This means that very high pulse energies, which lie close to the thermal threshold of the material, are needed. Another option of the same experiment would be to suspend scattering microparticles such as Titania or Polystyrene microspheres in a laser dye solution, or to embed them into a laser-dye doped polymeric matrix.

But before we proceed lets remember what happens to light on highly scattering random media assumed to have no gain? On a macroscopic level as mentioned before the picture is very simple and seen in every day life: the incoming beam is attenuated due to scattering and a diffuse glow emanates from the medium. On the microscopic level, however, the situation is extremely complicated. The light could be scattered

several thousands of times before leaving the medium. Depending on the scattering there are two different regimes. The weakly scattering regime, where the density of the scatterers is small, thus the probability of light to be scattered more than once is extremely small. In this case, the mean free path of the light is much larger than the sample size and the scattering acts only as a small perturbation on the incident light.

On the other hand when strong scattering takes place the scatterers' density is very high and thus the light is multiply scattered. In this regime, the scattering is a very strong perturbation on the incident light field. The field amplitude at any given scatterer is strongly modified by the presence of other scatterers. It is in the multiple scattering regime that most of the random laser experiments have been performed in and consequently, in which we will be interested and concentrated in this thesis.

The transport of light in multiply scattering media can be described at three different levels [9]. At the first, gross level of an incoherent energy transport (shown to be valid for $kl>1$ where k is the wave vector and l is the transport mean free path of the light inside the medium), light can be thought of consisting of particles bouncing of randomly distributed scattering centers with the probability of scattering being unity (the so-called bouncing photon picture). This random walk problem is accurately described by a diffusion equation for the light energy density at large length scales ($L>>l$). More sophisticated theory of persisted random walks where the photons retain some directional memory have been developed and accurately describe both the ballistic transport at short length scales ($L \sim l$) and the diffusive transport at large length scales ($L>>l$), as described in the next chapter.

At the second level of description in terms of a wave transport (necessary at $kl \sim 1$), interference of the scattered light becomes very important. Coherent backscattering of light where an enhanced scattering (doubling of the intensity) occurs within a cone of directions around the backscattered direction is perhaps the most well known phenomenon of such an (constructive) interference effect in disordered media. Very important in strongly scattering media are recurrent scattering events, where the photons continuously travel through a closed loop path involving the same set of scatterers. These paths can form random cavities and cause feedback much like a ring laser cavity. In fact, for very strongly scattering media, the effects of such interference and recurrent scattering can result in total spatial localization of light (Anderson localization) [10,11]. This was predicted to occur when the mean free path of light became very small ($kl \leq 1$) and has been experimentally found to occur [12,13]. In

this situation, light simply stops flowing over long length scales, i.e. the energy is spatially trapped over a length scale known as the localization length. In other words, the diffusion coefficient becomes zero and "light stands still".

The third level of description at a quantum optical point of view, involves the photon statistics and field quantization in random media. This would enable us to understand the very nature of the random lasing and asses whether it has all the properties that a conventional laser does, namely stimulated emission and coherence. **Beenakker et al.** have worked extensively on the photon statistics problem in one-dimensional random media [14]. Recently photon-counting experiments have been performed, in an attempt to measure the photon statistics of a real random laser when excited by ultra-fast lasers, with contradictory results, depending on the type of the material [15,16]. However, much remains to be made in this area both theoretically and experimentally.

Let us know consider a multiply scattering amplifying (gain) medium with weak, dense scatterers, in which the diffusion theory is still valid. The light emitted spontaneously by the medium will have to undergo a long random walk inside the medium (which could be orders of magnitude larger than that in a homogeneous medium) before exiting. During every path of this random walk, the light is continuously amplified due to stimulated emission. Thus, gain can become larger than losses and lasing action can be caused by diffusive feedback. The output loss is proportional to the surface of the medium through which the light exits, while the gain is proportional to the overall volume of the medium [17]. As the size of the random amplifying medium is increased, the gain becomes larger than the loss and a strong flash of light occurs in all directions. This is analogous to what happens in a fission nuclear bomb or reactor, where neutrons are scattered and amplified by nuclear fission – the system becomes super -critical beyond a critical size. In a random laser, there will be a large gain narrowing of the emitted spectrum, as photons at the emission maximum would be much more amplified in their long passage through the medium. Thus, lasing action is caused by a "feed–forward mechanism" compared to the feedback mechanism in a conventional laser. It is this extension of the path length in the random amplifying medium due to multiple scattering, which is responsible for the lowering of the threshold pump intensity. Note that in comparison to the unidirectional output of a conventional laser, the random laser will emit in all directions. Also due to the very large intensities, which occur during the lasing, the

population inversion in the medium is quickly depleted, leading to a sharp temporal peak or pulse shortening of the fluorescence emission. If the exciting pump beam is still present, then the population inversion will again build up and deplete successively, resulting in a train of spikes in the emission.

Finally, we look at very strongly scattering ($kl \sim 1$) and amplifying media where the diffusion picture breaks down and localization effects become important. Also, in the above picture of light diffusion with gain, the amplification could very well have been an incoherent process (such as in the generation of neutrons in a nuclear fission reaction where the outgoing neutrons have no phase correlations with the incoming neutrons). Stimulated emission is, however, a coherent process where the emitted photons have the same phase and direction as the incoming photon. This property of coherent amplification of light coupled with the coherent feedback offered by Anderson localization can result in a new kind of coherent laser output. This enhancement of amplification due to synergy between coherent amplification and wave confinement by localization was theoretically predicted by **Pradhan and Kumar** in 1994 [18]. In this case, the recurrent multiple scattering events forming closed loops provide feedback much like in the ring cavity lasers. Of course, due to the random nature of the medium, a distribution of many such random cavities with different Q factors would exist. As the pump laser intensity is increased, the laser threshold condition (gain = loss) would be satisfied first in the cavities with the highest Q factors. Laser oscillation would occur at frequencies determined by the cavity resonances. Thus, the laser emission would consist of sharp discrete lines. At higher pump intensities, oscillations would begin even in lossier cavities and more lines would be added to the emission spectrum. One notes, that the random cavities formed by recurrent multiple scattering would be totally different in different samples. Thus, the lasing lines would vary from sample to sample, a typical effect found in disordered systems. Also the random cavities would have outputs in different directions and the emitted spectrum would be different in different directions and we have a multimode laser in all directions. In the recent experiments of **Frolov et al.** and **H. Cao et al**. involving very strongly scattering semiconductor powders (ZnO, GaN), all the above effects were observed to occur [7,8]. The lasing lines had extremely small spectral linewidths (~ 0.2 nm). Thus, a random laser with coherent feedback was claimed. However, even though there are doubts that the fine spectrum observed in these experiments could be due to a reduced dimensionality of the system when

localization effects are easier to achieve, there is no doubt that the coherent feedback mechanism due to Anderson localization has been demonstrated.

The ability to perform experiments on media with multiple scattering and gain – either with powdered laser crystals or micro-particle suspensions in laser dyes – has opened up a new field of research, with constantly increasing interest during the past years. All the multiple scattering phenomena previously studied on passive (absorbing) materials can now be explored in active - amplifying systems. Moreover, the effect of strong scattering on laser action from different materials can also be investigated.

3.3 Applications

Random lasers can be implemented into a variety of applications ranging from industrial to medical and market fields. Some of the concepts have already been forwarded, since the field exhibits an increasing interest among, both researchers and marketing people.

To begin with, in machine vision applications, plastics can be impregnated with random lasers with different chromophores to produce lasing screws, nuts, bolts and manufactured parts. The 3 nm wide lasing signature can in turn be used as a wavelength domain labeling code. This simple orientation and shape independent method enables a robotic arm with an optical fiber conduit to sort and select parts.

Another very promising application of random lasers is the manufacturing of photonic codes. Using a very thin coating (~200 μm) of such material, everything could be coded and read by only one excitation laser pulse. Such codes could be used in the identification of military objects, for "marking" of harmful materials and contact-safe identification or for the replacement of the very common bar codes used in almost all modern product. The most recent development in photonic coding is the invention of **Nabil Lawandy at Spectra Systems Co.** who produced photonic codes that can be printed to any material using a common inkjet printer.

Furthermore, these photonic codes could be used in the manufacturing of new, safer cards, by substituting the existing magnetic codes. These cards would be consisted of stripes of different photonic polymers, every one of which would lase at a

different wavelength. Sixteen stripes could produce 1 billion of different photonic codes, making the reproduction of fake cards almost impossible.

In the area of search and rescue, there is currently an urgent need for a rugged, passive and low-cost method of identifying downed ships, aircraft and satellites. In most cases, once an aircraft crashes, the sophisticated transponder equipment on board is disabled, making conventional visual sighting and lidar methods the only way to find survivors. Random lasers along with eye-safe ranging lasers at 1.5 μm will enable search craft to identify downed vehicles and survivors by a unique narrow band return signal emanating from painted fuselages, hulls, tarps, sails and life jackets.

In the biomedical arena, the materials high conversion efficiency per unit volume ($\geq$ 50 percent in a 250 μm thickness) allows for wavelength-shifted catheters and laser creams, potentially useful for the removal of tattoos and other skin discolorations. In addition, random lasers can be used for wavelength shifting the installed base of lasers for other applications such as photodynamic therapy where narrow-band excitations are required for drugs such as benzoporphyrin derivatives (BPD). As far as detection is concerned random lasers could be implemented in various applications such as medical imaging. The combined use of these materials with chromophores that are selectively absorbed by malignant tumors and the narrowband emission along with the high-emitted intensity could boost the detection efficiency.

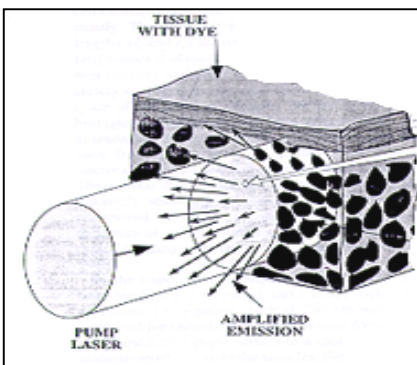**Fig. 3.5**: *Schematic representation of random lasing used in medical detection [19].*

Moreover, substituting other more chemically robust gain media for dyes opens the door for more applications. Photo-conducting polymers such as PPV can be used as both a gain medium and a host, while high quantum efficiency, high gain doped quantum dots can be incorporated into glasses or polymers for use as lasing pixels on

television screens. This results in a broad and expanded color pallet that circumvents the brightness limitation reached when phosphors saturate and may finally eliminate the requirement for the bulky vacuum tube.

Future development of this technology is focused on eliminating the need for optical pumping for applications such as flat panel, automotive and cockpit displays. Early work in these areas is employing polymeric diode devices formed from the families of materials such as PPV sandwiched between transparent indium tin oxide and appropriate metal or semiconductor electrodes. The incorporation of scatterers in these systems is expected to lead to higher efficiency LED and laser diodes potentially operating in the blue-green part of the spectrum. A very promising idea is the combination of random lasers with the photonic band gap materials. In other words the combination of an order structure characterizing photonic band gaps and disorder characterizing random lasers, in an attempt to manipulate and confine the random output of scattering gain media. A first attempt was made with the work of **Frolov et al.** regarding the laser-like emission from opal SiO_2 crystals, [20]. For an introduction to photonic band gap materials see **Yablonovitch** and **John et al**. [21, 22].

In the contents of this thesis the basic theoretical aspects of scattering, gain and random lasing will be described, as well as the latest developments of the theory in this field. As mentioned also in the previous sections much debate is still going on concerning the underlying mechanisms of random lasing and they are currently investigated by many research groups. In the **Chapters** section the experimental results of this thesis will be described and discussed.

References

1. J. T. Verdeyen, *"Laser Electronics"*, Third Edition, Prentice Hall, New Jersey (2000)

2. D. S. Wiersma *"Light in strongly scattering and amplifying random media"*, PhD Thesis, Amsterdam (1995). D. S. Wiersma, A. Lagendijk, *"Laser action in very white paint"*, **http://www.science.uva.nl/research/scm/index.html**V. S. Letokhov, *Sov. Phys. JEPT* **26**, 835 (1968)

4. C. Gouedard, D. Husson, C. Sauteret, F. Auzel and A. Migus, *J. Opt. Soc. Am.* **B10**, 2358 (1993)

5. A. Z. Genack and J. M. Drake, *Nature* **368**, 400 (1994)

6. N. M. Lawandy, R. M. Balachandran, A. S. L. Gomes and E. Sauvain, *Nature* **368**, 436 (1994)

7. S. V. Frolov, Z. V. Vardeny, K. Yoshino, A. Zakhidov and R. H. Baughman, *Phys. Rev. B* **59**, R5284 (1999)

8. H. Cao, Y. G. Zhao, S. T. Ho, E. W. Seelig, Q. H. Wang and R. P. Chang, *Phys. Rev. Lett.* **82**, 2278 (1999)

9. S. A. Ramakrishna, *Bull. Indian Laser Academy* **11**, 1 (1999)

10. P. W. Anderson, *Philos. Magaz.* B **52**, 505 (1985)

11. S. John, *Physics Today* **44**, 32 (1991)

12. M. Mitchell and M. Segev, *Nature* **387**, 880 (1997)

13. D. S. Wiersma, P. Bartolini, A. Lagendijk and R. Righini, *Nature* **390** 671 (1997)

14. C. W. J. Beenaker, *Phys. Rev. Lett.* **81**, 1829 (1998)

15. G. Zacharakis, N. A. Papadogiannis, G. Filippidis and T. G. Papazoglou, *Opt. Lett.* **25**, 923 (2000)

16. H. Cao, Y. Ling, J. Y. Xu, C. Q. Cao and P. Kumar, *Phys. Rev. Lett.* **86**, 4524 (2001)

17. D. S. Wiersma, *Nature*, **406**, 132 (2000)

18. P. Pradhan and N. Kumar, *Phys. Rev. B* **50**, 9644 (1994)

19. M. Siddique, Li Yang, Q. Z. Wang, R. R. Alfano, *Opt. Comm.* **117**, 475 (1995)

20. S. V. Frolov, Z. V. Vardeny, A. A. Zakhidov, R. H. Baughman, *Opt. Comm.* **162**, 241 (1999)

21. E. Yablonovitch, *Phys. Rev. Lett.* **58**, 2059 (1987)

22. S. John and T Quang, *Phys. Rev. Lett.* **74**, 3419 (1995)

4. Theory

In this part an overview of the theoretical aspects of the interaction of light and matter will be attempted. The processes of absorption, scattering and spontaneous emission (fluorescence), which take place when photons interact with matter will be described. Then the interest will be concentrated on describing the processes that govern a medium (random laser), which combines all of the above and on explaining both the emission and the properties of the emitted light. The current status of the theory on random lasing will be described both after one- and two- photon excitation. Finally, the coherent properties of the emitted light will be discussed both theoretically and experimentally.

4.1 Interactions of light with matter

4.1.1 Maxwell's equations

The interaction of light with matter can be described by the well-known Maxwell's equations:

$$\nabla \times \mathbf{E} = -\frac{\partial \mathbf{B}}{\partial t} \tag{4.1}$$

$$\nabla \times \mathbf{H} = \mathbf{J} + \frac{\partial \mathbf{D}}{\partial t} \tag{4.2}$$

$$\nabla \cdot \mathbf{D} = \rho \tag{4.3}$$

$$\nabla \cdot \mathbf{B} = 0 \tag{4.4}$$

where,

$$\mathbf{D} = \varepsilon_o \mathbf{E} + \mathbf{P(E)} \,,$$

$$\mathbf{B} = \mu_o \mathbf{H} + \mathbf{J(H)} \text{ and} \tag{4.5}$$

$$\mathbf{J} = \xi \mathbf{E}$$

The interaction of the light electric field with the charges of the material (electrons and ions) can be described by coupling the **wave equation** (for the electric field vector, since the magnetic component can be usually neglected):

$$\nabla^2 \mathbf{E} - \frac{1}{c^2} \frac{\partial^2 \mathbf{E}}{\partial t^2} - \frac{\partial}{\partial t} (\nabla \cdot \mathbf{E}) = \mu_o \frac{\partial^2 \mathbf{P(E)}}{\partial t^2} \tag{4.6}$$

with the **time-dependent Schrödinger equation:**

$$H(\mathbf{r},t)\Psi(\mathbf{r},t) = i\frac{h}{2\pi}\frac{\partial \Psi(\mathbf{r},t)}{\partial t} \tag{4.7}$$

The Hamilton operator H represents the total energy of the light-matter system and the wave function Ψ the quantum state of this system.

4.1.2 Absorption

Absorption is the process in which a photon from the incident field is absorbed by an atom or molecule of the material, which is then driven to an excited state. The energy $E = h\nu$ of the photon corresponds to the energy difference of the two states (resonance condition) and is then converted into other forms of energy [1-3]. The rate at which this process is taking place depends on the concentration of the absorbing atoms or molecules and the incident field. If $W(\nu)$ is the energy density per frequency interval, $\mathbf{B_{12}}$ is the **Einstein's coefficient** of absorption and N_1, N_2 the populations in the ground and excited state of a two level atomic system respectively we obtain:

$$\frac{dN_2}{dt} = B_{12}N_1W(\nu) = -\frac{dN_1}{dt} \tag{4.8}$$

However, the absorption of light is a complicated quantum process. A description in the microscopic level would require the use of quantum electrodynamics, which would have been outside of the contents and the aim of this thesis. The description that follows will account for the macroscopic effect of the absorption of light in matter, which is the attenuation of the number of photons transmitted through a given material.
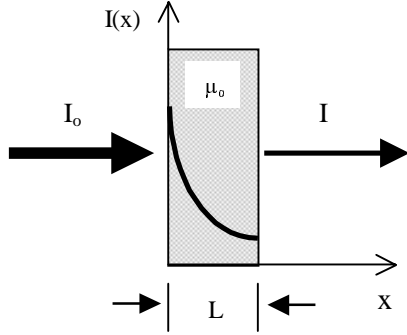
In linear optics the incremental decrease of the intensity I is proportional to the intensity itself:

$$dI(z) = -\mu_\alpha I(z) \qquad (4.9)$$

where μ_α is the **absorption coefficient** measured in mm^{-1}.

Integration of this equation leads t the well-known **Lambert-Beer law**:

$$I = I_o e^{-\mu_a L} \qquad (4.10)$$

where I_o is the incident and I is the transmitted intensity and L is the width of the material that photons have to travel through.

For the determination of absorption the incident intensity I_o and the transmitted intensity I have to be measured. Then the transmission T can be calculated by:

$T = \dfrac{I}{I_o}$ and thus the absorption coefficient can be determined as: $\mu_a = \dfrac{\ln(T)}{L}$

The inverse of the absorption coefficient gives the mean free path between two absorption events or absorption length l_α measured in mm.

In terms of the particle density ρ and absorption cross section σ_{abs}: $\mu_a = \rho \sigma_{abs}$

The absorption coefficient is related to the imaginary part of the complex refractive index: $n_{complex} = n_{real} + i n_{imag}$ by:

$$\mu_\alpha = \frac{4\pi}{\lambda} n_{imag} . \qquad (4.11)$$

The dependence of the absorption coefficient on the wavelength for the different chromophores comprising biological tissue can be seen in figure 4.1, where the absorption of proteins, melanin, hemoglobin and water are shown. It is clear that the absorption of water dominates the IR (Infra-Red) region of the spectrum and the macromolecules and pigments dominate over the visible and UV regions. However, since the absorption of both water and macromolecules is minimized over the NIR region, a therapeutic window is opened between roughly 600 nm and 1100 nm, which is also referred to as "biological window". In this spectral range the radiation penetrates deeper in biological tissue and it is in these wavelengths that all the attempts for optical imaging inside tissue have been performed.
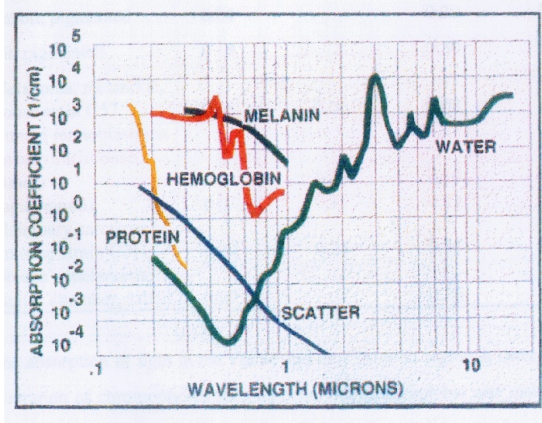
Fig. 4.1*: The wavelength dependence of the absorption coefficient of the most important components of biological tissue. The wavelength dependence of the overall scattering coefficient of tissue is also shown.*

4.1.3 Spontaneous emission

The spontaneous emission, as the name implies, is the process where an atom or molecule that is on an excited state after absorbing a photon, decays spontaneously to the ground state by emitting one photon[1,2]. The energy of the photon is identical to the energy difference of the two states. If the population density in the excited state 2 of a two level system was N_2, the decay to state one is given by:

$$\frac{dN_2}{dt} = -A_{21}N_2 \tag{4.12}$$

where **A_{21}** is the **Einstein's coefficient** giving the spontaneous emission probability, and the lifetime of the excited state as: $\qquad \tau_{sp} = (A_{21})^{-1}$

Since the probability is constant over time an ensemble of excited atoms or molecules will decay exponentially. The spontaneous emission intensity will be given by:

$$I_{sp}(t) = I_o e^{-t/\tau_{sp}} \tag{4.13}$$

The exponential decay curve that represents the intensity behavior is depicted in figure 4.2.

From the uncertainty principle it follows that this transition must have a minimum homogeneous spectral width, which is represented by a **Lorentzian line shape**, as shown in figure 4.2.

However, for the large molecules, which are involved in the present study, if they are organic dye molecules or the natural chromophores of biological tissue, the process of spontaneous emission is more complicated. If the emission of light does not require the molecule to pass from a state with different spin multiplicity as the

initial one, the radiative process is called **fluorescence**. The mechanism is schematically depicted in figure 4.2, where the exponential fluorescence decay is also shown. The incident radiation excites a molecule from the **singlet** (electron spin 0) electronic ground state S_o into an excited singlet state S_1. The molecule during this transition is also excited vibrationally and after collisions with the surrounding medium (a gas, a liquid solvent or a solid lattice) it is de-excited non-radiatively to the lowest vibrational level of state S_1 (**internal conversion**), with a characteristic time of the order of 10^{-12} sec. Thereafter, two different channels of energy loss can occur. The energy can be transferred non-radiatively to the surrounding medium or to a **triplet** (electron spin 1) excited electronic state via a process, which is called **intersystem crossing**, which eventually will lead to the emission of phosphorescence. The other channel is the radiative decay to state S_o with the emission of fluorescence (figure 4.2), with characteristic lifetime of the order of 10^{-9} sec.
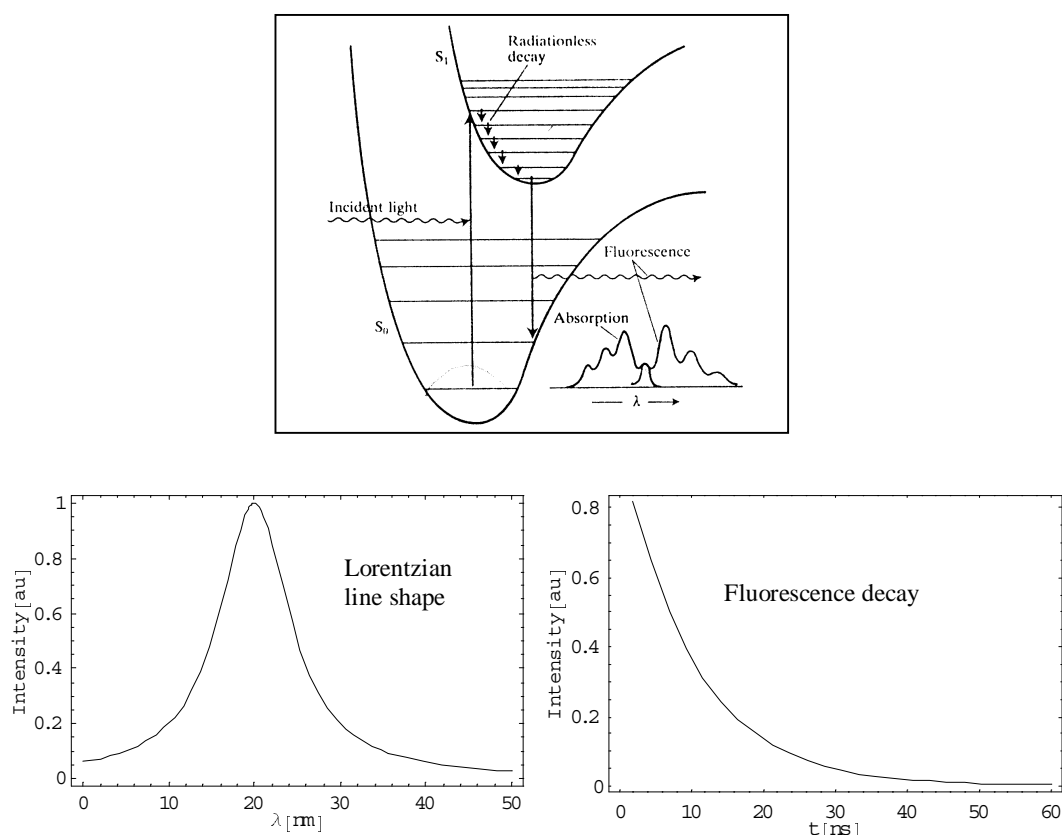

Fig.4.2*: Schematic diagram of the mechanism of fluorescence of a large organic molecule. The emission spectral and temporal characteristics are also presented.*

As seen also from figure 4.2, the fluorescence light is emitted at higher wavelengths than the incident light. The energy difference corresponds to the vibrational energy lost during the internal conversion and to the environment and is referred to as Stokes shift.

The **fluorescence lifetime** is identical to the lifetime of the emitting state and is directly connected to the natural spectral width Δv_{nat} of the transition and the decay time of the non-radiative processes τ_r:

$$\frac{1}{\tau_f} = \frac{1}{\tau_{nat}} + \frac{1}{\tau_r} = 2\pi\Delta v_{nat} + \frac{1}{\tau_r} \tag{4.14}$$

However, because of the broadening of the electronic transitions the fluorescence lifetime cannot be determined from spectral measurements and thus time-resolved measurements are required.

The **quantum yield** of the fluorescence is given by the ratio of the spontaneously emitted photon with the total number of photons absorbed by the molecules:

$$\Phi_{yield} = \frac{N_{spontaneous}}{N_{absorbed}} = \frac{\tau_f}{\tau_r} \tag{4.15}$$

Thus by measuring the quantum yield the radiative transitions from the excited state can be differentiated from the non-radiative ones.

4.1.4 Stimulated emission and lasing

In this section the basic aspects of stimulated emission and laser radiation will be reviewed [2,4,5]. The process of stimulated emission is the inverse of absorption. The atom or molecule that lies on an excited state is forced to return back to the ground state by emitting a photon and thus giving its energy hv to the field. The stimulatively emitted photon has the same frequency, phase and polarization and propagates in the same direction as the photon that induced the transition. The rate of the stimulated emission depends on the density of atoms or molecules and the strength of the stimulating field:

$$\frac{dN_2}{dt} = -B_{21}N_2W(v) = -\frac{dN_1}{dt} \tag{4.16}$$

From the basic electromagnetic theory arises the following relationship of the Einstein's coefficients:

$$A_{21} = \frac{8\pi h n^2 n_g}{c^3} v^3 B_{21} = \frac{8\pi h n^2 n_g}{c^3} v^3 B_{12} \qquad (4.17)$$

where n accounts for all the allowed values of the field energy and n_g for the group refractive index of the material.

All the above considerations were made with the assumption that the energy density of the field follows the blackbody radiation theory and the fact that the multiplicity factors of all the involved states are equal. However, when dealing with a real laser system we have to account for the fact that the gain medium emits a narrow band of frequencies or a **lineshape** $\gamma(v)$ with a certain width Δv. Thus, the **stimulated emission cross section** can be calculated as:

$$\sigma_{em}(v) = A_{21} \frac{\lambda^2}{8\pi n^2} \gamma(v) \qquad (4.18)$$

The amplification of the intensity of the field travelling inside a cavity is given by:

$$\frac{dI_v}{dz} = g(v)I_v \quad \text{where:} \quad g(v) = \sigma_{em}(v)\left(N_2 - \frac{g_2}{g_1}N_1\right) \qquad (4.19)$$

is the gain coefficient of the lasing medium. The condition for positive gain and amplification is $N_2 > (g_2/g_1)N_1$, the well know **population inversion** condition.
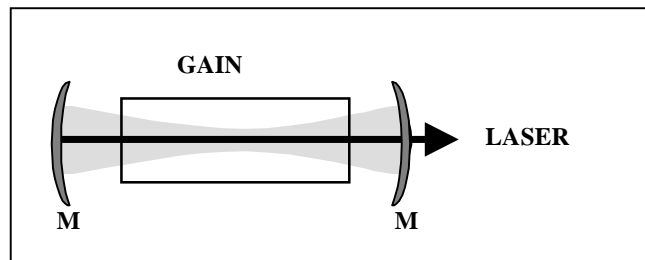

Fig. 4.3: *Schematic representation of a laser cavity, with the gain medium and the lasing output*

Taking all these into account the basic coupled lasing equations, which describe the rate of the energy density of the field traveling inside the cavity and the rate of the number of molecules of each state, can be derived:

$$\frac{dW_{em}}{dt} = -DW + \sigma_{em}cN_1W_{em} + \frac{N_1}{\tau_{sp}} \quad \text{and} \quad \frac{dN_1}{dt} = R - \sigma_{em}cN_1W_{em} - \frac{N_1}{\tau_{sp}} \qquad (4.20)$$

where D is a factor that accounts for all the losses of energy that are caused by the cavity and R is the pumping rate that produces the population inversion. In the following sections a connection of these rate equations with diffusion and random lasing theory will be tried.

4.1.5 Light scattering

Scattering is the process during which the propagation direction of an electromagnetic wave, which is incident on a particle, is altered. It takes place when the light electric field induces dipoles upon incident on the medium, which re-emit the light in the plane perpendicular to the dipole (figure 4.4). Interpretation of scattering can be made in terms of the ratio between the wavelength of the incident light $k = \frac{2\pi n}{\lambda}$ and the size of the scattering particle α. k is the wavenumber, λ the wavelength and n the refractive index of the medium in which the field is traveling. The difference of the refractive indices of the medium and the scattering particle is also very important. When $k\alpha \ll 1$ the interaction is called **Rayleigh scattering** and when $k\alpha \approx 1$ it is called **Mie scattering**. Both processes are **elastic,** meaning that the energy of the photons is conserved. However, there are other scattering processes in which the energy and frequency of photons are changed (**inelastic scattering**), such as **Raman** and **Brillouin** scattering, which are outside the contents of this thesis [1,3,6].
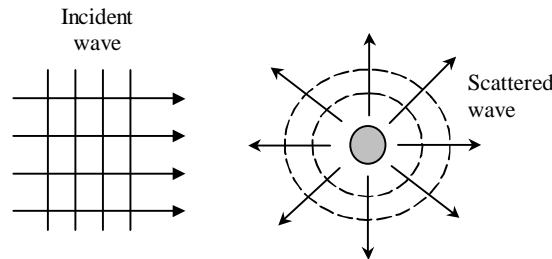

Fig.4.4: *Schematic representation of scattering by a localized object.*

Single scattering

In **Rayleigh scattering** the particles (atoms, molecules or very fine dust) are very small compared to the wavelength of the incident field ($k\alpha \ll 1$) as mentioned above. The angular distribution of the scattered energy is governed by the incoherent scattering from the dipole scatterers and depends on the state of polarization of the incident wave. The total scattering cross section for Rayleigh scattering is given by:

$$\sigma_R = \frac{8}{3}\left[\frac{\pi\left(n^2-1\right)}{N\lambda^2}\right]^2 \propto \frac{1}{\lambda^4} \tag{4.21}$$

where n is the refractive index of the scatterer, N the concentration of scattering particles and λ the wavelength of the incident light. The above formula is the well-known **Rayleigh law**, which describes very accurately the scattering of light in the atmosphere, which is responsible for the colors of the sunset and blue sky since blue light is scattered more effectively than red. A typical value of this cross section of the air with density of 2.5×10^{19} cm^{-3} at 500 nm is $\sigma_R = 6.91 \times 10^{-28}$ cm^2 [2].

On the other hand when the particle's size is comparable with the wavelength of the incident light field ($k\alpha \approx 1$) **Mie scattering** occurs. These particles can be aerosols or other fine particles in the air or colloids in a solution. The scattering intensity and angular distribution is a complicated function of the particle size, distributions and complex refractive indices. The problem can be solved only by a formal solution of the Maxwell's equations, which can be applied only for certain simple symmetric shapes such as a sphere or a cylinder. However, the scattering cross section of Mie scattering shows a weaker dependence on wavelength than for Rayleigh scattering:

$$\sigma_{Mie} \propto \frac{1}{\lambda^x} \tag{4.22}$$

where x could be $0.4 \leq x \geq 1.6$ [2,3]. Moreover, Mie scattering takes place preferably in the forward direction, whereas Rayleigh scattering is proportional to $1+\cos^2\left(\theta\right)$, i.e. forward and backward directions are the same.

This is depicted in figure 4.5 where the intensity distribution of the scattered light is shown. The particle's dimension is **a)** $k\alpha \ll 1$, **b)** $k\alpha = \frac{1}{4}$ and **c)** $k\alpha \gg 1$ [7].
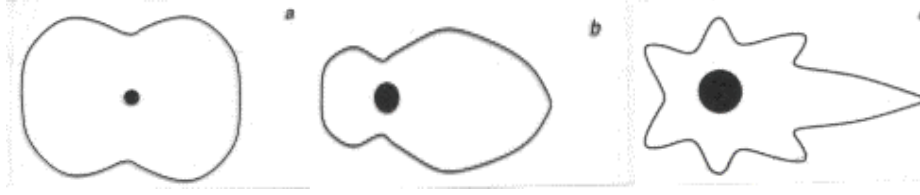
Fig. 4.5*: Intensity distribution of light scattered from particles of:*
***a)*** *kα<<1,* ***b)*** *kα = ¼ and* ***c)*** *kα>>1.*

Multiple scattering

However, when a macroscopic medium is studied, the total scattering of the radiation should be accounted for, which is the effect of multiple scattering events cause by an ensemble of scattering centers on the propagating light field. In that case a macroscopic optical parameter can be defined. This parameter is the **scattering coefficient μ_s** measured in mm^{-1}. Then the attenuation of the light intensity is defined from:

$$dI(z) = -\mu_s I(z) \tag{4.23}$$

and integration over z gives:

$$I = I_o e^{-\mu_s L} \tag{4.24}$$
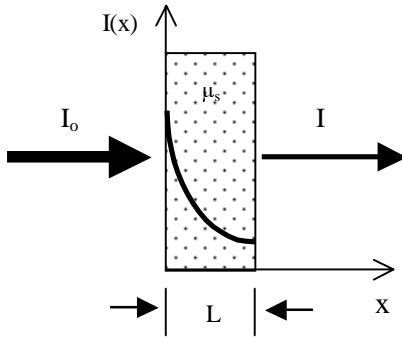
where I_o is the incident and I is the transmitted intensity and L is the width of the material that photons have to travel through. From the scattering coefficient the **scattering mean free path** between two scattering events can be defined as: $l_s = 1/\mu_s$ measured in mm. However, since in multiple scattering materials many random scattering events take place, it is important to define a probability function $p(\theta)$ of a photon to be scattered at an angle θ. If $p(\theta)$ does not depend on the angle then the scattering is **isotropic**. Otherwise, **anisotropic scattering** occurs. A measure of the anisotropy of scattering is given by the **anisotropy factor g**, where g = 1 denoted purely forward, g = -1 purely backward and g = 0 isotropic scattering. By definition g represents the average of the cosine of the scattering angle θ:

$$g = \langle \cos\theta \rangle = \frac{\int_{4\pi} p(\theta)\cos\theta \sin\theta d\theta d\phi}{\int_{4\pi} p(\theta)\sin\theta d\theta d\phi} \tag{4.25}$$

In very complex media such as biological tissue (as discussed in the following section) the scattering coefficient is usually determined coupled to the anisotropy factor as the **reduced scattering coefficient** $\mu_s^{'}$, defined as:

$$\mu_s^{'} = (1-g)\mu_s \qquad (4.26)$$

The probability function *p(θ)*, which is also called phase function, is normalized by:

$$\frac{1}{4\pi}\int_{4\pi} p(\theta)\sin\theta d\theta d\phi = 1 \qquad (4.27)$$

Several theoretical phase functions *p(θ)* have been proposed, but the most commonly used and the most accurate for describing light transport in tissue is the **Henyey - Greenstein** function, which was first used for the description of light scattering in galaxies:

$$p(\theta) = \frac{1-g^2}{\left(1+g^2-2g\cos\theta\right)^{3/2}} \qquad (4.28)$$

Scattering in biological tissue

Biological tissue is one of the most complicated materials combining both absorption (section 4.1.2) and multiple scattering. In such media a total **attenuation coefficient** $\mu_t = \mu_\alpha + \mu_s$ can be defined to account for both processes. The behavior of tissue cannot be accurately explained either with Rayleigh nor Mie scattering and thus only macroscopic description can be made as illustrated in the following sections. The scattering inside biological tissue is due to the microscopic components that it consists of such as cells, intracellular organelles or collagen fibers. In figure 4.6 the relative size of these scattering components compared with the wavelength of the light is depicted.
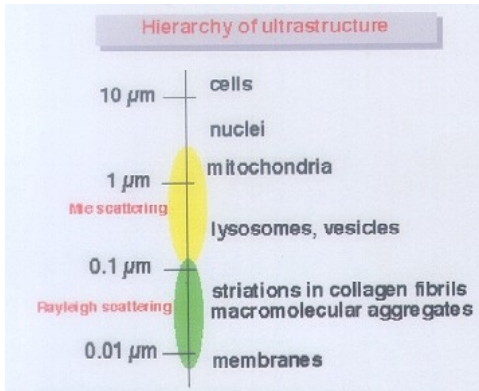

Fig. 4.6: Schematic representation of the relative sizes of the scattering components of biological tissue and the corresponding scattering mechanism.

4.2 Diffusion in turbid media

In turbid material light is scattered and absorbed due to the inhomogeneities and absorption characteristics of the medium. A mathematical description of the propagation and scattering characteristics of light can be made using two different approaches: analytical theory and transport theory.

Analytical theory starts with the Maxwell's equations takes into account the statistical nature of the medium and considers the statistical moments of the wave. In principle this is the most fundamental approach, including all diffraction effects. However, its drawback is the mathematical complexities involved and thus its usefulness is limited.

On the other hand, transport theory deals directly with the transport of power through turbid media. The development of transport theory is heuristic and lacks the rigor of analytical theory. However, it has been used extensively and experimental evidence shows that it is applicable to a large number of practical problems [8,9].

In the following sections, first the photon transport theory and the diffusion approximation are reviewed. Then the time-resolved transmission of ultra-short laser pulses through turbid media is described.

4.2.1 Photon transport theory

The fundamental quantity in transport theory is the radiance $J(\mathbf{r}, \mathbf{s})$, which is expressed in W cm^{-2} sr^{-1} and denotes the power flux density in a specific direction $\mathbf{s}$ within a unit solid angle [10]. The governing time-dependent differential equation for the radiance is called transport equation and is given by:

$$\frac{n}{c}\frac{\partial J(\mathbf{r},\mathbf{s})}{\partial t} = -\nabla \cdot J(\mathbf{r},\mathbf{s}) - \mu_t J(\mathbf{r},\mathbf{s}) + \frac{\mu_t}{4\pi}\int_{4\pi} p(\mathbf{s},\mathbf{s}')J(\mathbf{r},\mathbf{s}')d\omega' + \varepsilon(\mathbf{r},\mathbf{s}) \quad (4.29)$$

where n is the refractive index of the medium, c the speed of light, *p(s, s')* is the phase function of a photon to be scattered from direction *s'* into *s*, ds is an infinitesimal path length and $d\omega'$ is the elementary solid angle about the direction *s'*. The last term $\varepsilon(\mathbf{r}, \mathbf{s})$ represents the power radiated by the medium itself per unit volume and per unit solid angle. If the scattering is symmetric about the direction of the incident wave, the phase function can be set *p(s, s') = p(θ)* with θ being the scattering angle as defined in

Section 4.1.5. However, in experiments the observable quantity is the **Intensity** (measured in W cm^{-2}, which is derived from the radiance by integration over the solid angle:

$$I(\mathbf{r}) = \int_{4\pi} J(\mathbf{r},\mathbf{s}) d\omega \qquad (4.30)$$

On the other hand, the radiance can be expressed in terms of the intensity by:

$$J(\mathbf{r},\mathbf{s}) = I(\mathbf{r})\delta(\omega - \omega_s), \qquad (4.31)$$

where $\delta(\omega - \omega_s)$ is a solid angle delta function pointing into the direction given by s.

When a laser beam is incident on a turbid medium, the radiance inside the medium can be divided into a coherent and a diffuse component according to the following relation: $J = J_c + J_d$

The coherent radiance is reduced by attenuation due to absorption and scattering of the direct beam and can thus be calculated by:

$$\frac{dJ_c}{ds} = -\mu_t J_c \text{ , with solution: } J_c = I_o \delta(\omega - \omega_s) \exp(-d), \qquad (4.32)$$

where I_o is the incident intensity and d is the optical depth defined by: $d = \int_0^s \mu_t ds'$.

The boundary condition on the surface of a turbid medium is that no diffuse radiance enters the turbid medium: $J_d(\mathbf{s}) = 0$, when s is pointing inward.

The main problem that the transport theory has to solve is the evaluation of the diffused radiance, since scattered photons do not follow a determined path. Therefore, adequate approximations and statistical approaches for the solution must be chosen, depending on whether absorption or scattering is the dominant process of attenuation. Some of these approaches are **First-Order Scattering** for $J_c \gg J_d$ and **Kubelka-Munk Theory** for $J_c \ll J_d$ (analytically) or **Monte Carlo Simulation** (numerically). However, the most general applicable approach for scattering dominating over absorption is the **Diffusion Approximation** described in the following section.

4.2.2 Diffusion approximation

As shown in the previous section when a laser beam enters a medium, the radiance can be expressed as a sum of a coherent and a diffuse component. If the medium is mostly scattering, the diffuse radiance tends to be almost isotropic and the

diffuse radiance has a broad angular spread. Therefore, the diffuse radiance can be expended in a series of spherical harmonics. The two first terms of the expansion constitute the diffusion approximation:

$$J_d = \sum_{n=0}^{\infty} J_n = \frac{1}{4\pi} \left(I_d + 3\mathbf{F}_d \cdot \mathbf{s} + ... \right) \tag{4.33}$$

where I_d is the diffuse intensity and $\mathbf{F}_d$ is the vector flux determined by:

$$\mathbf{F}_d(\mathbf{r}) = \int_{4\pi} J_d(\mathbf{r},\mathbf{s}) \cdot \mathbf{s} d\omega \tag{4.34}$$

The diffuse intensity then satisfies the following diffusion equation:

$$\frac{n}{c} \frac{\partial I_d(\mathbf{r})}{\partial t} - D\nabla^2 I_d(\mathbf{r}) + \mu_a I_d(\mathbf{r}) = S(\mathbf{r}) \tag{4.35}$$

where n is the refractive index of the medium, c the speed of light, S($\mathbf{r}$) is the photon source and D is the diffusion coefficient defined by:

$$D = \frac{1}{3\left[\mu_a + (1-g)\mu_s \right]} \tag{4.36}$$

The diffusion of light inside a turbid medium can be described by an effective attenuation coefficient μ_{eff} given by:

$$l_{eff}^{-1} = \mu_{eff} = \sqrt{3\mu_a \left(\mu_a + \mu_s (1-g) \right)} \tag{4.37}$$

and thus the diffusion approximation states that:

$$I = I_c + I_d = A\exp(-\mu_t z) + B\exp(-\mu_{eff} z), \text{ where } A + B = I_o. \tag{4.38}$$

When an optical beam enters a turbid medium, the first-order scattering is dominant near the surface and as the observation point moves into the medium second-order and higher-order scattering increases. The diffusion solution is an approximation representing the limiting case where the multiple scattering is dominant. It is therefore clear that near the surface (or for very thin media) the diffusion solution may not be applicable.

4.2.3 Time-resolved transmission

When a short light pulse is propagating through a turbid medium it will suffer multiple scattering events. This will cause both the temporal and spatial point spread

functions to broaden. In figure 4.7 a schematic representation of the transmission of a short (picosecond) laser pulse through a highly scattering medium (tissue section) is shown. The transmitted pulse is expanded in the nanosecond regime after multiple scattering events. This temporal spreading of the short light pulse is very valuable since it contains information about the optical properties of the medium and is key to this problem. The solution will provide the optical properties of the medium (e.g. biological tissue) and thus the possibility to optically characterize different media. This problem has been addressed by many research groups, however in the followings the approach proposed by Patterson et al. will be described since this is the model that was used also during the experiments [11].
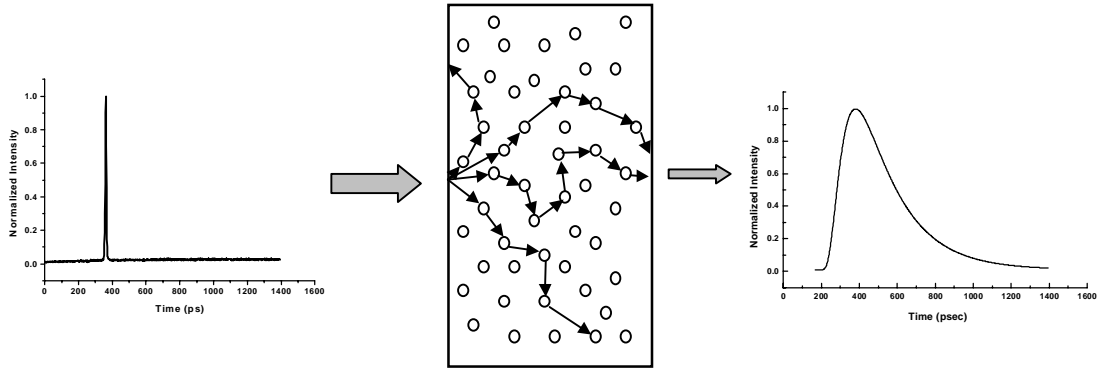

Fig 4.7*: Schematic illustration of the diffuse propagation of a short light pulse through a thick turbid medium (e.g. tissue section). A narrow beam of short light pulses is incident and is temporally and spatially dispersed as well as strongly attenuated after the transmission, because of the multiple scattering events.*

The geometry of the addressed problem is illustrated in figure 4.8. A narrow collimated pulsed light beam is normally incident on a finite homogeneous tissue slab. As shown in the previous section the diffuse intensity satisfies the time-dependent diffusion equation.

$$\frac{n}{c}\frac{\partial I_d(\mathbf{r},t)}{\partial t} - D\nabla^2 I_d(\mathbf{r},t) + \mu_a I_d(\mathbf{r},t) = S(\mathbf{r},t) \qquad (4.39)$$

The fluence rate can be accurately calculated if $\mu_a \ll (1\text{-}g)\mu_s$ and if the point of interest is far from sources or boundaries. The first is well applied for soft tissue in the spectral range between 650-1300 nm. For a short pulse from an isotropic source (laser pulse) $S(r, t) = \delta(0, 0)$ and for the geometry of figure 4.8 it can be shown that the solution of Eq. 4.39 is:

$$I_d(r,t) = c(4\pi Dct)^{-3/2} e^{-\frac{r^2}{4Dct} - \mu_\alpha ct}$$

(4.40)

We can use the corresponding Green's function to solve the problem by making two assumptions. First that all the incident photons are initially scattered at a depth:

$$z_0 = [(1-g)\mu_s]^{-1}$$

(4.41)

so that the actual source term becomes the simple delta function described above. The second assumption is that the diffused intensity must be zero at the boundary of the tissue:

$I_d(r,0,t) = 0$ and $I_d(r,d,t) = 0$

In order to satisfy these boundary conditions an infinite number of dipole photon sources (positive-negative sources) is introduced in the tissue slab (as shown in figure 4.8).

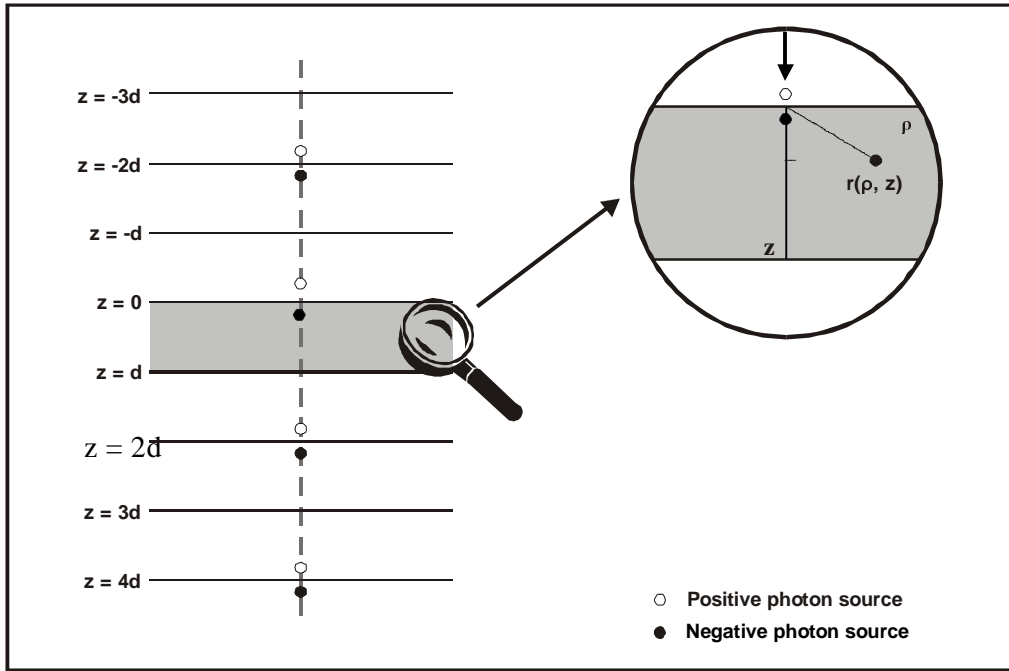**Fig. 4.8**: *Geometry for the calculation of the time resolved diffused reflectance and transmittance from a homogeneous finite slab of width d.*

The diffused transmittance can be calculated from **Fick's law** for a distance d as:

$$J(\rho,d,t) = -D\nabla I_d(\rho,z,t)\big|_{z=d} \text{ and } T(\rho,d,t) = |J(\rho,d,t)|$$

(4.42)

If only four of the dipoles are retained then the transmittance is given by:

48

$$T(\rho,d,t) = (4\pi Dc)^{-3/2} t^{-5/2} e^{-\mu_\alpha ct} e^{-\frac{\rho^2}{4Dct}}$$

$$\times \left\{ (d-z_0)e^{-\frac{(d-z_0)^2}{4Dct}} - (d+z_0)e^{-\frac{(d+z_0)^2}{4Dct}} + (3d-z_0)e^{-\frac{(3d-z_0)^2}{4Dct}} - (3d+z_0)e^{-\frac{(3d+z_0)^2}{4Dct}} \right\}$$

The spatially integrated transmittance is then calculated as:

$$T(d,t) = (4\pi Dc)^{-1/2} t^{-3/2} e^{-\mu_\alpha ct}$$

$$\times \left\{ (d-z_0)e^{-\frac{(d-z_0)^2}{4Dct}} - (d+z_0)e^{-\frac{(d+z_0)^2}{4Dct}} + (3d-z_0)e^{-\frac{(3d-z_0)^2}{4Dct}} - (3d+z_0)e^{-\frac{(3d+z_0)^2}{4Dct}} \right\}$$

This formula, which we shall address as **Patterson's equation**, was used for the fitting of the experimental transmission curves and for the calculation of the optical properties (μ_a and μ_s') of different types of excised female breast tissue, as will be described in detail in Chapter 6.1. The shape of the temporal distribution resulting from the Patterson's formula can be seen in figure 4.7 in the plot of the transmitted light.

4.3 Light scattering with gain

In the previous paragraphs a brief description of the interactions involving light and matter has been given. The processes of absorption, spontaneous and stimulated emission and light scattering have been reviewed. However, one of the most interesting theoretical problems in physics still remains the combination of intense scattering and gain (i.e. light amplification due to stimulated emission) and lasing inside random amplifying media. In the followings, a review of the theory proposed to explain the characteristics of such radiation will be presented from the first theoretical prediction of the phenomenon to the latest developments to date.

4.3.1 Theory of random lasers

The first theoretical prediction of the emission of light from random amplifying media was made in 1968 by Letokhov who converted the diffusion equation 4.39 by

adding a **negative absorption** term Q_ω [12]. This term accounted for the amplification of light inside the scattering gain medium consisting of N_o dielectric particles. The approach was made for the case when the photon wavelength is smaller than the scattering mean free path, which in turn is much smaller than the dimension of the scattering region, that is for a highly random medium: $\lambda \ll l_s \ll R$. The equation describing the emission from such media becomes:

$$\frac{n}{c}\frac{\partial \Phi_\omega(\mathbf{r},t)}{\partial t} = -D\nabla^2\Phi_\omega(\mathbf{r},t) + Q_\omega(\mathbf{r},t)N_o\Phi_\omega(\mathbf{r},t) \qquad (4.43)$$

From this equation he was able to predict the threshold condition, the emission spectrum and the number of modes consisting the emitted light: $N \simeq \Omega_g / (\lambda/2R)^2$, where Ω_g is the generation solid angle and R the radius of the generation region.

The next approach was made simultaneously by John et al. and by Wiersma et al. in 1996, which both tried to couple the diffusion equation proposed by Letokhov with the rate equations describing a lasing material [13, 14]. They proposed that when strong multiple scattering occurs the scattered photons may return to the amplification region, thus performing closed loop paths and the amplified mode itself may consist of a multiple scattering path. This scenario of the formation of micro-cavities strongly resembles the amplification after several passes inside a laser cavity (hence the name mirror-less lasing). At the threshold for photon localization ($l_s \ll \lambda$) [15], the diffusion modes of light interfere strongly and are converted into a continuous spectrum of localized cavity modes in the extended medium, in which the emitted light may self-organize into a coherent state. However, by using this approach it is not possible to describe the discrete lasing modes observed in recent experiments [16].

This was made possible with the work of Soukoulis et al. and Sebbah et al. who coupled the Maxwell's equations with the rate equations of electron population within a semi-classical theory [17, 18]. Both groups use the well-established finite-difference time-domain method to calculate the wave propagation in random media with gain. The work of Soukoulis et al. concerns a one-dimensional simplification of the real experiments, which consists of many dielectric layers of real dielectric constant of fixed thickness, sandwiched between two surfaces, with the spacing between the layers filled with gain media. The distance between the neighboring dielectric layers

is assumed to be a random variable. This model described the field pattern and spectra of localized lasing modes inside the system.

A more developed model is the model of Sebbah et al. [18], which describes a two-dimensional disordered medium of size L^2 made of circular scatterers with radius *r*, optical index n_2 and surface filling fraction *Φ*, embedded in a matrix of index n_1. The matrix is chosen as the active part of the medium, in order to control the randomness and the gain independently. Furthermore, they introduce gain to the system by including to the Maxwell's equations a polarization term due to atomic population inversion. This model has predicted that the lasing modes are the same with the eigenmodes of the passive (without gain) disordered system.

However, the behavior of random active media (random lasers) has yet to be fully understood and described with a complete theoretical model and the research effort in this direction is continuous [19].

4.3.2 One- and two- photon excitation

On this basis and in the contents of this thesis an attempt was made to describe the excitation models used during the experiments. These excitation schemes can be seen in figures 4.9 and 4.10 for one- and two-photon excitation respectively. The gain medium (i.e. the lasing organic dye) is modeled with a typical four level laser system. The ground state (g) is pumped via one- or two-photon excitation onto the excited state (2), which immediately populates state (1). The laser transition takes place from state (1) to state (0), which in turn decays rapidly into the ground state. Assuming that states (2) and (0) are practically unpopulated a single population rate equation is adequate for describing the system.
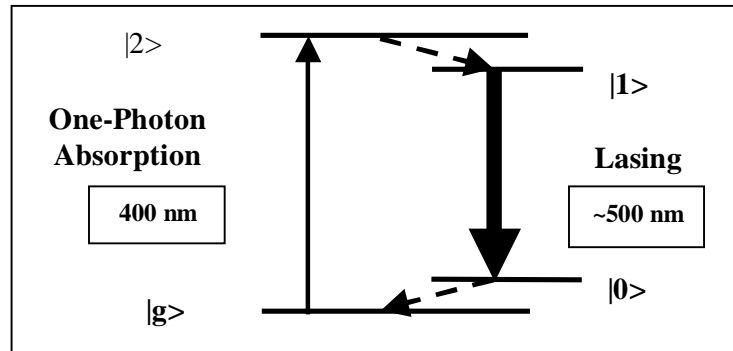

Fig 4.9*: One-photon excitation scheme of the gain medium (organic dye) used for the random lasing.*

The coupled differential equations describing the behavior of the system in space and time are formed by two diffusion equations for the pump and emitted light (W_P and W_E are the corresponding energy densities) and the rate equation for the concentration N_1 of molecules in the lasing state (1):

$$\dot{W}_P = D\nabla^2 W_P - \sigma_{abs}c\left[N_t - N_1\right]W_P + \frac{1}{l}I_P \tag{4.44}$$

$$\dot{W}_E = D\nabla^2 W_E + \sigma_{em}cN_1W_E + \frac{1}{\tau_e}N_1 \tag{4.45}$$

$$\dot{N}_1 = \sigma_{abs}c\left[N_t - N_1\right]W_P - \sigma_{em}cN_1W_E - \frac{1}{\tau_e}N_1 \tag{4.46}$$

where c is the velocity of light inside the medium, l is the transport mean free path, σ_{abs} and σ_{em} are the absorption and emission cross sections respectively, τ_e is the life time of the excited state (1) and N_T is the total concentration of dye molecules. D is the diffusion constant and I_P is the pump pulse intensity.

The modified scheme for the two-photon excitation is given below, where the difference is the non-linear absorption cross section for the two-photon interaction $\sigma_{abs}^{(2)}$. In addition in this case the dependence of the emitted intensity is expected to be quadratic to I_P [20].
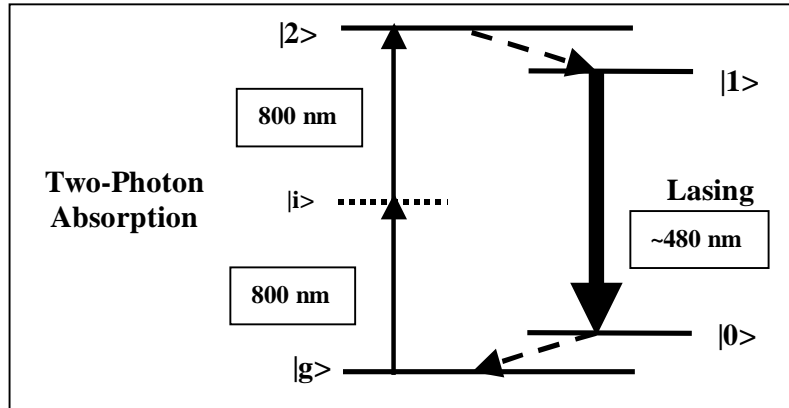

Fig 4.9: *Two-photon excitation scheme of the gain medium (organic dye) used for the random lasing.*

$$\dot{W}_P = D\nabla^2 W_P - \sigma_{abs}^{(2)}c\left[N_T - N_1\right]W_P{}^2 + \frac{1}{l}I_P \tag{4.47}$$

$$\dot{W}_E = D\nabla^2 W_E + \sigma_{em}cN_1W_E + \frac{1}{\tau_e}N_1 \tag{4.48}$$

$$\dot{N}_1 = \sigma_{abs}{}^{(2)} c \left[N_T - N_1 \right] W_P^2 - \sigma_{em} c N_1 W_E - \frac{1}{\tau_e} N_1 \qquad (4.49)$$

The numerical solution of the above set of equations will give all relevant information on the spatial and temporal distribution of the energy densities of the pump light and the amplified spontaneous emission as well as of the gain coefficient of the lasing medium $\kappa_g = \sigma_{em} N_1$.

4.4 Photon statistics

In this paragraph a description of the statistics of the photons emitted from a light source owed to the quantum nature of light will be given. Since photons are bosons they can occupy the same quantum state. However, from the uncertainty relation of quantum mechanics it results that they should follow a certain statistical behavior. These statistics can be measured by performing single photon counting experiments, in order to obtain the average photon number $\langle n \rangle$ on a time interval Δt, which is smaller than the coherence time T_c of the light field: $\Delta t < T_c$. From these measurements the probability $P(n)$ of n photons to be detected over this time interval Δt can be calculated [21,22]. This probability can be directly related to the coherent properties of the light source and can be used to distinguish between coherent and incoherent light. Coherent (i.e. laser) light shows Poissonian distribution whereas incoherent (i.e. thermal) light shows Bose-Einstein distribution, both given in equations 4.50. The two ensembles are depicted in figure 4.10 for an average number of photons $\langle n \rangle$ =5. In the same figure the linear combination of the two distributions (Eq. 4.51) is shown as well, for the same average photon number. The linear combination was proposed to characterize the statistics of a partially coherent light source. Such light sources could be considered to be the random lasers where the light is emitted from a highly scattering environment, which can affect in a great extent the coherent properties of the otherwise coherent emission of the micro-cavities [23,24].

Poisson   Bose-Einstein

$$P(n) = \langle n \rangle^n \, e^{-\langle n \rangle} / n! \qquad\qquad P(n) = \langle n \rangle^n / \left[1 + \langle n \rangle \right]^{n+1} \qquad (4.50)$$

Linear combination

$$P(n) = m \frac{\langle n \rangle^n e^{-\langle n \rangle}}{n!} + (1-m) \frac{\langle n \rangle^n}{\left[1 + \langle n \rangle \right]^{n+1}} \qquad (4.51)$$
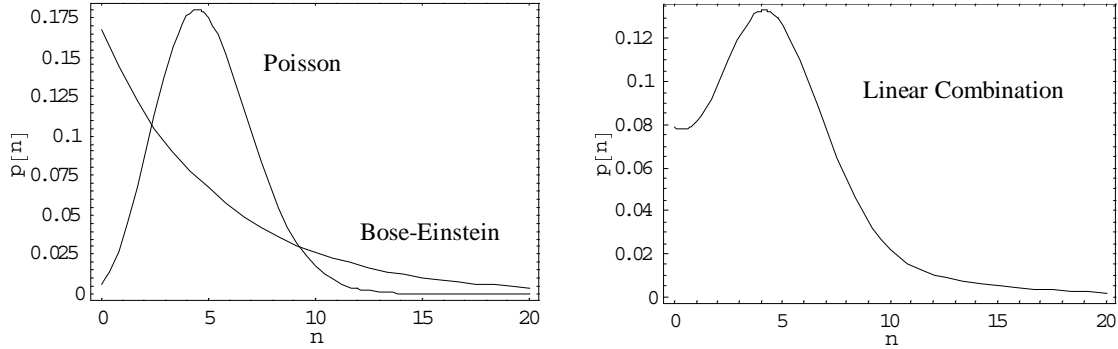

Fig. 4.10*: Probability P(n) of finding n photons per time unit for $\langle n \rangle$ =5. Both Poissonian and Bose-Einstein distributions are shown as well as their linear combination describing a partially coherent light source.*

In figure 4.11 the statistical distribution of photons for a laser and a thermal source are depicted. The counting statistics of the coherent laser light are the same as those found for the arrival of raindrops in a steady downpour whereas the statistics of the thermal source have no correlation whatsoever.
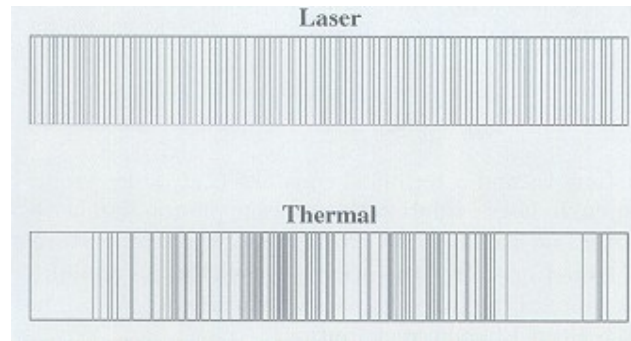
Fig 4.11*:Statistical distribution of photons from a laser and a thermal source for $\langle n \rangle$ =20 [2]*

However, it should be noted that these considerations are valid only for $\Delta t < T_c$. If the time interval of detection is increased then the statistics of the chaotic light approach those of the coherent light. Consequently, special care must be paid when arranging the detection setup to ensure that this condition is fulfilled. The details as well as the code used for the measurement and calculation of the count distributions will be given in section 5.8.

References

1. J. D. Jackson, *"Classical Electrodynamics"*, Third Edition, John Wiley & Sons, New York (1998)

2. R. Menzel, *"Photonics: Linear and Nonlinear interactions of Laser light and matter"*, Springer-Verlag, Berlin (2001)

3. M. H. Niemz, *"Laser-Tissue Interactions: Fundamentals and Applications"*, Springer-Verlag, Berlin (1996)

4. J. T. Verdeyen, *"Laser Electronics"*, Third Edition, Prentice Hall, New Jersey (2000)

5. G. van Soest, *"Experiments on random lasers"*, PhD Thesis, Amsterdam (2001)

6. H. C. van de Hulst, *"Light scattering by small particles"*, Dover Publications Inc., New York (1981)

7. H. Ramachandran, *Curr. Sci.* **76**, 1334 (1999)

8. A. Ishimaru, *"Wave Propagation and Scattering in Random Media"*, Academic Press, Vol. I, New York (1978)

9. A. Ishimaru, *Appl. Opt.* **28**, 2210 (1989)

10. J. Ripoll-Lorenzo, *"Light diffusion in turbid media with biomedical application"*, PhD Thesis, Madrid (2000)

11. M. S. Patterson, B. Chance and B. C. Wilson, *Appl. Opt.* **28**, 2331 (1989)

12. V. S. Letokhov, *Sov. Phys. JEPT* **26**, 835 (1968)

13. S. John, G. Pang, *Phys. Rev.* **A54**, 3642 (1996)

14. D. S. Wiersma, A. Lagendijk, *Phys. Rev.* **E54**, 4256 (1996)

15. P. W. Anderson, *Philos. Magaz.* **B52**, 505 (1985)

16. H. Cao, Y. G. Zhao, S. T. Ho, E. W. Seelig, Q. H. Wang and R. P. H. Chang, *Phys. Rev. Lett.* **82**, 2278 (1999)

17. X. Jiang, C. M. Soukoulis, *Phys. Rev. Lett.* **85**, 70 (2000)

18. C. Vanneste and P. Sebbah, *Phys. Rev. Lett.* **87**, 183903 (2001)

19. A. L. Burin, M. A. Ratner, H. Cao and R. P. H. Chang, *Phys. Rev. Lett.* **87**, 215503 (2001)

20. G. Zacharakis, N. A. Papadogiannis, A. B. Pravdin, S. P. Chernova, V. V. Tuchin and T. G. Papazoglou, subm. to Phys. Rev. A

21. R. Loudon, *"The quantum theory of light"*, Second edition, Oxford Science Publishing, Oxford University Press, Oxford (1983)

22. C. W. J. Beenaker, *Phys. Rev. Lett.* **81**, 1829 (1998)

23. G. Zacharakis, N. A. Papadogiannis, G. Filippidis and T. G. Papazoglou, *Opt. Lett.* **25**, 923 (2000)

24. H. Cao, Y. Ling, J. Y. Xu, C. Q. Cao and P. Kumar, *Phys. Rev. Lett.* **86**, 4524 (2001)

5. Experimental

*In the followings the experimental arrangements, which were used during this thesis will be described. A detailed analysis of the sources of the ultra-short (femtosecond) pulses as well as the detecting device will be given, in an effort to give the potential experimentalist all the information needed to repeat the experiments based on the text of this chapter. In **Section 5.1** the detection system used during the experiments (Streak Camera), is described. **Section 5.2** will give the details of the different laser systems used in the different experiments. **Sections 5.3** and **5.4** describe the spectral calibration of the apparatus and the sample preparation procedures respectively. **Sections 5.5** through **5.8** present the details of the different experiments, as they will be described analytically in the next chapters.*

5.1 Streak Camera
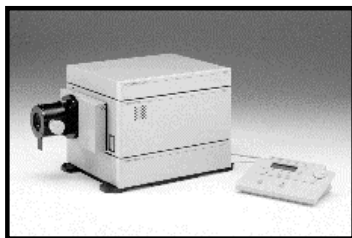
The C5680 Streak Camera

The detection system used during the measurements consisted of a Hamamatsu C5680 Streak Camera with a superb temporal resolution of 2 ps and a high sensitivity CCD camera. A streak camera is quite different from the video and still cameras, which take the pictures using ordinary film. The streak camera is a device that measures ultra-fast light phenomena and delivers 3-dimensionl images of the light intensity vs. time vs. position. It's name dates back to the early days of the high speed rotating drum cameras. These cameras would streak reflected light onto a film. No other instruments that directly detect ultra-fast light phenomena have better temporal resolution than the

streak camera. Since it is a two dimensional device, it can be used to detect several tens of different light channels simultaneously. For example when used together with a spectrograph, time variations of the incident light intensity with respect to wavelength can be measured (time resolved spectroscopy). Used in combination with proper optics, it is possible to measure time variation of the incident light with respect to position (time and space-resolved measurements).

5.1.1 Operating principle

In Figure 5.1 the operating principle is shown. The light passes through a slit and is imaged by the input optics on the photocathode of the streak tube. Lets assume that four optical pulses which vary slightly in terms of both time and space and which have different optical intensities, are input through the slit and arrive at the photocathode. The incident photons on the photocathode are converted into a number of electrons proportional to the intensity of the light. The ratio between the number of incident photons and the number of photoelectrons generated defines the quantum efficiency of the photocathode. Then the four electron pulses pass through a pair of accelerating electrodes, where a high voltage is applied to them at a timing synchronized to the incident light (figure 5.2). Since this voltage is time dependent it initiates a high-speed sweep (the electrons are swept from top to bottom). During the high-speed sweep, the electrons, which arrive at slightly different times, are deflected in slightly different angles in the vertical direction and enter the Micro-Channel Plate (MCP[*]).

As the electrons pass the MCP, they are multiplied several thousands of times, enabling ultra-high sensitivity with single photoelectron detection in the photon counting mode. After the MCP the electrons impact against a phosphor screen, where they are converted again into photons. On the phosphor screen, the image corresponding to the optical pulse, which was the earliest to arrive is placed in the uppermost position, with the others being arranged in sequential order from top to bottom. In other words the vertical direction serves as the time axis. The brightness of the various phosphor images is proportional to the intensity of the respective incident

---

[*] The MCP is an electron multiplier consisting of many thin glass capillaries (channels) with internal diameters ranging from 10 to 20 μm, bundled together to form a disk-shaped plate with a thickness of 0.5 to 1 mm. The internal walls of each individual channel are coated with a secondary electron emitting material, so that as the electrons come flying through the channels, they bump against the walls and the repeated impact causes them to multiply in number. A single electron can be multiplied into as many as 10^4 times.

light pulse. The position in horizontal direction corresponds to the horizontal location of the incident light. The spectral transmittance characteristics covered the range from 200 to 850 nm, with a wide dynamic range up to 1:1000, defined as the ratio between the strongest and the weakest measured pulse.

Fig.5.1*: Operating principle of the Streak Tube*
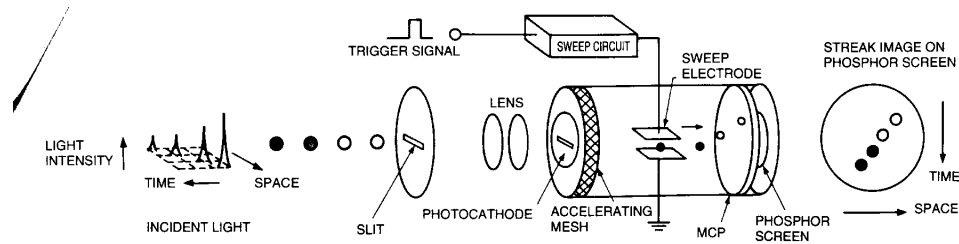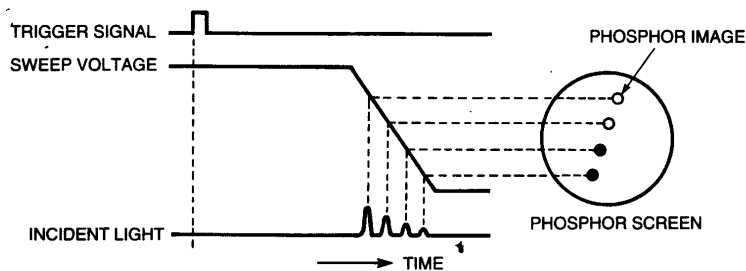

Fig.5.2*: Operation timing at the time of the sweep*
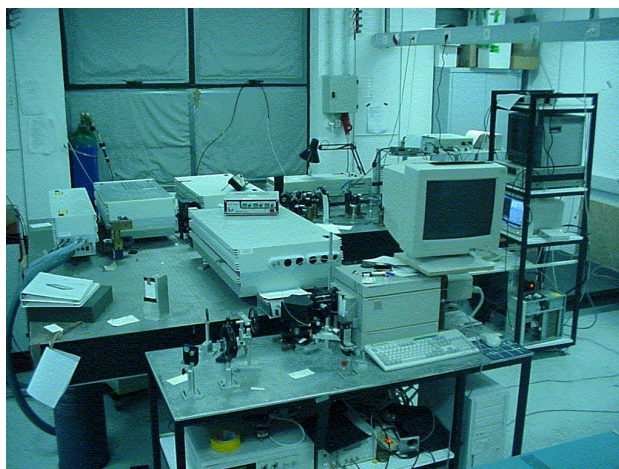
5.1.2 System Configuration

Fig. 5.3*: A picture of the experimental setup showing the streak camera and the regenerative amplifier laser system.*

The streak camera system together with the femtosecond Ti:Sapphire based regenerative amplifier laser system can be seen in figure 5.3. A schematic

representation of the system configuration can be found in figure 5.4. The discrete parts will be described in detail in the following paragraphs. These comprise of the temporal synchronization component, the sweep voltage control and the readout system.
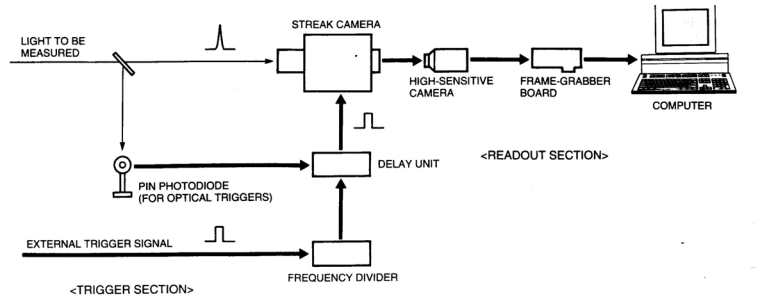

Fig. 5.4: *Basic System Configuration of Streak Camera*

Trigger unit

The trigger unit controls the timing of the streak sweep. It has to be adjusted so that the streak sweep is initiated when the measured light arrives at the streak camera. For this purpose a delay unit and a frequency divider are used. The first controls how long the trigger signal is delayed and the latter can be used when the repetition frequency of the external trigger is too high. In cases where a suitable trigger signal cannot be produced from the laser, it can be produced from a small portion of the measured light pulse with the use of a PIN photodiode. The advantage of the optical trigger compared to the electronic one is that it eliminates the laser jitter when it is too high in cases where for example an excimer laser is used. A serious drawback, which arises from the operating principle of the streak camera, is the relatively long internal delay time (70 ns), which is required for the electronics to be operational. This imposes the construction of an optical delay where the light is traveling an equivalent distance to compensate for this delay time.

During the experiments two different trigger units were used. For single shot operation with low repetition rate the C1097-01 trigger unit was used enabling delay times from 30 ps to 31.96 ns. However, the optical delay line could not be avoided. For synchroscan operation the same delay unit was used, but since the streak camera was synchronized with the mode-lock clock frequency the delay line was not needed. In the cases where the regenerative amplifier (described below) was used, both the kilohertz (from the **delay1** output of the Meddox drive of the Pockels cell) and the mode-locked (obtained optically using the fast Hamamatsu PIN photodiode) signals

were combined in the C4792-01 delay unit. This produced the appropriate streak trigger signal with the proper negative delay, making the optical delay not necessary. This was accomplished by locking the kilohertz pulse (1 ms period) on a mode locked pulse (12 ns period) and by generating a trigger pulse with negative delay time -70 ns. The delay times achieved with this trigger unit ranges from 100 ps to 999 ns.

5.1.3 Sweep voltages

Depending on the repetition frequency of the phenomenon that is under investigation different sweep voltages are applied to the deflection plates using two different plug-ins.
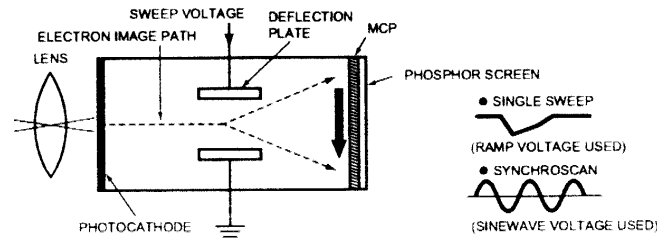

Fig.5.5: *Sweep voltages for Single sweep and Synchroscan units*

Synchroscan Unit (M5675)

When the high repetition rate mode-locked Ti:Sapphire laser was used, it was combined with the Synchroscan unit (Hamamatsu M5675), which is manufactured to be synchronized with the mode locking 82 MHz frequency of the laser. The voltage, which is applied by this unit, is a sinusoidal function. For the deflection of the electrons only the part that can be considered to be linear (half the magnitude between two adjacent maxima of the sine wave accomplishes 99% linearity) was used. This unit could operate in four different sweep speeds covering temporal ranges from 200 ps to 2 ns and the temporal resolution that can be accomplished was ≤ 2 ps.

Single-sweep unit (M5676)

For repetition rates from single-shot up to 10 KHz depending on the trigger signal the single sweep unit (Hamamatsu M5676) was used. The applied voltage in this case was a saw tooth function creating a ramp synchronized with the trigger signal from the photodiode. This plug-in covered a temporal range from 200 ps to 50 ns and the accomplished temporal resolution was 2 ps. To avoid the return sweep of

the voltage, which creates an opposite temporal behavior, a blanking unit was used. This unit imposes a horizontal sweep during the return sweep and sends the electrons out of the phosphor screen.

5.1.4 Readout system

The readout system employs a high sensitivity Hamamatsu C4880 CCD camera that detects the images of the phosphor screen and a computer equipped with a frame grabber board. The recording and the analysis of the streak images were performed using special software for digital temporal analysis. This had the ability to record images with 24-bit color information (using pseudo-colors) and simultaneously give values for the intensity in time and space domains of every image pixel. A characteristic streak image is shown in Figure 5.6. The detectable wavelength range covered the regime from 200 to 1100 nm. For better image quality the background, accounting for the electronic noise (dark current), the leaks from the optics or the temperature of the photocathode, was subtracted after the acquisition of each image, keeping all the settings the same. Additionally to the background subtraction, the camera offers correction for the shading and for the curvature of the images, which are inherent problems of the CCD and streak camera operation respectively. The CCD chip is cooled by a thermoelectric device employing a Peltier cooler, which enables temperatures down to –50 ^{o}C, thus reducing the dark current and achieving better signal to noise (S/N) ratios. Thus, a high dynamic range better than 1:5000 can be achieved. It is defined as the ratio of the CCD saturation charge volume to the readout noise In addition, very weak signals can be detected by increasing the acquisition time or by performing single photon counting.
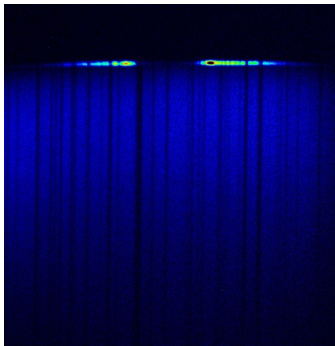

Fig. 5.6: *Characteristic image recorded with the streak camera*

5.1.5 Photon counting mode

The photoelectrons emitted from the photocathode of the streak tube are multiplied at a high integration rate by the MCP. One photoelectron is accounted as one intensity point on the phosphor screen. This photoelectron image is read out by the CCD camera, which is coupled to the streak tube and then undergoes A/D conversion. Because of the exceptionally low noise level of the CCD, the photoelectron image can be clearly separated from the noise by setting a threshold level. This is done by obtaining an intensity histogram with closed shutter and thus recording only the electronic noise. The threshold is set to be the intensity value, which is not exceeded by any pixel. Positions in the photoelectron image, which are above the threshold value are detected and are integrated in the memory, enabling noise to be eliminated completely. By performing photon counting measurements the photon statistics of the observed light can be calculated and thus its coherent properties can be investigated.
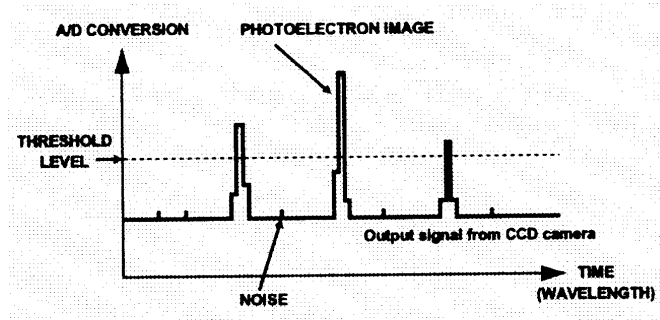
Fig. 5.7: *Setting the threshold level for photon counting*

5.1.6 High Performance Digital Temporal Analyzer (HPD-TA)

The HPD-TA is a high performance digital image processing system for reading out from the phosphor screen of the streak camera. It enables precise acquisition and quantitative analysis of two-dimensional streak data, including a full range of data correction (shading, background, curvature) and calibration functions. It provides also remote control of the streak camera functions via GPIB interface. The acquisition time, the number of integrated images, the MCP gain, the photon counting threshold can be controlled with the software. During the measurements the acquisition time varied between 200 ms and 2 s and the MCP Gain from 0 to 63. In Figure 5.8 the

HPD-TA program as it appears on the screen of the computer when it is operating, is shown.
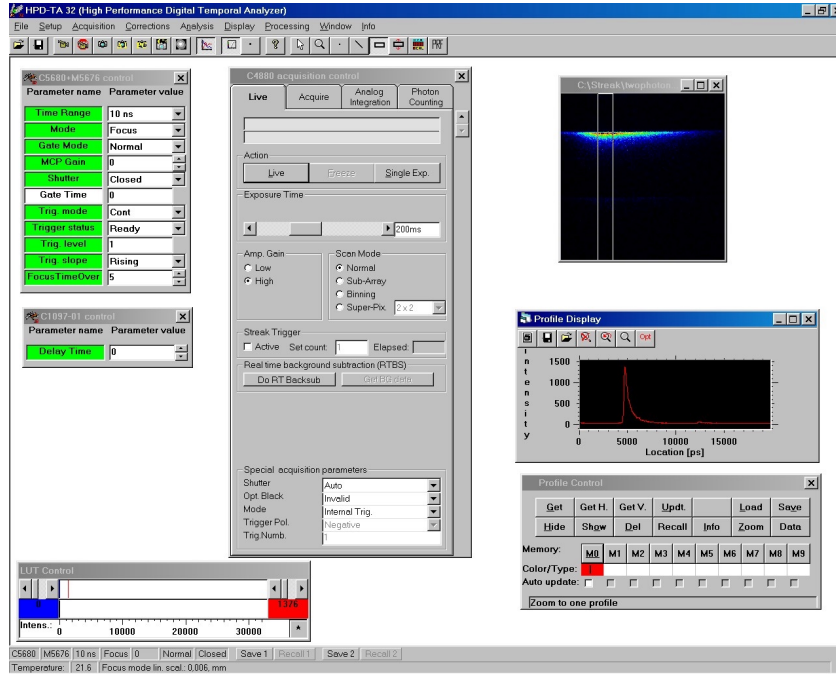
Fig. 5.8*: The HPD-TA software of the operation of the streak camera*

5.2 Laser systems

5.2.1 Mode-locked Ti:Sapphire Oscillator

The tissue optical characterization measurements were performed using a mode-locked Ti:Sapphire laser emitting 200 fs pulses at 800 nm. This laser was pumped by a Spectra Physics Ar^+ laser (or the second harmonic of a Spectra Physics diode-pumped Nd:YAG laser) operating with a power of 9 W. The repetition rate of the Ti:Sapphire was 82 MHz with an average power of ≤ 1 W. However, the intensity irradiating the tissue samples was kept bellow the solar constant of 2 mW/cm^2.

5.2.2 Distributed feedback dye laser

The laser system used for the one-photon excitation of the random lasers made by polymer samples consisted of a Lambda Physik distributed feedback dye laser emitting at 496 nm. The output energy was of the order of 10 µJ and the repetition

rate ranging from 1-10 Hz. The duration of the pulses was 500 fs. This laser was pumped by a XeCl excimer laser emitting 25 ns pulses at 308 nm and with output energy of 80 mJ.

5.2.3 Regenerative amplifier

The laser system that was used for the photon statistics experiment and for the two-photon excitation of the random lasers consisted of the following parts. The source of the 200 fsec pulses was a mode-locked Ti:Sapphire laser emitting at 800 nm, pumped by the second harmonic of a Spectra Physics diode-pumped Nd:YAG laser operating with a power of 5 W. The repetition rate of the Ti:Sapphire oscillator was 82 MHz with an average power of ~1 W. The pulses were fed to an amplifying system consisting of a stretcher-compressor setup and an amplifier pumped by the second harmonic of an $Nd:LiYF_4$ pulsed laser. As a result of the Q-switching rate of the regenerative amplifier implemented by the operation of a Pockels cell, the repetition rate of the amplified beam was 1 KHz.

5.3 Spectral calibration

For the simultaneous recording of spectral and temporal information, the spectral analysis was performed using a 0.10 m spectrograph employing a 450 grooves/mm holographic grating mounted in front of the horizontal entrance slit of the streak camera. Wavelength calibration was performed using a commercial mercury lamp. The spectral resolution was of the order of 1 nm defined by the width of the detected mercury spectral lines. The recording of the continuous emission of the mercury lamp was done with the streak camera operating in the focus mode. That is without the sweep voltage being applied to the deflection plates, namely it operated as an image intensifier and thus without the temporal analysis of the incoming signals. A characteristic image of the emission of the mercury lamp is shown in Figure 5.9. The total size of the recorded image window corresponded to a spectral region of about 100 nm. This resulted from the effective width of the photocathode (6 mm) and the dispersion of the grating used in the spectrograph (20 nm/mm).

The delivery of the measured light was utilized with a one-meter long step index multimode optical fiber. The temporal dispersion induced by the optical fiber to the propagating femtosecond pulses was shorter than the temporal evolution of the investigated event. The fiber was placed in front of the sample such that the collection of the light was done in 45° with respect to the normal of the surface of the sample. The irradiation was made normal to the surface. This arrangement eliminated the reflected laser light that could be coupled into the fiber.
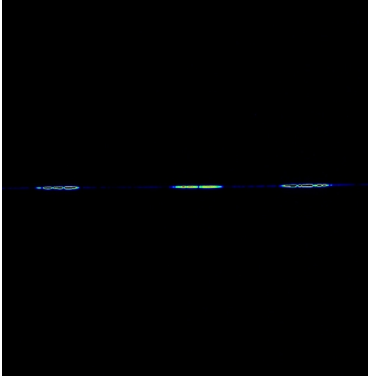

Fig.5.9*: Characteristic image of the mercury lamp, used for the spectral calibration of the readout system*

5.4 Sample preparation

5.4.1 Tissue samples

The tissue samples were excised from female breast during tumor extraction or biopsy operations. The study concerned tissue from twenty cases in total. Twelve of them were macroscopically characterized as fat deposited and eight of them as fibrous. All tissues were obtained half an hour after excision and were returned after the measurement to the Department of Surgical Oncology of the University Hospital for histological analysis. The thickness of the samples varied from 5 to 30 mm and they were placed on a X-Y translation stage in order to take measurement from more than one point on each tissue. The calculation of the optical parameters of the large samples, with thickness more than 5 mm, was made using the well-known Patterson equation, which is derived from the diffusion theory (see Chapter 1). For the biopsy samples with thickness less than 5 mm the calculation of the optical properties is based on the Laguerre expansion of the kernels method. The distance of the backside of the tissue to the front face of the detector was kept constant at 1 cm throughout the

measurements thus, keeping the observation angle constant. This was very important for the correct calculation of the parameters since the detected light would have the same characteristics for all measurements.

5.4.2 Liquid samples

The first attempt to investigate the laser-like behavior of active disordered media was made using liquid samples. They were consisted of solutions of dyes in methanol and suspended scattering microparticles placed inside a 1cm x 1cm x 3cm glass cuvette. The dyes used were Rhodamine101, Rhogamine6G and DCM (Lambda Chrome part numbers LC 6400, LC 5900 and LC 6500 respectively). Samples of different dye ($3x10^{-3}$ M to 10^{-2} M) and scatterer ($2-5x10^{18}$ cm^{-3}) concentrations were prepared. The scattering particles were polystyrene microspheres with concentrations of 3 - $10x10^{10}$ cm^{-3} (393 nm in diameter PL-LATEX Plain White microparticles from Polymer Laboratories). The corresponding absorption (measured in methanol solution) and scattering (calculated as $l_s = 4\pi/n\sigma$) mean free paths were of the order of 1 mm and tens of μm respectively.

5.4.3 Polymer samples

The polymer samples were prepared by mixing Poly-methylmethacrylate (PMMA) (Aldrich) and dye solutions in dichloromethane - CH_2Cl_2, in a 1cm x 1cm x 2cm Teflon cuvette, together with the scattering particles. The scatterers were TiO_2 nanoparticles (~400 nm diameter, ~ 4 kg/l density, R-900 Ti-Pure from E.I. du-Pont de Nemours & Co., Inc.). The PL-LATEX microparticles could not be used in this case since they are dissolved from the dichloromethane. The slow evaporation of the solvent resulted to the creation of the ca. 1 mm thick polymer pellet. The dyes used were Coumarin 307, Coumarin 151, Rhodamine101, Rhodamine6G and DCM (4-Dicyanomethylene-2methyl-6-(p-dimethylaminostyryl)-4H-pyran) (Lambda Chrome part numbers LC 6400, LC 5900 and LC 6500 respectively) depending on the required spectral response. An attempt was done also to investigate the behavior of a system with two different dyes embedded in the same sample. The goal was to asses whether this could lead to dichromatic emission of random laser. Samples of different dye (ranging from $3x10^{-3}$ M to 10^{-2} M) and scatterer (10^{12} - 10^{14} cm^{-3}) concentrations were prepared and irradiated with different excitation energies varying from 0.5 to 30 μJ/pulse by means of a variable density filter. The particles concentration

corresponded to a scattering mean free path of the order of a micrometer. The concentration of the dye corresponded to absorption length of the order of 1 mm (measured in a methanol solution).

5.4.4 Gel samples

The gel samples were made in order to simulate the conditions occurred inside the tissue. Therefore, these tissue phantom models were prepared as highly scattering samples containing Coumarin 307. They were made in the form of 1x1x1 cm gelatin or collagen cubes. First, two stock solutions ($4x10^{-3}$ M and $1.33x10^{-3}$ M) of Coumarin307 in ethanol and a series of stock suspensions of TiO_2 (Du Pont, Ti-Pure R-900, average particle diameter 400 nm) in water, containing from 1-40 mg/ml, were prepared. To obtain the gel base of the sample, 0.45 ml of appropriate stock suspension was added to 0.1 g of gelatin (Sigma G-2500), the suspension having been treated in an ultrasound bath for about 30 min. Then the mixture was melted in a water bath at 50-60 ^{o}C under intense stirring. 0.45 ml of appropriate Coumarin solution was added during stirring just before casting the mixture into a Teflon mold. After 15 min hardening in the refrigerator the sample was removed from the mold. To prevent drying before and between measurements, samples were kept in a water-ethanol vapor chamber in the refrigerator. The use of high repetition rate pumping results in the rather fast deterioration of the samples. Consequently all our measurements were based on 3 seconds long acquisition (3000 pulses). Initial measurements indicate that the lowering of the laser repetition rate improves the lifetime of the samples.

5.5 Calculation of optical parameters

Different kinds of tissue are being optically characterized using the transmitted part of the diffused photons. Since this part of the propagating pulse was more affected by the extensive scattering, the photon path inside the tissue was longer. Therefore, the provided information is statistically better than the corresponding to early arriving photons. The diffused part of the temporal distribution was described very accurately by the analytical expression used for the calculation derived from

diffusion theory. The variability of the calculated optical parameters of one type of tissue among different tissue samples was very small.

5.5.1 Patterson's equation

Temporal profiles were obtained in order to extract the temporal information. Intensity versus time graphs could then be constructed. The optical parameters (absorption and reduced scattering coefficients) of the samples were calculated by fitting the diffusion curves with the Patterson analytical expression (derived from the diffusion theory), modified to fit the data from the streak camera:

The fixed parameters of the equation were the thickness of the sample (d), the time corresponding to the position of the maximum of the reference pulse (t_o) and the speed of light (c). The output of the calculation was the absorption and the inverse reduced scattering coefficient (μ_a and $1/\mu_s'$ respectively). Since the scattering coefficient cannot be calculated independently of the anisotropy factor g, the transport mean free path ($1/\mu_s'$) was used for the characterization of each type of tissue.

5.5.2 Laguerre expansion of kernels

However, for the small biopsy samples it is apparent that due to their limited thickness the spreading of the transmitted pulse is limited and this set of measurements cannot be treated by the photon diffusion approximation by simply fitting the data to one of the closed form solutions. Each set of incident and transmitted laser pulse was de-convoluted using the Laguerre expansion technique and the characteristic kernels as well the coefficients of the expansion were recorded for each sample and compared with the histological analysis.

The Laguerre expansion technique was introduced in order to best describe nonlinear physiological systems stimulated with broad band random inputs. However, this technique can be used to study systems with either random or deterministic inputs as described in Chapter 2.

5.6 Random lasing after one- and two-photon excitation

The study of the highly scattering gain media was performed using different laser systems depending on the excitation scheme. The behavior of these systems was

investigated after one- and two-photon excitation. The goal of the experiments was the extensive study of the dependence of the spectral and temporal characteristics of the fluophore emission on different parameters (different dyes and host matrix, excitation energy, concentration of scatterers).

One-photon excitation was performed using either the distributed feedback dye laser or the second harmonic (400 nm) of the regenerative amplifier system described in section 5.2. The two-photon excitation was performed using the regenerative amplifier system at 800 nm. The detection system was for all cases the same spectrograph- streak camera setup. The detailed description of the experimental arrangements will be given in chapters 3, 4 and 5.

The use of ultra-short-pulse lasers was imposed by the need for excitation of the fluorescent agents with delta-like functions compared to the emission. In addition, since two-photon excitation was employed, high pumping power was necessary to attain an acceptable rate of two-photon absorption, which had a nonlinear dependence on the laser intensity. In our case a femtosecond pulsed laser, combined with an amplifying setup, was used in delivering the necessary excitation.

5.8 Photon statistics

As described in the previous sections the streak camera could perform photon-counting measurements. This made possible to record photon number distributions and thus experimentally asses the coherent properties of the temporally and spectrally narrowed emission of laser-induced fluorescence of organic dyes hosted inside artificial scattering matrices ("random lasers"). The details of the experimental arrangement will be given in Chapter 4 together with the obtained results.

5.8.1 Photon-count distribution code

The following simple program can be used under the Origin environment for the calculation of the photon count distributions. It is activated by creating a new button in the active worksheet with the "Button Edit" function and by simply copying the code. The calculation is performed on 2D data obtained from the photon count window of the streak camera's software.

```
//METRAEI THN EPANALEIPSH TWN ARITHMWN STON PINAKA
 if (col(No)[1]==0)  //testarei an exei ginei o ypologismos
  {
         type -b "You have done it allready";
         break 1;
  };
b=wks.nrows;
  getnumber -s  (# of rows) b (max # of photons) n (no);
r=%(%h,@#);    //diabazei ton arithmo twn sthlwn
      wks.col1.type=1;
        work -c No;    work -c Times;
  v=$(r)+1;    wks.col$(v).type=4;  //sets col(No) as x-col.
 for (vap=0; vap<=$(n); vap+=1) //loop gia kathe # photoniwn
{
 p=$(vap);
 a=0;    //a = # pou epanalambanetai kathe arithmos fwtoniwn
      for (var=1; var<=$(r); var+=1) //loop stis steiles
    {
     d=$(var);
          for (i=1; i<=$(b); i+=1)  //loop stis grammes
      {   if    (COL($(d))[i]==$(p))
          {a+=1;};
        };
    };
col(No)[$(p)+1]=$(p);  col(Times)[$(p)+1]=$(a);
      // type -a "$(p) $(a)";
};
```

6. Chapters

In the following chapters the experimental results obtained during this thesis are presented, in the form of journal articles. Details about the experimental procedures used to obtain these results are also given. The first two chapters describe the experiments aiming towards optical biopsy of female breast tissue of various sizes and optical properties. On the other hand the last three chapters describe the emission from the highly disordered gain media (random lasers) and their unexpected properties.

Chapter 1

In vitro optical characterization and discrimination of female breast tissue during near infrared fsec laser pulses propagation

Ultra-short infrared laser pulses were transmitted through excised female breast tissue. The resulted signal was recorded by a streak camera with a time resolution of the order of a few picoseconds. Experimental data of the temporal spread of the ultra-short pulse during the transmission through the tissue have been analyzed using the Patterson analytical expression derived from the diffusion theory. This resulted in the calculation of the absorption and reduced scattering coefficients, which are related to the optical characteristics of each type of tissue. The goal of the study was to use the theoretical values of the coefficients to discriminate different kinds of tissue.

Introduction

Optical Tomography has been a subject of extensive study by many research groups. Over the last years the goal has been the replacement of ionizing radiation, such as X-rays, with visible or near infrared (NIR) light. This breakthrough will provide a non - invasive imaging technique using non-ionizing radiation in contrast with the commonly used X-rays. The large penetration depth of NIR photons owed to

the scattering mechanism taking place inside the tissue is the most important reason for using this type of light for imaging purposes. Early-arriving photons of a transmitted ultra-short laser pulse can carry image information while late-arriving photons due to their extensive scattering will bear little information [1-4]. Various time-resolved techniques have been used in order to detect objects hidden in such turbid media. Enhancement of the early part of the propagating pulse via non-linear techniques or time gating imaging has been used in order to discriminate between these photons.

On the other hand the temporal spreading of a short light pulse as it propagates through the scattering medium may also provide further information about the optical coefficients of the medium [5], taking advantage of the extensive scattering. In previous published works measurements have been made both *in vitro* and *in vivo* in human volunteers, both in the temporal and spectral domains [6-12]. The results have been based on the known topography of the sample under investigation, which supported the extrapolation of the properties of the different kinds of tissue consisting the sample. In the literature, measurements of optical coefficients have been made using the entire female breast. The fact that fat tissue scatters more effectively than the potentially pathogenic fibrous has been extrapolated from the geometry of the measurements, knowing the histology of the female breast. However, this is not a conclusion one can rely on since no distinct measurements of specific types of tissue have been reported to date.

This is the subject of this work where, different kinds of tissue are being optically characterized using the transmitted part of the diffused photons. Since this part of the propagating pulse was more affected by the extensive scattering, the photon path inside the tissue was longer. Therefore, the provided information is statistically better than the corresponding to early arriving photons. The diffused part of the temporal distribution was described very accurately by the analytical expression used for the calculation derived from diffusion theory. The variability of the calculated optical parameters of one type of tissue among different tissue samples was very small.

Experimental procedure

The tissue samples were obtained from female breast during tumor extraction or biopsy operations. The study concerned tissue from twenty cases in total. Twelve of

75

them were macroscopically characterized as fat deposited and eight of them as fibrous. All tissues were obtained half an hour after excision and were returned after the measurement to the Department of Surgical Oncology of the University Hospital for histologic analysis. The thickness of the samples varied from 5 to 30 mm and they were placed on a X-Y translation stage in order to take measurement from more than one point on each tissue. For biopsy samples with thickness less than 5 mm the calculation of the optical properties is based on the Laguerre expansion of the kernels method reported elsewhere [13]. The distance of the backside of the tissue to the front face of the detector was kept constant at 1 cm thus, keeping the observation angle constant.

Fig.1*: Experimental setup of trans-illumination system*
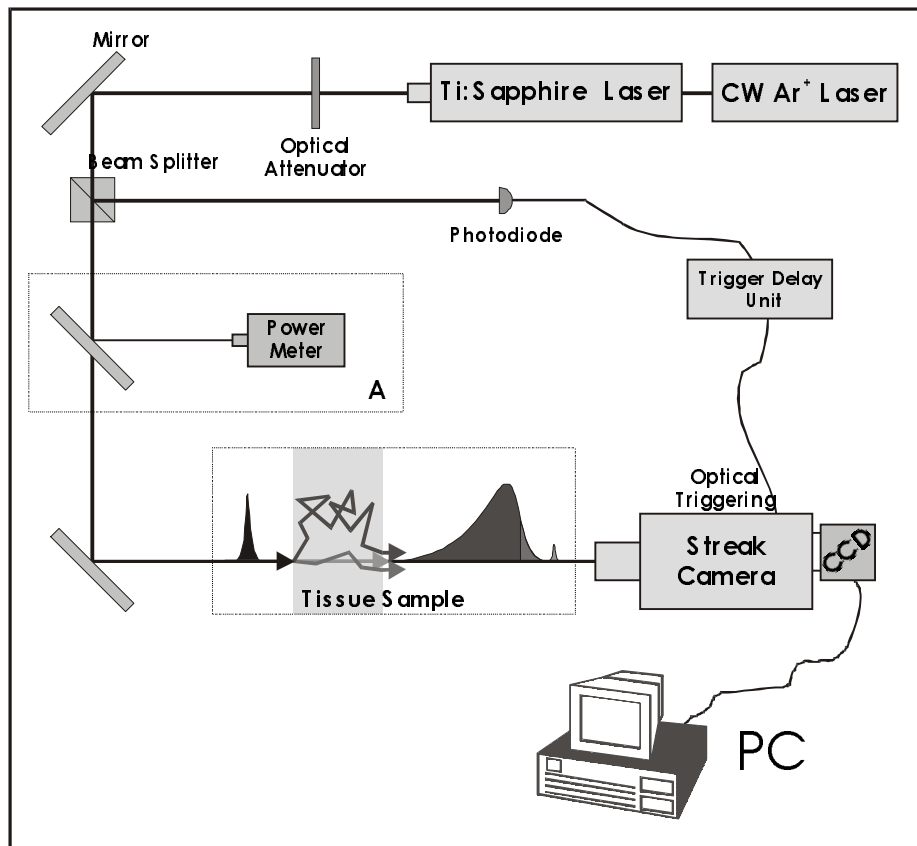
A schematic representation of the set-up used for the transmission measurements is shown in figure 1. The source of the fsec pulses is a mode-locked Ti:Sapphire laser emitting at 800 nm, pumped by a Spectra Physics Ar^+ laser operating with a power of 9 W. The repetition rate of the Ti:Sapphire was 82 MHz with an average power of ~1 W. A Hamamatsu C 5680 Streak Camera with a

temporal resolution of 2 psec was used as the detector. A CCD camera operating at - 50°C for reduced dark noise was used for the recording of the signals. The resulting signal was fed to a PC for further processing. Two different signals were simultaneously recorded. The diffused pulse emerging from the sample and a small portion of the original pulse, which provided the time reference. This part of the pulse was coupled into an optical fiber and directed to the entrance slit of the camera. The position of the coupler was adjusted so that the two signals arrive at the same time without the sample. The width of the entrance slit of the streak camera was 28 mm and during the experiments it was opened 5-10 μm in order to achieve the maximum temporal resolution. A Hamamatsu PIN photodiode provided the optical trigger to the streak camera using a very small part (few mW) of the original pulse. The diameter of the beam was about 3 mm while the samples were irradiated with a power of 100 mW.

Calculation of the optical parameters

Time profiles are obtained in order to extract the temporal information. Intensity versus time graphs can then be constructed. The optical parameters (absorption and reduced scattering coefficient) of the samples were calculated by fitting the diffusion curves with the Patterson analytical expression [14] (derived from the diffusion theory), modified to fit the data from the streak camera:

$$T(d,t) = (4\pi Dc)^{-1/2} t^{-3/2} e^{-\mu_\alpha ct}$$

$$\times \left\{ (d - z_0)e^{-\frac{(d-z_0)^2}{4Dct}} - (d + z_0)e^{-\frac{(d+z_0)^2}{4Dct}} + (3d - z_0)e^{-\frac{(3d-z_0)^2}{4Dct}} - (3d + z_0)e^{-\frac{(3d+z_0)^2}{4Dct}} \right\}$$

where,

$$t = t - t_o, \quad z = l_t = ((1-g)\,\mu_s)^{-1} = 1/\mu_s{}' \text{ and } D = (3(\mu_a + (1/z)))^{-1}$$

The fixed parameters of the equation were the thickness of the sample (d), the time corresponding to the position of the maximum of the reference pulse (t_o) and the speed of light (c). The value of the latter was calculated for water (0.214×10^9 m/sec, with $n_{water} = 1.4$) [15].

B and y_o, were parameters that had to do with specific characteristics of each curve and are important for the adjustment of the theoretical curve to the data. The

output of the calculation was the absorption and the inverse reduced scattering coefficient (μ_a and $1/\mu_s'$ respectively). Since the scattering coefficient cannot be calculated independently of the anisotropy factor g, the transport mean free path ($1/\mu_s'$) was used for the characterization of each type of tissue.

Fig.2*: Characteristic temporal profile of fat tissue obtained from the 3D streak image. The dashed curve corresponds to the experimental data whereas the solid curve represents the analytical fitting.*
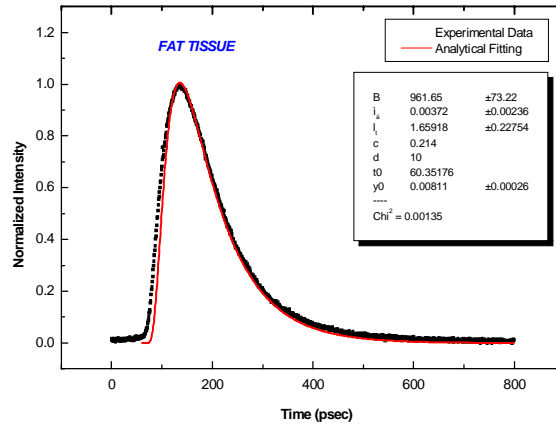

Fig.3*: Characteristic temporal profile of fibrous tissue obtained from the 3D streak image. The dashed curve corresponds to the experimental data whereas the solid curve represents the analytical fitting.*
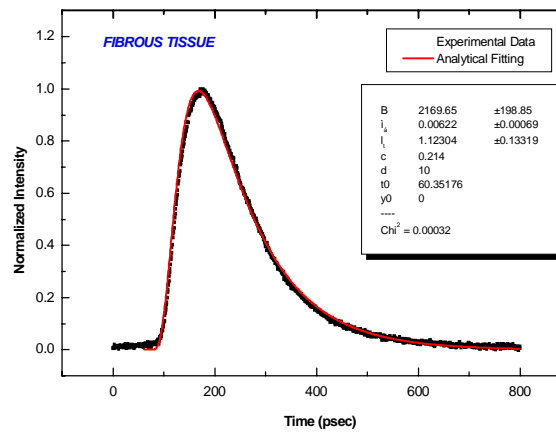
78

Characteristic profiles for fat and fibrous tissue are presented in figure 2 and 3 respectively (scatter graph), where the results of the analytical fitting are also given in the inset as well as the fitted curves (solid line). To make the differences more pronounced the two curves are plotted in the same graph (figure 4). The larger temporal spreading and the longer delay of the curve corresponding to fibrous tissue suggests that fibrous tissue has higher scattering properties compared to the fat tissue. This is in contradiction with already published results. However, as mentioned in the introduction part the investigation was made in the entire breast and not in separate tissue samples.
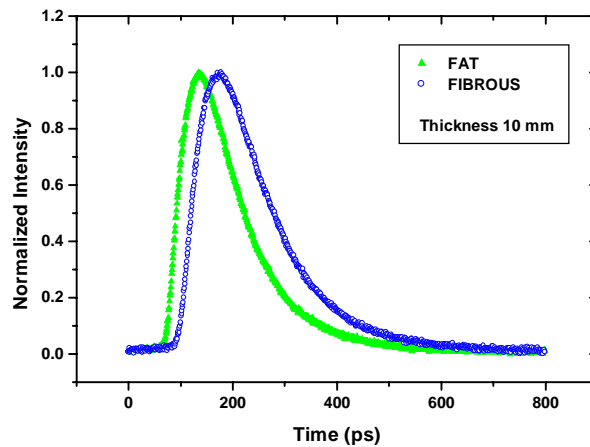

Fig. 4: *Curves corresponding to fat (solid triangles) and fibrous tissue (open circles) with the same thickness and recorded under the same conditions (Laser intensity, observation geometry and time scale).*

The difference of the mean values of the reduced scattering coefficient was used in order to discriminate the different types of tissue as described below. The absorption coefficient was not taken into account since it did not affect significantly the fitting of the theoretical curve and furthermore its values were at least two orders of magnitude smaller and had a large deviation for the same tissue. This conclusion is also supported by the fact that the absorption of tissue in the near infrared is associated with the presence of blood and when dealing with tissues *in vitro* the blood content varies between tissue samples. Moreover, the absorption is negligible because of the minimum of hemoglobin absorption around 700 nm. Therefore, it could not be

connected to the characterization of the tissue. The values obtained were (0.0040 $\pm$ 0.0010) mm^{-1} for lipid tissue and (0.0045 $\pm$ 0.0021) mm^{-1} for fibrous tissue. These values are in good agreement with already published work even though slightly different wavelengths or techniques might have been used for the investigation of the tissue samples [16, 17]. In particular the values obtained for fibrocystic tissue were in perfect agreement with the values reported by Peters et al. [17], even though this tissue was not taken into account in our study since it concerned only one set of measurements.
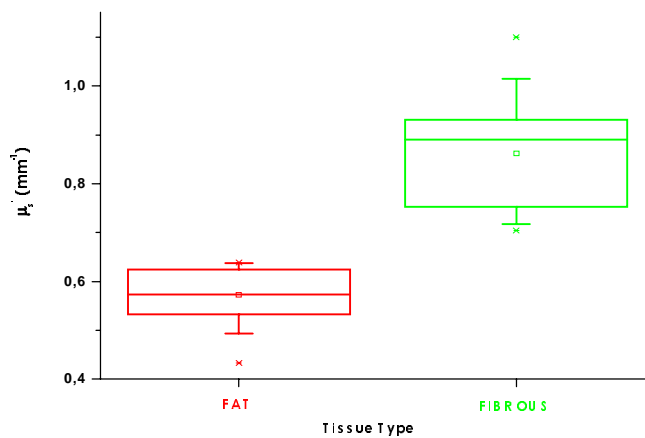

Fig.5*: Statistical plot constructed using the values calculated from the theoretical fitting. The horizontal lines from bottom to top represent the 25th, 50th and 75th percentile respectively. The 5th and the 95th percentile are used as error bars. Finally, the 1st and 99th percentile, are depicted as stars.*

The values obtained from the fittings were plotted in statistical graphs as the one shown in figure 5, where the percentile distribution was plotted. In this graph the horizontal lines from bottom to top represent the 25th, 50th and 75th percentile respectively. This meant that for example the values above the 25th percentile were larger than the 25 percent of the range of the values. The error bars represented the 5th and the 95th percentile while the stars the 1st and 99th (meaning, in this case, the first and last value of the distribution) respectively. The square inside the box was the mean value of the distribution. It could be seen clearly from the plot that using as criterion the reduced scattering coefficient, the discrimination between lipid and fibrous tissue was possible since a different range of values corresponded to the two

80

types of tissue studied here. For the lipid tissue the values lid in the interval [0.43 - 0.64] mm^{-1} and for the fibrous tissue in the interval [0.71 - 1.1] mm^{-1}. Values, which, were between the two distributions, were assumed to correspond to tissue with different percentage of fat and fiber. This classification was based on the corresponding histologic analysis. The same method could also be used for the discrimination of the other components of the breast.

Conclusions

The result of the study was the discrimination between lipid, fibrous and benign tissue with the latter being a sensitive indicator of the presence of a histological deviation (precancerous lesion, benign or malignant tumor). This could lead to a non-invasive technique, which may eventually operate synergistically with biopsy, which requires the extraction of tissue sample from the patient. Optical topography, meaning calculation of the scattering coefficient in specific and very distinct positions of the tissue, could assist in achieving that goal.

References

1. F. Liu, K. M. Yoo and R. R. Alfano, "Transmitted photon intensity through biological tissues within various time windows", Opt. Lett. **19,** 740 (1994).

2. B. B. Das, K. M. Yoo, F. Liu, J. Cleary, R. Prudente, E. Celmer, R. R. Alfano, "Spectral optical-density measurements of small particles and breast tissues", Appl. Opt. **32,** 549-553 (1993).

3. J. C. Hebden, and D. T. Delpy, "Enhanced time-resolved imaging with a diffusion model of photon transport", Opt. Lett. **19,** 311 (1994)

4. S. Andersson-Engels, R. Berg, S. Svanberg, and O. Jarlman, "Time-resolved transillumination for medical diagnosis", Opt. Lett. **15**, 1179-1181 (1990)

5. J. C. Hebden, "Evaluating the spatial resolution performance of a time-resolved optical system", Med. Phys. **19,** 1081-1087 (1992)

6. K. A. Kang, B. Chance, S. Zhao, S. Srinivassan, E. Patterson and R. Troupin, "Breast tumor characterization using near-infrared spectroscopy", SPIE, **Vol. 1888**, 487-499 (1993)

7. J. Kölzer, G. Mitic, J. Otto and W. Zinth, "Measurements of the optical properties of breast tissue using time-resolved transillumination", SPIE **Vol. 2326**, 143-152 (1994)

8. H. Heusmann, J. Kölzer, J. Otto, R. Puls, T. Friedrich, S. Heywang-Köbrunner, W. Zinth, "Spectral transillumination of female breasts and breast tissue-like material" SPIE **Vol. 2326**, 370-382 (1994)

9. L. T. Perelman, J. Wu, I. Itzkan and M. S. Feld, "Photon migration in turbid media using path integrals" Phys. Rev. Lett. **72**, 1341-1344 (1994)

10. K. M. Yoo, F. Liu and R. R. Alfano, "When does the diffusion approximation fail to describe photon transport in random media?" Phys. Rev. Lett. **64**, 2647-2650 (1990)

11. B. B. Das, K. M. Yoo and R. R. Alfano, "Ultrafast time-gated imaging in thick tissues: a step toward optical mammography" Opt. Lett. **18**, 1092-1094 (1993)

12. L. Wang, X. Liang, P. Galland, P. P. Ho and R. R. Alfano, "True scattering coefficient of turbid matter measured by early-time gating" Opt. Lett. **20**, 913-915 (1995)

13. G. Zacharakis, A. Zolindaki, V. Sakkalis, G. Filippidis, E. Koumantakis and T. G. Papazoglou, "Nonparametric characterization of human breast tissue by the Laguerre expansion of the kernels technique applied on propagating femtosecond laser pulses through biopsy samples" Appl. Phys. Lett. **74**, 771-772 (1999)

14. M. S. Patterson, B. Chance and B. C. Wilson, "Time resolved reflectance and transmittance for the noninvasive measurement of tissue optical properties", Appl. Opt. **28**, 2331-2336 (1989)

15. D.T. Delpy, M. Cope, P. van der Zee, S. Arridge, S. Wray, J. Wyatt, "Estimation of optical pathlength through tissue from direct time of flight measurement", SPIE **Vol. MS 102** (1994)

16. G. Mitic, J. Kolzer, J. Otto, E. Plies, G. Solkner and W. Zinth, "Time-gated transillumination of biological tissues and tissuelike phantoms", Appl. Opt. **33**, 6699-6710 (1994)

17. V. G. Peters, D. R. Wyman, M.S. Patterson and G. L. Frank, "Optical properties of normal and diseased human breast tissues in the visible and near infrared", Phys. Med. Biol., **35**, 1317-1334 (1990)

Chapter2

Non-parametric characterization of human breast tissue by the Laguerre expansion of the kernels technique applied on propagating femtosecond laser pulses through biopsy samples

Ultra-fast laser pulses transmitted through excised human breast tissue have been detected by a streak camera. Experimental data of the temporal spread of the ultrafast pulse during the transmission through the tissue have been analyzed using the Laguerre expansion technique. This method treats the medium of propagation as a "black box system" and using data sets of incident – transmitted pulse it relates to this system a set of coefficients as well the first order system kernels. This analysis could present an alternative method of tissue characterization when, due to the limited optical thickness of small biopsy samples, the photon diffusion approximation cannot be used successfully.

Most of any image-bearing light that propagates through a highly scattering medium undergoes multiple scattering, which causes broadening on both the temporal

and spatial point spread functions [1-3]. Various time-resolved techniques have been used in order to detect objects hidden in such turbid media. Early-arriving photons of a transmitted ultra-short laser pulse can carry the image information while late-arriving photons, due to their extensive scattering will bear little information [4]. Enhancement of the early part of the propagating pulse via non-linear techniques or time gating imaging has been used in order to discriminate between these photons [5-6]. The temporal spreading of a short light pulse as it propagates through the scattering medium may also provide further information about the optical coefficients of the medium[5]. In this letter the temporal point spread functions were recorded when the beam propagated through different types of human breast tissue of limited size (<4 mm) such as the samples removed during biopsy are and when the photon diffusion theory does not represent a good model approach.
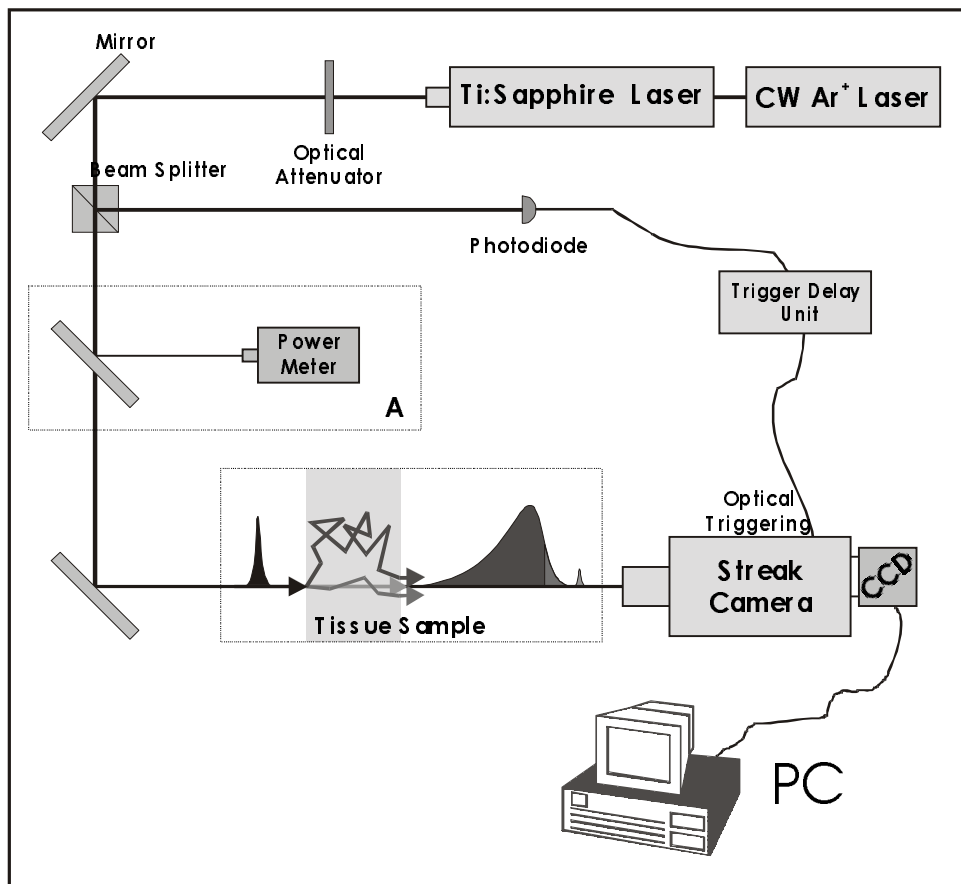

Fig.1*: Experimental setup of trans-illumination system*

The experimental imaging system is illustrated in Figure 1. Near-infrared (~ 790 nm), sub-100 femtosecond pulses are produced at a rate of ~82 MHz by a Spectra-Physics Ti:Sapphire laser pumped by a Spectra-Physics Ar^+ laser. Beam diameter was less than 2 mm. After neutral density filter attenuation, less than 20 mW of laser light is relayed to the sample object. Transmitted light emerging from the back surface of the sample was directly relayed to the input slit of a Hamamatsu C5680 streak camera. A Hamamatsu PIN photodiode provided the optical trigger to the streak camera using a very small part (few mW) of the original pulse. The temporal resolution of the camera, in the range of 1 ps, with negligible laser jitter, was very much smaller than the temporal range, which was studied. The length of the entrance slit of the streak camera was 14 mm and during the experiments its width was 5-10 μm in order to obtain the maximum temporal resolution. The transmitted light was imaged onto the photocathode through the slit. A CCD camera operating at -50°C for reduced dark noise was used for the recording of the signals. The resulting signal was fed to a PC for further processing. Transverse sample manipulation was done by an x-y translation stage. Samples were taken from 20 different breast biopsies at the department of Surgical Oncology of the University Hospital.

Fig.2 a)*: A set of transmitted laser pulses on lipid (OUT 1, OUT 2, OUT 4) and fibrous (OUT 3 and OUT 5) samples taken during exploratory biopsy sampling and the incident laser pulse (IN) (a). Corresponding first order kernels calculated using the Laguerre expansion technique. L1, L2, L4 for lipid and L3, L5 for fibrous samples respectively*

A typical set of incident-transmitted laser pulses is shown in figure 2a. It is apparent that due to the limited thickness of the biopsy sample the spreading of the transmitted pulse is limited and this set of measurements cannot be treated by the photon diffusion approximation by simply fitting the data to one of the closed form solutions. Each set of incident and transmitted laser pulse was de-convoluted using the Laguerre expansion technique and the characteristic kernels as well the coefficients of the expansion were recorded for each sample and compared with the histologic analysis.
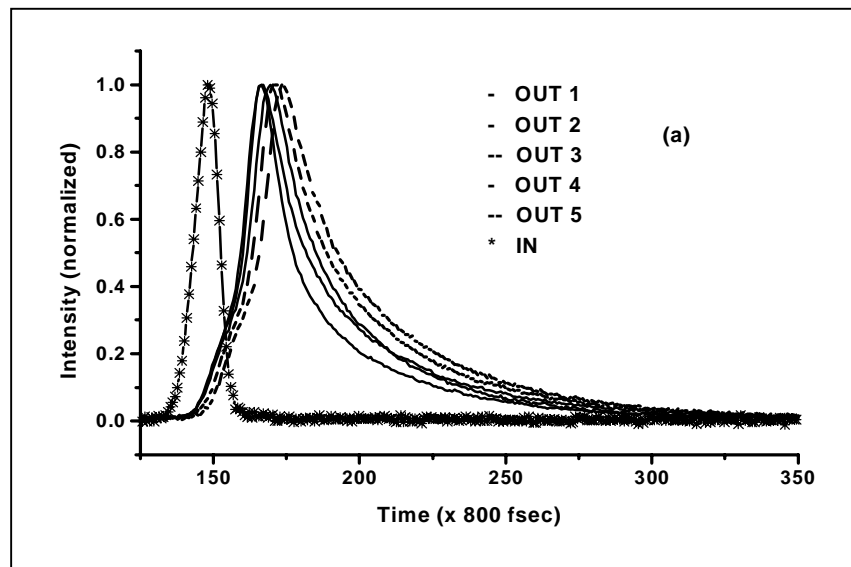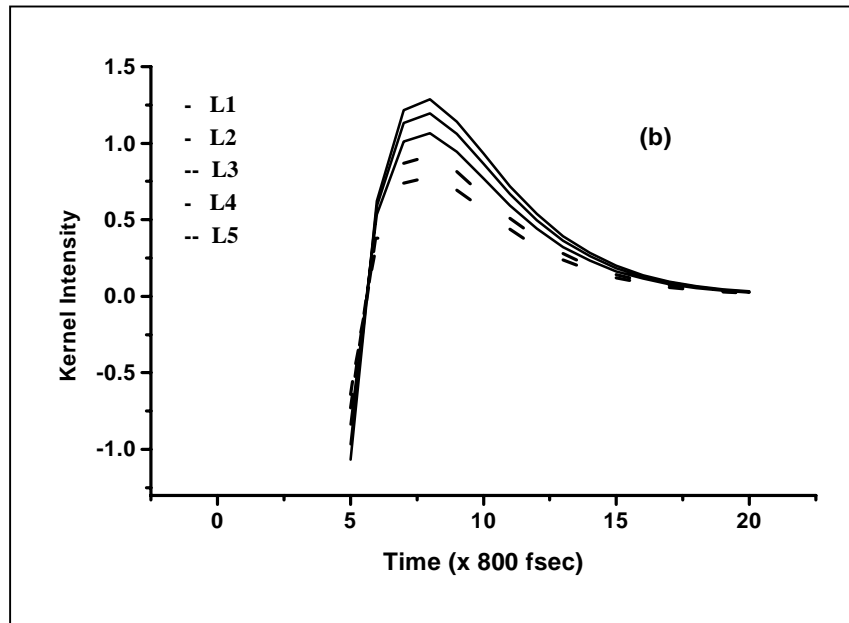

Fig.2 b): A set of transmitted laser pulses on lipid (OUT 1, OUT 2, OUT 4) and fibrous (OUT 3 and OUT 5) samples taken during exploratory biopsy sampling and the incident laser pulse (IN). All samples were 4 mm thick

The Laguerre expansion technique was introduced in order to best describe nonlinear physiological systems stimulated with broadband random inputs [7, 8]. However, this technique can be used to study systems with either random or deterministic inputs. In the discrete time case, the de-convoluting of the sampled incident laser pulse, L(n), from the transmitted T(n) laser pulse becomes:

$$T(n) = \sum_m L(m)R(n-m) \quad (1)$$

where R(n) is the response function of the medium. Expansion of this function over the orthogonal Laguerre basis $\{b_j(n)\}$ gives

87

$$R(n) = \sum_j c(j)b_j(n) \quad (2)$$

that transforms the first equation into

$$T(n) = \sum_j c(j) \sum_m b_j(m)L(n-m) \quad (3)$$

where c(j) represents the Laguerre expansion coefficients of R(n). The Laguerre functions $\{b_j(m)\}$ are defined as

$$b_j(m) = a^{(m-j)/2}(1-a)^{1/2} \sum_{k=0}^{j} (-1)^k \binom{m}{k}\binom{j}{k} a^{j-k}(1-a)^k, (m \geq 0) \quad (4)$$

where α $(0 < \alpha < 1)$ is the Laguerre parameter which describes the asymptotic descent of the kernel R(n). The Laguerre expansion technique yields estimates of R(n) by determining the expansion coefficients for a selected Laguerre parameter α. The number of Laguerre functions used in the expansion and the Laguerre parameter α were selected through an ascending order search procedure using a least-squares fitting algorithm for each combination of parameters. The Laguerre parameter was varied further in order to minimize the χ^2, yielding optimal parameters for α and c(j). All calculations were performed using the LYSIS computational package, available from the Biomedical Simulations Resource of the University of Southern California.

A set of transmitted pulses for lipid tissue (OUT 1, OUT 2, OUT 4) coming from a breast which was diagnosed for cancer and fibrous tissue which was taken from the tumor area (OUT 3, OUT 5) are shown in figure 2a. The corresponding first order kernels are depicted in figure 2b (L1, L2, L4 and L3, L5). The grouping of the corresponding kernels appear to be related to both the different time-spreading of the pulses as they propagate through different tissue and also due to the different time-delay of the laser pulse as it propagated through the two different types of tissue. The main discriminatory feature of the "lipid kernels" is the wider range of their values in both the positive and negative direction of the y-axis. In addition the 0th and 1st order Laguerre expansion coefficients for the two main groups of tissue (lipid vs. fibrous) were calculated to be c(0) = 0.38±0.01, c(1) = -2.56±0.24 for lipid and c(0) = -0.27±0.03, c(1) = -1.83±0.14 for fibrous tissue respectively.

In conclusion, our analysis suggests that the Laguerre expansion technique can identify fibrous and lipid tissue from analysis of the temporal point spread functions of the transmitted ultrafast laser pulse. We are in the process of further data analysis

in order to determine the sensitivity and selectivity of this approach on a wider variety of tissues that are obtained from various diagnostic procedures.

References

1. F. Liu, K. M. Yoo and R. R. Alfano, "Transmitted photon intensity through biological tissues within various time windows", Opt. Lett. **19,** 740 (1994).

2. B. B. Das, K. M. Yoo, F. Liu, J. Cleary, R. Prudente, E. Celmer, R. R. Alfano, "Spectral optical-density measurements of small particles and breast tissues", Appl. Opt. **32,** 549-553 (1993).

3. J. C. Hebden, and D. T. Delpy, "Enhanced time-resolved imaging with a diffusion model of photon transport", Opt. Lett. **19,** 311 (1994)

4. S. Andersson-Engels, R. Berg, S. Svanberg, and O. Jarlman, "Time-resolved transillumination for medical diagnosis", Opt. Lett. **15**, 1179-1181 (1990)

5. J. C. Hebden, "Evaluating the spatial resolution performance of a time-resolved optical system", Med. Phys. **19,** 1081-1087 (1992)

6. K. Yoo, Q. Xing, and R. R. Alfano, "Imaging objects hidden in highly scattering media using femtosecond second-harmonic-generation cross-correlation time gating", Opt. Lett. **16,** 1019-1021 (1991)

7. V.Z. Marmarelis, "Indentification of nonlinear biological systems using Laguerre expansions of Kernels", Annals of Biomed. Eng. **21**, 573-589 (1993)

8. V.Z. Marmarelis, in Advanced methods of physiological system modeling, edited by V.Z. Marmarelis (Plenum Press, New York and London, 1994), vol. 3, pp 229-242

Chapter 3

Investigation of the laser-like behavior of polymeric scattering gain media under sub-picosecond laser excitation

The narrowing effects of scatterers on the lifetime and spectral width of laser-induced fluorescence of organic dyes hosted inside poly-methylmethacrylate (PMMA) polymer sheets were studied. The excitation source was a distributed feedback dye laser emitting 500 femtosecond pulses at 496 nm. Spectral and temporal features were simultaneously recorded on a spectrograph- streak camera detection system. The results were then compared with those obtained from dye solutions in methanol, recorded in previous experiments. The effects of the different host environment on the fluorescence characteristics of the dye were thus investigated. These effects are currently studied when the dye is inserted in human tissue, in an attempt to boost tumor detection and Photodynamic Therapy (PDT) efficiency, and some initial results are presented.

Introduction

Scattering has always been considered detrimental to laser action because it alters the direction and spatial coherence of the photon paths. However, 5 years ago Lawandy et al [1] demonstrated isotropic laser-like emission from an optically pumped solution of Rhodamine 640 perchlorate in methanol containing TiO_2 scattering nanoparticles in suspension. Letokhov [2], who theoretically investigated the optical properties of a random medium, which simultaneously amplifies and scatters light, proposed this effect in 1968.

The remarkable observation of Lawandy et al provided a starting point for the investigation of the properties of such materials, often described as random lasers. Since then, experiments have been carried out by several research groups in order to examine the origins and various features of the narrow-linewidth emission observed [3-5, 10]. All these experiments have confirmed that the scatterers play a role analogous to that of mirrors in a conventional laser cavity providing the necessary feedback for laser action. In parallel, several theoretical studies [6-8] have been carried out in order to provide models that will efficiently describe the behavior of these materials and assist in understanding the underlying mechanisms that are responsible for their laser-like characteristics.

The behavior of disordered media with organic dyes can be described with a four level laser model in which the effects of the diffusion of both the pumping and the stimulately emitted photons must be accounted for, as Wiersma and Lagendijk [8] have shown. This system is pumped into an excited state (2), which decays rapidly to a metastable state (1). The laser transition occurs from this metastable state to a state (0') just above the ground state, which decays rapidly to the actual ground state (0). This means that state (2) and (0') are nearly unpopulated and that the population of state (1) can be described by one rate equation.

The total set of coupled differential equations describing the system is formed by two diffusion equations for pump light and amplified spontaneous emission ($W_p(\vec{r},t)$ and $W_E(\vec{r},t)$ are the corresponding energy densities) and the rate equation for the concentration $N_1(\vec{r},t)$ of molecules in the lasing state (1):

$$\dot{W}_P = D\nabla^2 W_P - \sigma_{abs}c[N_t - N_1]W_P + \frac{1}{l}I_P \qquad (1)$$

$$\dot{W}_E = D\nabla^2 W_E + \sigma_{em} c N_1 W_E + \frac{1}{\tau_e} N_1 \qquad (2)$$

$$\dot{N}_1 = \sigma_{abs} c \left[N_t - N_1 \right] W_P - \sigma_{em} c N_1 W_E - \frac{1}{l} N_1 \qquad (3)$$

where c is the transport velocity of light inside the medium, s_{abs} and s_{em} are the absorption and emission cross sections respectively, t_e is the life time of the excited state (1) and N_T is the total concentration of the laser particles. D is the diffusion constant given by $D = cl/3$ and $I_P(\vec{r}, t)$ is the pump pulse intensity.

The numerical solution of the above set of equations will give all relevant information on the spatial and temporal distribution of the energy densities of the pump light and the amplified spontaneous emission as well as of the gain coefficient of the lasing medium $\kappa_g = \sigma_{em} N_1(\vec{r}, t)$.

Most recently, there has been a growing interest in a different kind of random laser that uses polymers instead of liquid solvents as host material [9-12]. These materials have the advantages of being broadly tunable sources of nearly monochromatic radiation combined with the practical convenience of polymers, and lend themselves to a great number of possible applications.

The goal of the experiments described herein was the extensive study of the dependence of the spectral and temporal characteristics of the recorded fluorescence signal on the excitation energy, on the concentration of the scatterers and the dye and on the host medium. Indeed, the different behavior observed in the solid polymer compared to that observed in solution suggests that the different embedding environment of the dye affects the fluorescence characteristics. Also the behavior of the different dyes in the same environment was investigated.

Experimental

The liquid samples were solutions of the dyes in methanol placed inside a 1cm x 1cm x 3cm glass cuvette. The scattering particles were polystyrene microspheres with concentrations of $3\text{-}10\text{x}10^{10}$ cm^{-3} (393 nm in diameter PL-LATEX Plain White microparticles from Polymer Laboratories). For preparing the polymer samples PMMA (Aldrich 9011-14-7) and corresponding dye were dissolved in dichloromethane; appropriate quantity of TiO_2 nanoparticles (~400 nm diameter, R-900 Ti-Pure from E.I. du-Pont de Nemours & Co., Inc.) was added to the resulting

solution and this was placed in a 1cm x 1cm x 2cm Teflon cuvette for casting. Slow evaporation of the solvent resulted in a 1 mm thick polymer sheet. The dyes used were Rhodamine101, Rhogamine6G and DCM (Lambda Chrome part numbers LC 6400, LC 5900 and LC 6500 respectively) [13]. Samples of different dye ($3x10^{-3}$ M to 10^{-2} M) and scatterer ($2\text{-}5x10^{18}$ cm^{-3}) concentrations were prepared and irradiated with different excitation energies varying from 0.5 to 30 µJ/pulse by means of a variable density filter. The particle concentration corresponded to a scattering mean free path of the order of a few nanometers calculated as $l_s = 4p/ns$ [14].

A schematic representation of the experimental setup used for the measurements is given in figure 1. The laser pumping the polymer dyes was a 500 fsec distributed feedback dye laser (DFDL) emitting at 496 nm. It was pumped by the output of a KrF excimer laser emitting at 248 nm. During the experiments the repetition rate was set at 4 Hz.
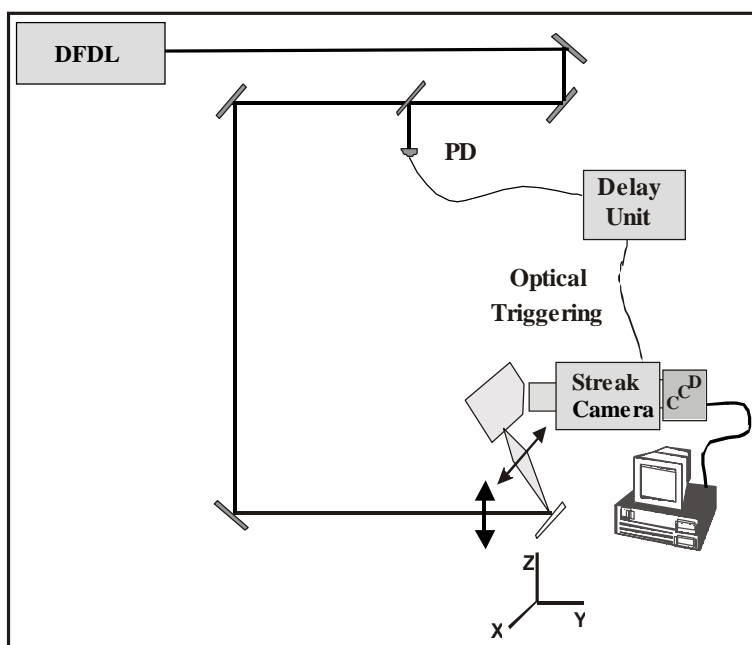

Fig. 1: *Schematic representation of the experimental setup M: Mirrors, BS: Beam Splitter, F: Lens, PD: Photodiode.*

The samples were placed on a X-Y-Z translation stage and the laser beam was slightly focused on its surface forming a 0.5 mm spot. The produced fluorescence signal, collected by the appropriate optics was focused on the entrance slit (100µm) of a 0.10 m spectrograph employing a 450 grooves mm^{-1} holographic grating. Wavelength calibration was performed with a mercury lamp. The spectrally dispersed fluorescence was focused on the entrance slit of a Hamamatsu C 5680 Streak Camera,

with a temporal resolution of 2 psec. The effective width of the photocathode (6 mm) resulted in a spectral window of approximately 100 nm, with a spectral resolution estimated to be of the order of 2 nm. The streak camera was operated in the fast sweep mode and the trigger signal was obtained from a photodiode monitoring the laser pulse. A Peltier-cooled CCD camera, operating at -50°C for reduced dark noise, was used for recording of the emission signals. Each streak image corresponded to the recording of the average of four pulses, since the acquisition time was set to 1 sec. Data acquisition and processing was done on a PC. Time and spectral profiles of the recorded 3D images were taken in order to extract the corresponding information. The temporal evolution of the fluorescence can be extracted after fitting the time profiles with the appropriate function.

Results and Discussion

A general and very spectacular result observed in all samples examined was that in both time and wavelength domains the width of the profile was dramatically reduced when the excitation energy was higher than a threshold value. Single- and double-exponential fitting of the decay curves were chosen for solutions and polymer sheets respectively, suggesting different decay mechanisms operating in the liquid or solid medium (figures 2a, 2b and 3a, 3b respectively). The spectral width of the spectrum was compared with the FWHM of the laser pulse for a qualitatively evaluation of the spectral narrowing of the fluorescence.

a   **b**
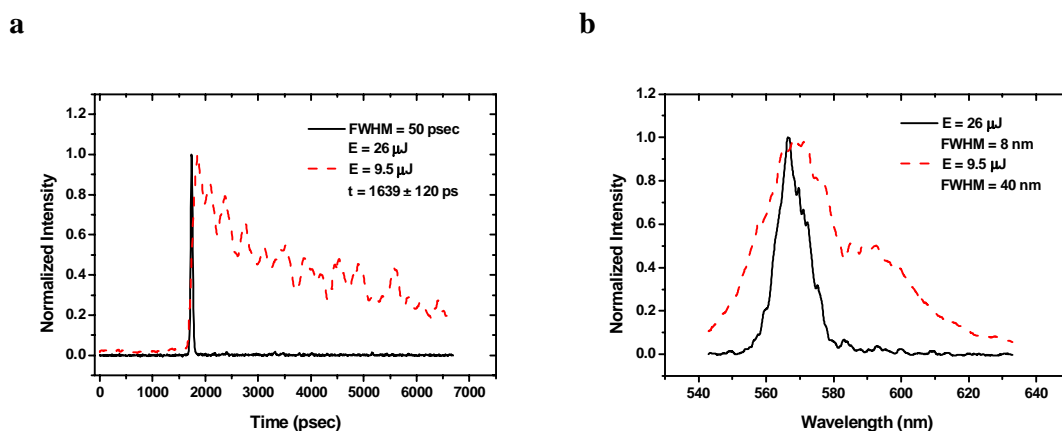
Fig. 2: a) *Time profile of the fluorescence decay of R6G solution (dye and scatterer concentration $8.2x10^{-3}$ M and $7.2x10^{10}$ cm^{-3} respectively) for excitation energies 9.5 μJ (dashed curve) and 26 μJ (solid curve).* ***b)*** *Spectral width of the fluorescence of R6G solution (dye and scatterer concentration $8.2x10^{-3}$ M and $7.2x10^{10}$ cm^{-3} respectively) for excitation energies 9.5 μJ (dashed curve) and 26 μJ (solid curve)*

The fittings of the decay curves lead to fluorescence lifetime in the order of 50 psec. The FWHM of the resulting spectrum was reduced to about 15 nm in contrast to the initial value, which is around 50 to 70 nm. This value was broader than that reported by other groups [9]. This happened because a femtosecond pump pulse was used, which had a broader spectral distribution than a nanosecond pulse for example. On the other hand the large refractive index mismatch of the air-polymer excitation boundary helped also on this effect. This accounted to spectral broadening by a factor of four [4], in comparison with the liquid samples where the boundary was methanol-glass-air.

a   **b**

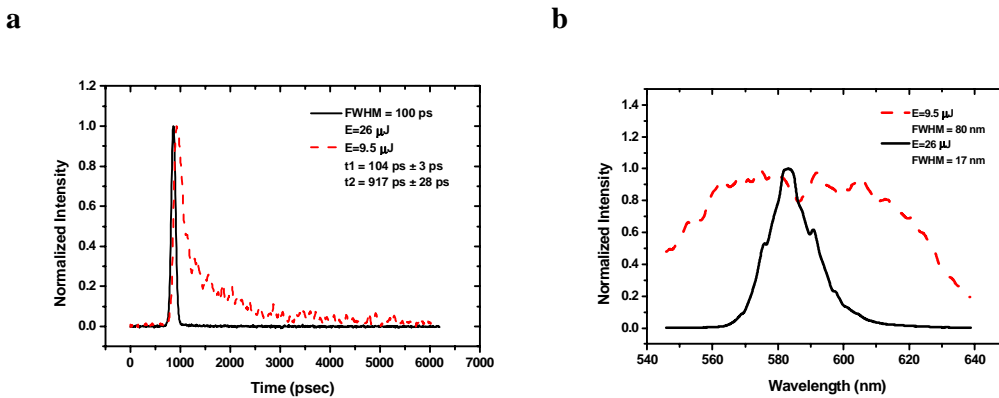***Fig. 4: a**) Time profile of the fluorescence decay of R6G polymer sheet (dye and scatterer concentration 10^{-2} M and $3.6x10^{19}$ cm^{-3} respectively) for excitation energies 9.5 µJ (dashed curve) and 26 µJ (solid curve). The characteristic time constants of the double exponential fitting are given in the inset. **b**) Spectral width of the fluorescence of R6G polymer sheet (dye and scatterer concentration 10^{-2} M and $3.6x10^{19}$ cm^{-3} respectively) for excitation energies 9.5 µJ (dashed curve) and 26 µJ (solid curve).*

The liquid samples presented a typical behavior, which has been reported several times in the past [3-5, 12]. When the energy was below the threshold the emission characteristics were identical to the fluorescence of the dyes in scattering-free methanol solution[13]. The decay curves could be fitted with a simple exponential decay and the typical values of the lifetime were around 3 nsec in agreement with the literature values. On the contrary, the polymer sheets presented a more complex decay mechanism, suggested by the double exponential fitting. The slow lifetime component (of the order of 1 nsec) resembled the corresponding of the liquid, even though the characteristic time constant was shorter, originated most likely from the different properties of the solid environment. In this case the dielectric constant was smaller by

a ten fold compared to that of the liquid (2.9 and 32.7 respectively). This resulted to an easier movement of the electrons along the chain and hence a faster decay from the excited state to the ground one. This was true even though the bonding of the dye molecules was stronger in the polymer than in the liquid. In a solid medium the embedded molecules are positioned inside the matrix of the polymer, while in the liquid van der Waals bonds are created. Furthermore, the fast component (lifetime of the order of 100 psec) is attribute to the inherent narrowing behavior of the spontaneous emission of the polymer chains when excited by ultra-short pulses (in the picosecond regime) [15]. An experimental proof of the faster behavior of the polymer samples can be extracted from the difference of the time that the maxima of the stimulated and spontaneous emission occur. The value for the solids was around 50 psec and for the liquids 150 psec. This difference represented the non-radiative decay from one of the vibrational levels of the first excited state to the ground vibrational level.
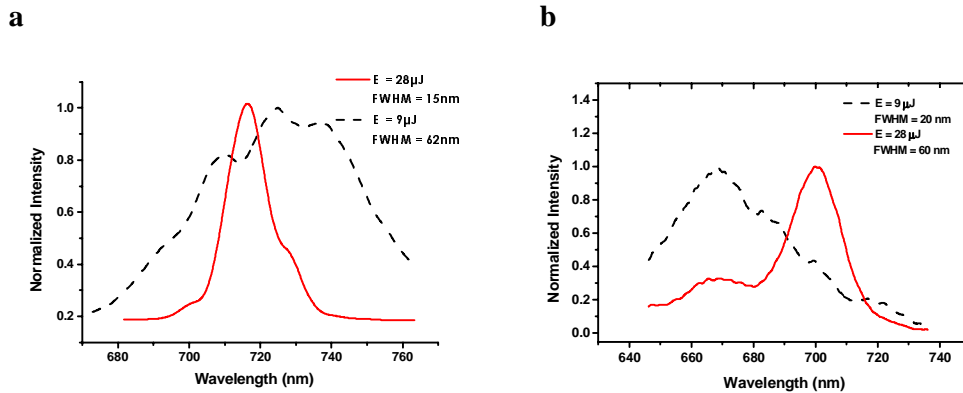
a   **b**

Fig. 5: a) *Spectral width of the fluorescence of R101 polymer sheet (dye and scatterer concentration 10^{-2} M and $5.6x10^{19}$ cm^{-3} respectively) for excitation energies 9 µJ (dashed curve) and 28 µJ (solid curve).* ***b)*** *Spectral width of the fluorescence of DCM polymer sheet (dye and scatterer concentration 10^{-2} M and $5.6x10^{19}$ cm^{-3} respectively) for excitation energies 9 µJ (dashed curve) and 28 µJ (solid curve).*

The spectral and temporal narrowing could occur in wavelengths other than the maximum of the fluorescence curve, suggesting gain curves, which depended strongly on the microcavities that were formed by the scatterers inside the polymer sheet, due to the different concentration and distribution of the particles inside the different samples. This observation was more pronounced for the DCM samples, but was also true for all the investigated dyes (figures 5a and 5b). This effect could be caused by the photon localization that starts taking place in the high particle concentration

regime ($l_s \leq \lambda$) as suggested by P. W. Anderson [16] and S. John [17]. Due to very strong scattering, recurrent scattering events arise. These are scattering events in which the light returns to a scatterer from which it was scattered before thereby forming closed loop paths. If the amplification along such a loop path would be strong enough, they could serve as random ring cavities resulting to emission of coherent light. In that case the system would lase in the modes allowed by these cavities. However, the solvent could also cause a shift in the fluorescence maxima, as proposed by the Lippert equation [18]. This shift was nevertheless always towards longer wavelengths, since the solvent causes a decrease of the energy gap between the ground and the first excited state of the dye molecule and this was not valid for all of our observations. The experimental confirmation of the coherence of the produced stimulated emission as well as the systematic investigation of this extraordinary behavior are under way and will be reported later.

The observed narrowing of the emission spectra of the sample at high dye concentration owes to the fact that the increased number of the dye molecules prevents the excitation photons to insert deeper and thus reacting with a great number of molecules. Since the excitation volume in the sample is minimized and well defined, the possibility of self-absorption is reduced, resulting to narrow fluorescence spectra. The stimulated emission observed when the excitation energy is above the necessary threshold value, leads also in this direction.

a   **b**
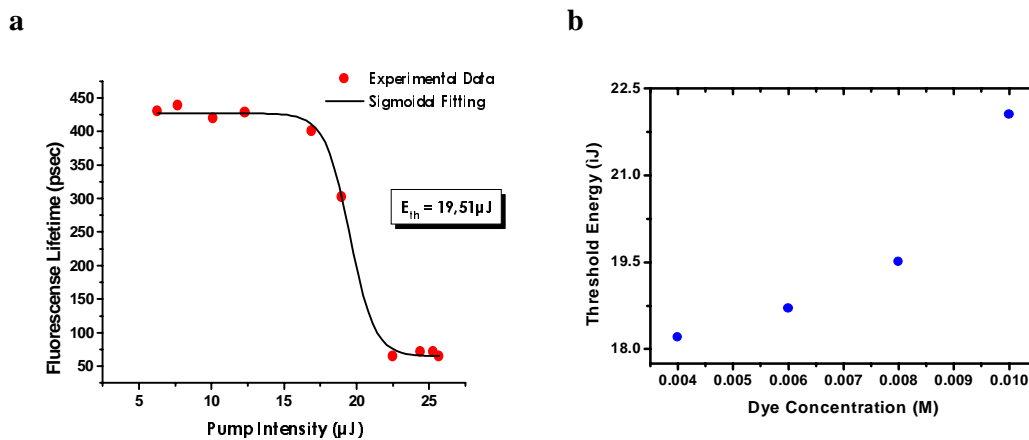
*Fig. 6: a) Dependence of fluorescence lifetime on excitation energy, recorded on R6G polymer sheet (dye and scatterer concentration $6x10^{-3}$ M and $3.6x10^{19}$ cm^{-3} respectively) with and without scatterers. Both experimental values and theoretical fitting are depicted. **b**) Dependence of the threshold energy on the dye (R6G) concentration. The scatterers' concentration is kept constant at $3.6x10^{19}$ cm^{-3}.*

In both spectral and temporal domains the features were plotted against the excitation energy in order to accurately calculate the threshold energy where the narrowing took place. The values were fitted with a sigmoidal curve (figure 6a) the turning point of which represented the threshold energy. This value was found to vary between 10 and 20 µJ, depending on the dye, and the same value was observed in both the spectral and temporal behavior (R6G: 18-22 µJ, R101: 10-15 µJ and DCM: 10-13 µJ). This distinct threshold energy supports the suggestion of a lasing behavior in random media. It also depended on the dye concentration as shown in figure 6b where the threshold energy against the dye concentration is plotted. This is true since the threshold energy accounts for the saturation energy of the dye. An increase of the concentration of the dye results in increase of the saturation energy of the solution, requiring accordingly increased laser energy.

Conclusions

In this paper we report a study of the effect of scattering particles on laser-induced fluorescence of organic dyes embedded inside polymer matrices. Lasing action in such materials can be interpreted in terms of increased path length inside the medium caused by multiple scattering. When the amplification of the produced fluorescence light overcomes a critical value the probability of stimulated emission becomes 1 (all the dye molecules decay only stimulately) and lasing action occurs.

The observed fluorescence signal quenches in both temporal and spectral domains. This happens when the excitation energy reaches and exceeds a threshold value. Above that value the narrowed fluorescence exhibits the same features as the excitation laser pulse. Lifetime in the order of 50 psec and spectral FWHM in the order of 10 nm were observed. The threshold energy was measured to vary between 10 and 20µJ. For energies bellow that value the amplification is negligible and the samples behave exactly as those without scatterers. As the excitation energy increases the laser action requirements are fulfilled and the sudden narrowing takes place.

In conclusion this is a study of the use of the spectral and temporal narrowing of fluorophore emission in a highly scattering environment. Similar studies are underway when various fluorophores are embedded in biological tissues [19]. An example from a very recent experiment is given in figure 7, where the autofluorescence of R6G is compared with the fluorescence recorded when the dye has been introduced in human arterial atherosclerotic tissue. The final goal is to take

advantage of this effect towards a more spatially and spectrally confined agent in Photodynamic Therapy of target tissue lesions on skin or other types of superficial lesions. Very promising in the field of skin PDT would be thin polymer sheets with various dyes, which could be applied directly on the lesion and allow the selection of different irradiation wavelengths using the same laser as excitation source. Thus, improving by far the efficiency of the destruction of different types of cancerous cells.
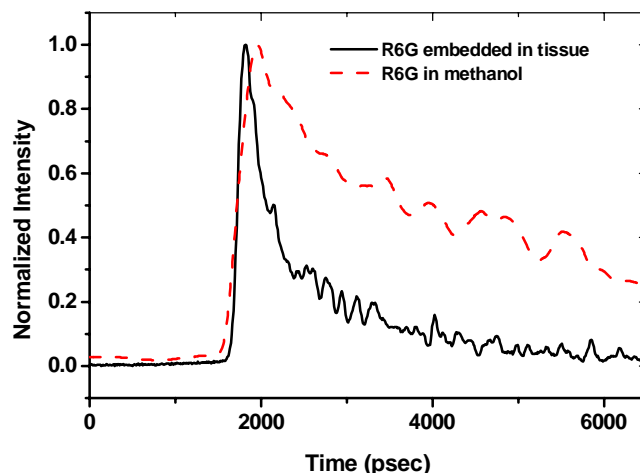

Fig. 7: *Lifetime of R6G embedded in human arterial tissue in comparison with the corresponding signal recorded from methanol solution.*

The absence of saturation, the very narrow emission spectrum and the instantaneous response of photonic polymers make them very versatile in many applications, in addition to PDT. Some of them are photonic marking for identification purposes (photonic codes, search and rescue missions, military applications, marking of hazardous material), substitution of ordinary lasing media in dye lasers and boosting the emission of LEDs and diode lasers in the blue region of the spectrum (if used with electroluminescent polymers).

For all these reasons these materials have created a very rapidly increasing interest among researchers and the number of experiments involving such media is constantly increasing. Further studies, needed for the interpretation of all the principles concerning polymeric scattering media, are under way. Different polymers (i.e. polystyrene), dyes (i.e. porphyrines) and excitation wavelengths are used in order to fully evaluate and understand these materials.

References

1. N. M. Lawandy, R. M. Balachandran, A. S. L. Gomes and E. Sauvain: "Laser action in strongly scattering media", Nature, **Vol. 368**, pp. 436, 1994

2. V. S. Letokhov: "Generation of light by a scattering medium with negative resonance absorption", Sov. Phys. JEPT **Vol. 26**, No. 4, pp. 835, 1968

3. W. L. Sha, C. H. Liu and R. R. Alfano: "Spectral and temporal measurements of laser action of Rhodamine 640 dye in strongly scattering media", Opt. Leet. **Vol. 19**, No. 23, pp.1922, 1994

4. R. M. Balachandran, N. M. Lawandy: "Interface reflection effects in photonic paint", Opt. Lett., **Vol. 20**, No. 11, pp.1271, 1995

5. W. Zhang, N. Cue and K. M. Yoo: "Emission linewidth of laser action in random gain media", Opt. Lett., **Vol. 20**, No. 9, pp. 961, 1995

6. S. John and G. Pang: "Theory of lasing in a multiple-scattering medium", Phys. Rev. **A54**, No. 4, pp. 3642, 1996

7. R. M. Balachandran, N. M. Lawandy, J.A. Moon: "Theory of laser action in scattering gain media", Opt. Lett., **Vol. 22**, No. 5, pp. 319, 1997

8. D. S. Wiersma, Ad Lagendijk: "Light diffusion with gain and random lasers", Phys. Rev. E, **V. 54**, No. 4, pp. 4256, 1996

9. R. M. Balachandran, D. P. Pacheco and N.M. Lawandy: "Laser action in polymeric gain media containing scattering particles", Appl. Opt. **V. 35**, No. 4, pp. 640, 1996

10. J. Martorell, R. M. Balachandran, N. M. Lawandy: "Radiative coupling between photonic paint layers", Opt. Lett., **Vol. 21**, No. 4, pp. 239, 1996

11. M. Siddique, R. R. Alfano, G. A. Berger, M. Kempe and A. Z. Genack: "Time-resolved studies of stimulated emission from colloidal dye solutions", Opt. Let., **Vol. 21**, No. 7, pp. 450, 1996

12. G. Zacharakis, D. Anglos, E. Vazgiouraki, T. G. Papazoglou: "Temporal and spectral effects of scatterers on sub-picosecond laser-induced fluorescence of organic dyes", CLEO proceedings, **Ctul99**, 1998

13. Ulrich Brackmann, "Lambdachrome Laser Dyes", Lambda Physik GmbH, Göttingen, 1994

14. Th. M. Nieuwenhuizen, J. M. Luck: "Skin layer of diffusive media", Phys. Rev. E, **V. 48**, No. 1, pp. 569, 1993

15. A. Haugeneder, M. Hilmer, C. Kallinger, M. Perner, W. Spirkl, U. Lemmer, J. Feldmann, U. Scherf: "Mechanism of gain narrowing in conjugated polymer thin films", Appl. Phys. B **66**, pp. 389, 1998

16. P. W. Anderson: "The question of classical localization. A theory of white paint?", Philos. Magaz. B, **V. 52**, No. 3, pp. 505, 1985

17. Sajeev John: "Localization of light", Physics Today, **V. 44**, No 5, pp. 32, 1991

18. J. R. Lackowicz: "Principles of fluorescence spectroscopy", Plenum Press, New York, 1983

19. M. Siddique, Li Yang, Q. Z. Wang, R. R. Alfano: "Mirrorless laser action from optically pumped dye-treated animal tissues" Opt. Comm. **No. 117**, pp.475, 1995

Chapter4

Photon statistics of the laser-like emission from polymeric scattering gain media

G. Zacharakis et al. Opt. Lett. **25**, *923 (2000)*

The coherent properties of the temporally and spectrally narrowed emission of laser-induced fluorescence of organic dyes hosted inside artificial scattering matrices ("random lasers") were investigated. The excitation source was a frequency doubled 200 femtosecond pulsed laser emitting at 400 nm. Spectral and temporal features were simultaneously recorded using a spectrograph and a streak camera operating on the photon counting mode. Photon number distributions were thus created. The temporal coherence of the laser-like emission above and bellow the excitation energy threshold has been investigated from the photon number distribution obtained.

Scattering has always been considered detrimental to laser action because it alters the direction and spatial coherence of the photon paths. Recently however, Lawandy et al [1] demonstrated isotropic laser-like emission from an optically pumped solution of Rhodamine 640 perchlorate with TiO_2 scatterers dispersed in a methanol solution. Letokhov [2], while investigating the optical properties of a random medium, which simultaneously amplifies and scatters light, theoretically proposed this effect in the mid-60s.

The remarkable observation of Lawandy et al provided a starting point for the investigation of the properties of such materials, often described as random lasers. Since then, a lot of experiments were carried out in order to examine the origins and various features of the narrow-linewidth emission observed [3-5]. All these experiments confirmed that the scatterers play the role of mirrors in a conventional laser in order to provide the necessary feedback for laser action. Simultaneously, several theoretical studies [6-8] have been made in order to provide models that will efficiently describe the behavior of these materials and help to understand the underlying mechanisms that are responsible for their laser-like characteristics.

Random laser action with coherent feedback in semiconductor powders was demonstrated very recently by Cao et al [9] for the first time. This effect is thought to be caused by the photon localization that starts taking place in the high particle concentration regime ($l_s \leq \lambda$) as suggested by P. W. Anderson [10] and S. John [11]. Due to very strong scattering, recurrent scattering events arise. These are scattering events in which the light returns again to the previous scattering center thereby forming closed loop paths. If the amplification along such a loop path would be strong enough, they could serve as random ring cavities resulting to emission of coherent light.

Nevertheless, the proof of coherent emission from such materials has yet to be demonstrated. In this study we try to investigate whether the emission from such samples is coherent, by measuring the photon statistics for different excitation conditions.

The polymer samples were prepared by mixing PMMA and dye solutions, in a 1cm x 1cm x 2cm Teflon cuvette, together with the scattering particles. The scatterers were TiO$_2$ nanoparticles (~400 nm diameter, ~ 4 kg/l density, R-900 Ti-Pure from E.I. du-Pont de Nemours & Co., Inc.). The evaporation of the solvent (dichloromethane - CH$_2$Cl$_2$) resulted to the creation of the 1 mm thick polymer sheet. The dye used was Rhodamine6G (Lambda Chrome part numbers LC 5900) and the concentration was 10^{-2} M, with the concentration of the scatterers being 1.2×10^{12} cm^{-3} (15 mg Ti-Pure in 0.1 cm^3 of the final solid phantom). The samples during the experiments were irradiated with different excitation energies varying from 1 to 12 μJ, by means of a variable density filter.
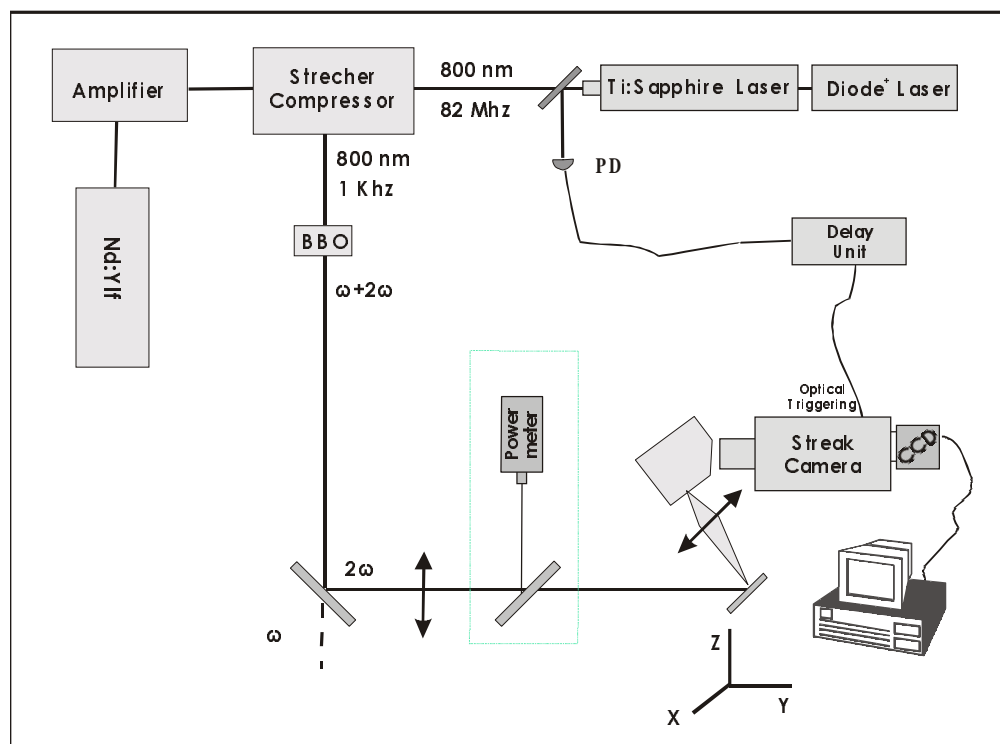
Fig.1*: Experimental setup*

A schematic representation of the experimental setup used for the measurements can be seen in figure 1. The source of the 200 fsec pulses is a mode-locked Ti:Sapphire laser emitting at 800 nm, pumped by a Spectra Physics diode laser operating with a power of 5 W. The repetition rate of the Ti:Sapphire oscillator was 82 MHz with an average power of ~1 W. The pulses were fed to an amplifying system consisting of a stretcher-compressor setup and an amplifier pumped by a Nd:Ylf pulsed laser. The repetition rate of the amplified beam was 1 KHz resulting from the Q-switching rate of the regenerative amplifier. This beam was then frequency doubled by means of a BBO crystal and after the separation of the fundamental from the second harmonic, the 400 nm, 200 fsec pulses were focused on the samples, which were placed on a X-Y-Z translation stage. The produced fluorescence signal was collected by the appropriate optics and focused at the entrance slit (100μm) of a 0.10 m spectrograph employing a 450 grooves mm^{-1} holographic grating. Wavelength

calibration was performed with a mercury lamp. After spectral analysis the signal was focused at the entrance slit of a Hamamatsu C 5680 Streak Camera, with a temporal resolution of 2 psec. The effective width of the photocathode (6 mm) resulted to an observable spectral window of approximately 100 nm, with a spectral resolution of the order of 1 nm. The streak camera was operated in the fast sweep mode and the trigger signal was obtained from a photodiode. A Peltier-cooled CCD camera, operating at -50°C for reduced dark noise, was used for the recording of the signals, which were then collected by a PC for further processing. The streak camera provided the possibility of eliminating the contribution of the dark current noise by experimentally measuring this noise and using a threshold value over which the real measurements took place. This setup provided also the ability to measure the photon number distributions for different time delays and at different wavelengths, reaching resolution down to a single photon event. Thus, the temporal coherence of the emitted light could be investigated.

A general and very spectacular result observed in all samples examined was that in both time and wavelength domains the width of the profile was dramatically reduced when the excitation energy was higher than a threshold value [13]. This remarkable effect is attributed to the stimulated emission caused by the increased path length of the fluorescence photons inside the multiple-scattering medium. This leads to the laser-like emission when the gain exceeds the losses of the scattering cavities. The coherence can be verified by performing photon statistics on the emitted light above and below threshold [14].

Nevertheless, before starting to study the coherence of the emitted fluorescence, photon counting must first be applied for the excitation laser pulse, recorded from a reflection from the sample. The resulted Poisson shaped distribution reveals the coherence of the excitation source, even though it is not pure.

The photon number distributions from the sample, for an image obtained while pumping above threshold (excitation energy 12 μJ), are shown in figure 2. The different graphs correspond to distributions measured for different time delays after the excitation has ended and for a time interval of 30 ps. The distribution for the short time delays is characteristic of coherent light. The divergence from the perfect Poisson distribution suggests that the light consists of a superposition of more than one pattern. These patterns could consist of incoherent as well as coherent light. Furthermore, one can see that as the time delay increases, the Poisson shaped

distribution is lost and is replaced by a Bose-Einstein distribution characteristic of incoherent light. This is a result of the scattering that the fluorescence light undergoes before exiting from the sample and which acts detrimentally to the characteristics of the emitted coherent light. The temporal coherence is lost completely 100 psec after the end of the excitation. This is shown in the inset of figure 2, where the photon-count distribution calculated for time delay 100 ps, plotted on a logarithmic scale, is presented. The two curves correspond to the fittings using Poisson (dash-dotted line) and Bose-Einstein (solid line) distributions. The theoretical values obtained after the fittings are 0.0025 and 0.005 respectively, whereas the measured value is 0.0045.
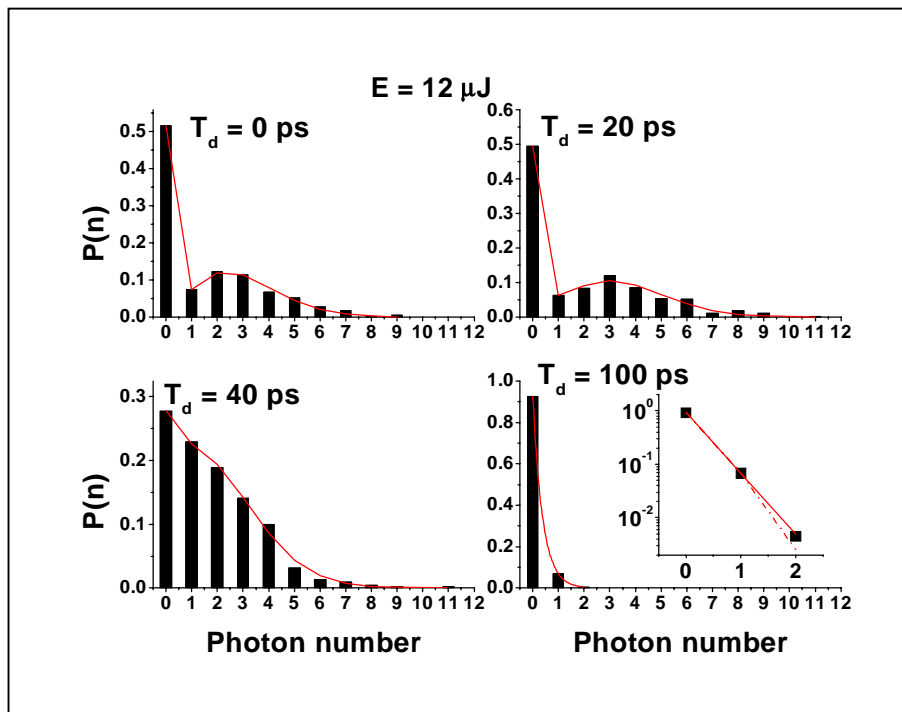

Fig.2*: Photon-count distributions of the laser like emission (above threshold E=12 μJ) in increasing time delays after the excitation has finished. Total number of photon counts is kept constant.*

In contrast to the high-energy case, when the excitation energy is below threshold, as in the case shown in figure 3 where the excitation energy is 1 μJ, the light that is emitted is completely incoherent. This is demonstrated by the Bose-Einstein distribution, which is independent on the time delay. But as the excitation energy is increased the Poisson like distribution is restored. Figure 4 depicts the

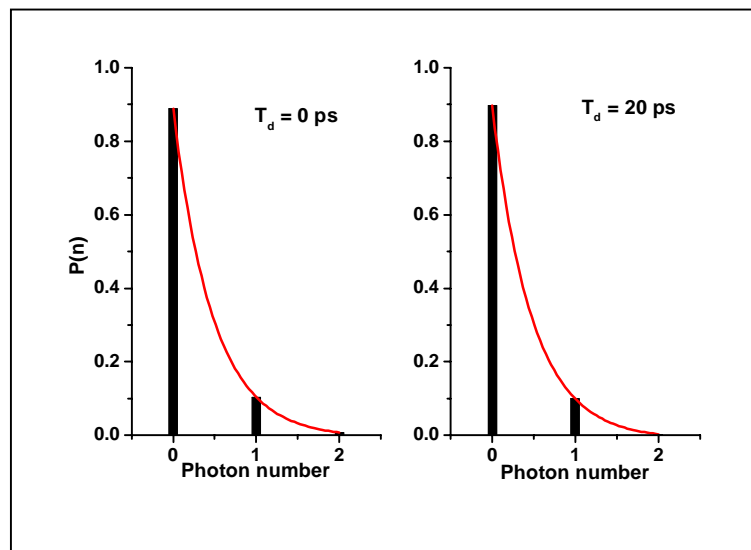statistics for the zero delay time for different measurements corresponding to decreasing excitation energy.

Fig. 3: *Photon-count distributions performed on the fluorescence bellow threshold (E=1µJ) for different time delays after the excitation*
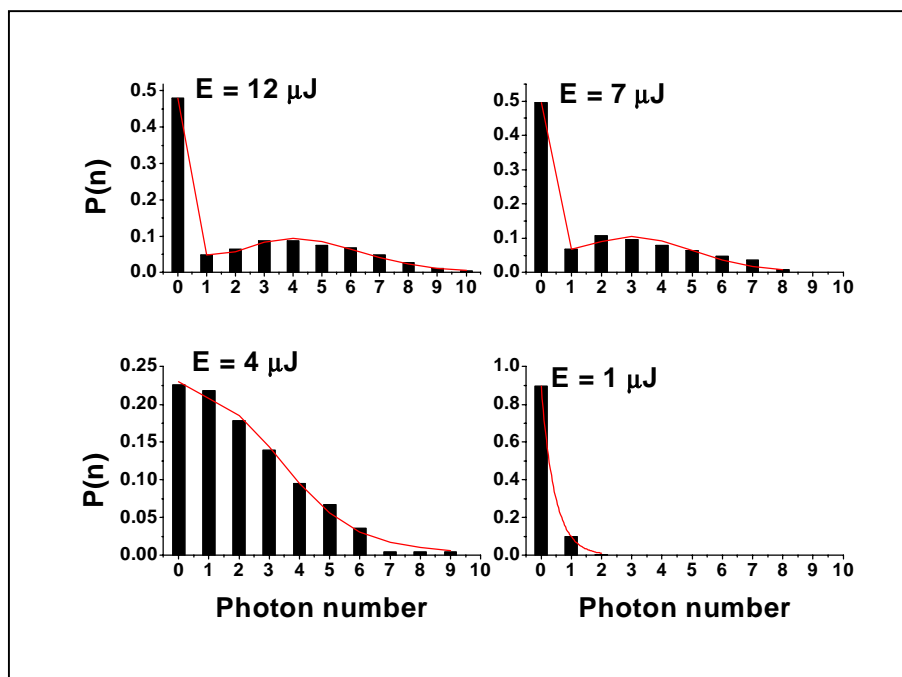

Fig. 4: *Photon-count distributions of the fluorescence for increasing excitation energies (1, 4, 7 and 12 µJ respectively). The distributions correspond to zero time delay.*

After fitting the curves with a linear superposition of a Poisson and a Bose-Einstein function, the percentages of the coherent and the incoherent component of the emitted light could be calculated. Figure 5 depicts these coherence percentages for different time delays with respect to the laser excitation and different laser excitation energies. For excitation energy 12 μJ and for zero delay time (T_d =0 ps) the coherent component corresponds to 51% of the total light, whereas after 100 ps the light is fully incoherent. This is an indication of the time needed for the total loss of coherence after laser excitation (de-phasing time). The coherence percentage increases fast as a function of laser excitation energy and reaches a plateau after about 7 μJ.
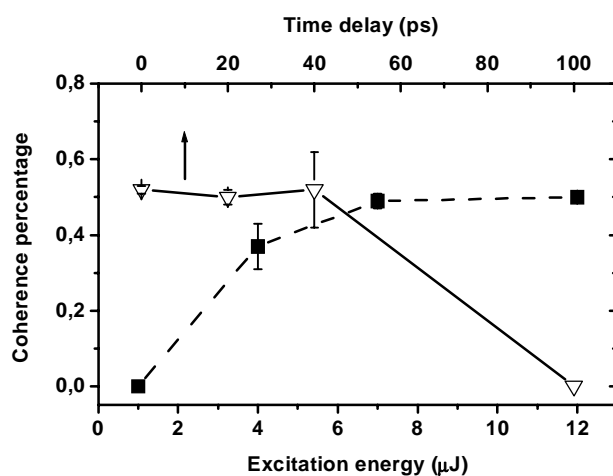
Fig. 5: *The coherent percentages of the photon-count distributions for different time delays (open triangles) and different excitation energies (solid squares), as calculated from the weight of the Poisson part of the fitting formula.*

In this study we demonstrated the emission of coherent light from random lasers. Even though the observed light was not purely coherent but rather a superposition of coherent and incoherent components, further refinements in the preparation procedure of the polymer matrices, with a more controlled construction, will improve also the observed photon statistics. The coherence of the fluorescence has yet to be observed when the host medium is a biological tissue. This will boost the efficiency of both the detection and photodynamic therapy of pathologic conditions at the cellular level.

References

1. N. M. Lawandy, R. M. Balachandran, A. S. L. Gomes and E. Sauvain, Nature **368**, 436 (1994)

2. V. S. Letokhov, Sov. Phys. JEPT **26**, 835 (1968)

3. W. L. Sha, C. H. Liu and R. R. Alfano, Opt. Lett. **19**, 1922 (1994)

4. R. M. Balachandran, N. M. Lawandy, Opt. Lett. **20**, 1271 (1995)

5. W. Zhang, N. Cue and K. M. Yoo, Opt. Lett. **20**, 961 (1995)

6. S. John and G. Pang, Phys. Rev. **A54**, 3642 (1996)

7. R. M. Balachandran, N. M. Lawandy, J.A. Moon, Opt. Lett. **22**, 319 (1997)

8. D. S. Wiersma, Ad Lagendijk, Phys. Rev. E **54**, 4256 (1996)

9. H. Cao, Y. G. Zhao, S. T. Ho, E. W. Seelig, Q. H. Wang and R. P. Chang, Phys. Rev. Lett. **82**, 2278 (1999)

10. P. W. Anderson, Philos. Magaz. B **52**, 505 (1985)

11. Sajeev John, Physics Today **44**, 32 (1991)

12. Th. M. Nieuwenhuizen, J. M. Luck, Phys. Rev. E **48**, 569 (1993)

13. G. Zacharakis, G. Heliotis, G. Filippidis, D. Anglos and T. G. Papazoglou, Appl. Opt. **38**, 6087 (1999)

14. R. Loudon, "The quantum theory of light", Second edition, Oxford Science Publishing, Oxford University Press, Oxford (1983)

Chapter 5

Coherent two-photon excited random lasing from highly scattering gain media

G. Zacharakis et al. Submitted to Physical Review A

We present the first experimental evidence of laser-like emission following two-photon excitation of dye agents in solid random gain media of biological significance. Excitation was performed with sub-picosecond laser pulses at 800 nm and emission (at 480 nm) was recorded with a spectrograph streak camera system. The coherent properties of the random lasing were also investigated by single photon counting. The proposed excitation-emission scheme would increase the efficiency of both the detection and photodynamic therapy of lesions, with minimized effect on healthy tissue.

I. **INTRODUCTION**

The detection of discontinuities inside turbid media, such as tumors inside biological tissue, has been the "holy grail" of biomedical imaging in recent years. However, it is well known that when light travels through turbid media it undergoes multiple random scattering events causing both the temporal and the spatial point-spread functions to broaden and altering the initial properties. Consequently, the imaging capabilities are degraded. Many techniques, including optical coherence

tomography, time gating and second harmonic generation tomography, have been used in the past in the attempt to boost imaging to the micrometer resolution range [1-3]. In addition, the remarkable observation, made by Lawandy [4] et al, of isotropic laser-like emission from optically pumped absorptive and scattering media, provided a starting point for the possible implementation of the so called random lasers in medical imaging. The very narrow temporal and spectral characteristics of this emission could boost the efficiency of tumor detection, if combined with the proper photosensitizer.

Here we report the first, to our knowledge, observation of laser-like emission from solid random media following two-photon excitation. The latter is expected to increase the spatial resolution of imaging due to the quadratic dependence of the emission on the input intensity, when combined with the spatially confined absorption of specific fluorophores in cancerous cells (two-photon laser scanning fluorescence microscopy) [5]. Furthermore, the long wavelength of the excitation photons results to deeper penetration, as well as to lower photobleaching of the fluorophores and to limited damage of the samples.

Recent experimental evidence suggests that the scatterers play the role of mirrors of the conventional laser cavity in order to provide the necessary feedback for laser action [6-11]. Simultaneously, several theoretical studies [12-17] have been made in order to provide models that will efficiently describe the behavior of such media and help to understand the underlying mechanisms that are responsible for the laser-like characteristics (temporal and spectral narrowing, coherence).

The behavior of random media enriched with organic dye molecules can be described with a four level laser model in which the effects of the diffusion of both the pumping and the emitted photons must be accounted for, as Wiersma and Lagendijk [14] have shown. A modified scheme is proposed below where the two-photon process is taken into account. The ground state (g) is pumped via two-photon absorption, onto the excited state (2), which immediately populates state (1). The laser transition takes place from state (1) to state (0), which in turn decays rapidly into the ground state. Assuming that states (2) and (0) are practically unpopulated a single rate equation is adequate for describing the system (figure 1). The coupled differential equations describing the behavior of the system in space and time is formed by two diffusion equations for the pump and emitted light (W_P and W_E are the corresponding

energy densities) and the rate equation for the concentration $N_1(\vec{r}, t)$ of molecules in the lasing state (1):
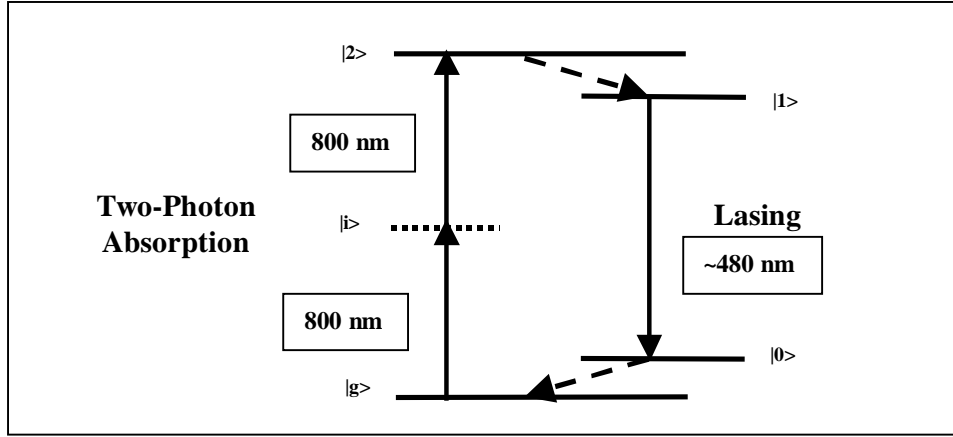

FIG. 1: *The four level scheme describing the two processes taking place inside the random laser material: the two-photon excitation (800 nm) and the laser action (480 nm).*

$$\dot{W}_P = D\nabla^2 W_P - \sigma_{abs}^{(2)} c [N_T - N_1] W_P^2 + \frac{1}{l} I_P \qquad (1)$$

$$\dot{W}_E = D\nabla^2 W_E + \sigma_{em} c N_1 W_E + \frac{1}{\tau_e} N_1 \qquad (2)$$

$$\dot{N}_1 = \sigma_{abs}^{(2)} c [N_T - N_1] W_P^2 - \sigma_{em} c N_1 W_E - \frac{1}{\tau_e} N_1 \qquad (3)$$

where c is the velocity of light inside the medium, l is the scattering mean free path, $\sigma_{abs}^{(2)}$ and σ_{em} are the two-photon absorption and single-photon emission cross sections respectively, τ_e is the life time of the excited state (1) and N_T is the total concentration of dye molecules. D is the diffusion constant and I_P is the pump pulse intensity. In this case the dependence of the emitted intensity is expected to be quadratic to I_P. The numerical solution of the above set of equations could in principle give all relevant information on the spatial and temporal distribution of the energy densities of the pump light and of the random lasing.

II. EXPERIMENT

The source of the ultra-short laser pulses (200 fsec) was a mode-locked Ti:Sapphire laser emitting at 800 nm with a repetition rate of 82 MHz, pumped by the

second harmonic of a Spectra Physics diode pumped Nd:YAG laser. The pulses were amplified with a regenerative amplifier system with a repetition rate of 1 KHz. After focusing the beam on the samples a spot size of 0.15 mm^2 was formed. The energy/pulse was controlled by a neutral density filter wheel and varied from 50 to 150 μJ. The resulting fluorescence signal was collected by appropriate optics and focused on the entrance slit of a 0.10 m spectrograph. The spectrally resolved signal was imaged on the entrance slit of a Hamamatsu C 5680 Streak Camera for temporal analysis (maximum temporal resolution of 2 psec). The spectral observation window was approximately 100 nm, with a spectral resolution of the order of 1 nm. A Peltier-cooled CCD camera, operating at -50°C for reduced dark noise, was used for the recording of the signals [9].
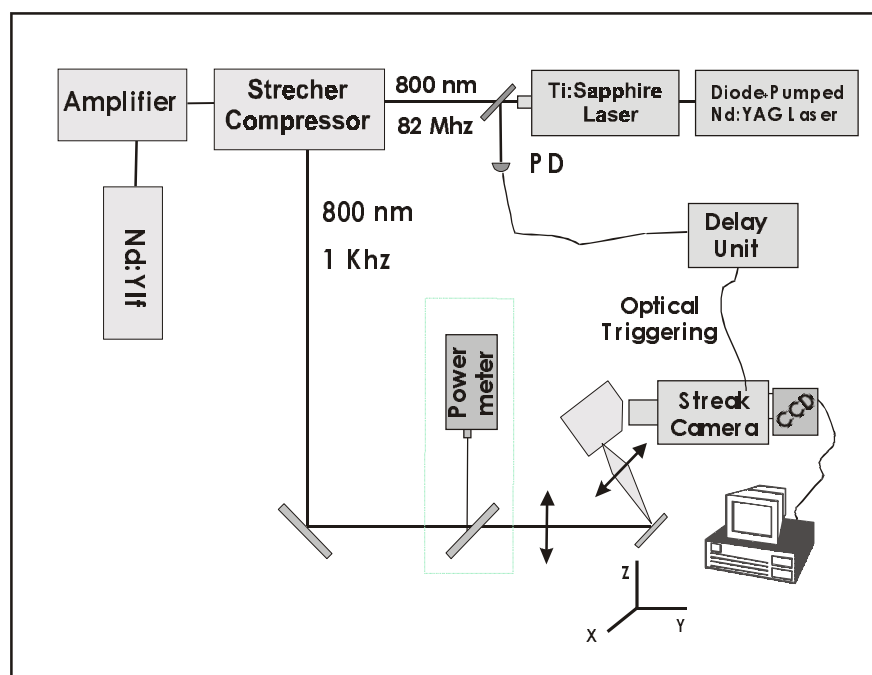
Fig. 2: Experimental setup for two-photon excitation of random lasers

Scattering samples containing Coumarin 307 were made in a form of 1x1x1 cm gelatin cubes. Two stock solutions (4x10^{-3} M and 1.33x10^{-3} M) of Coumarin307 (Lambda Chrome Dyes) in ethanol and a series of stock suspensions of TiO_2 (Du Pont, Ti-Pure R-900, average particle diameter 400 nm) in water, containing from 1-40 mg/ml TiO_2 powder, were prepared. To obtain the gel base of the sample, 0.45 ml of appropriate stock suspension was added to 0.1 g of gelatin (Sigma G-2500). Then

the mixture was melted in a water bath at 50-60 ^{o}C under intense stirring. 0.45 ml of appropriate Coumarin solution was added just before casting the mixture into a Teflon mold. According to the size and the concentration of the particles used, the scattering mean free path is calculated ($l_s = 4\pi/n\sigma$) in the order of tens of micrometers [15]. The concentration of the Coumarin 307 ($\sim10^{-3}$ mol/lt) corresponds to an absorption length at 400 nm in the order of 1 mm (measured in methanol solution).

III. DISCUSSION

The simultaneous spectro-temporal narrowing can be clearly seen in figure 3, where the fluorescence response of the Coumarin307 dye dissolved in Ethanol solution (3a) is compared with its response when it is embedded in the Gelatin matrix (concentrations 2×10^{-3} M and 1.8×10^{-3} M) in the presence of titania particles (3b).
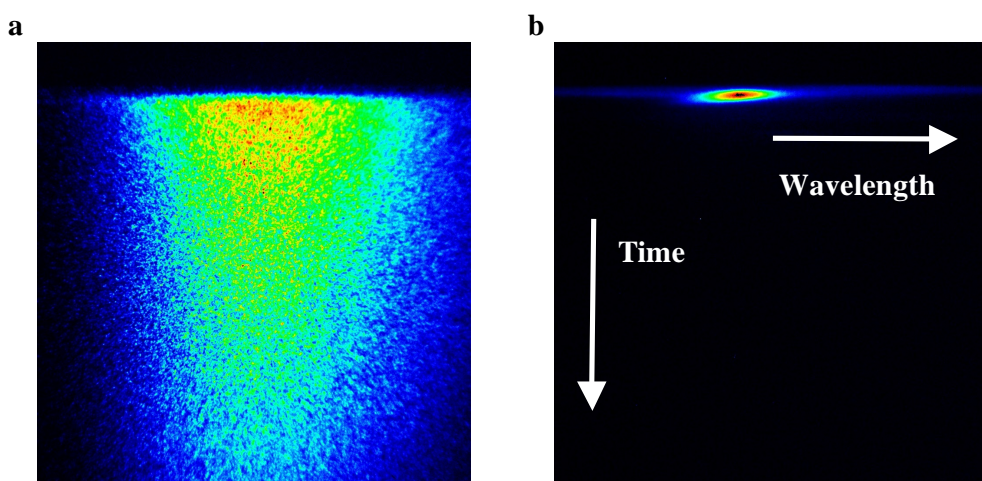
FIG. 3: a) Fluorescence emission of Coumarin 307 in ethanol solution (C= 2x10^{-3} M) and b) in Gelatin with high concentration of titania scatterers (10.8x10^{10} cm^{-3}). The overall length of the horizontal axis corresponds to 100nm spectral range whereas the vertical temporal axis covers 6.5 nsec.

Characteristic temporal and spectral profiles obtained from the streak images are shown in figures 4a and 4b respectively. The different curves correspond to the pure dye solution and to gel samples with different scatterers' concentration. In the case of the solution the narrowing effect is not observed and a single exponential fitting provides the decay time of 4.5 ns, which is characteristic of Coumarin 307. On the other hand, in the case of the gel samples and for pumping energy above threshold,

the narrowing effect is very strong, with the calculated decay times being two orders of magnitude shorter. For the highest concentration of scatterers (10.8×10^{10} cm^{-3}) the FWHM of the recorded fluorescence pulse is 20 ps, which is comparable to the duration of the recorded laser pulse, namely the instrument's response function. Furthermore, when stimulated emission is taking place, the rising slope is much steeper, resulting from the faster onset contrasted to the spontaneous emission.
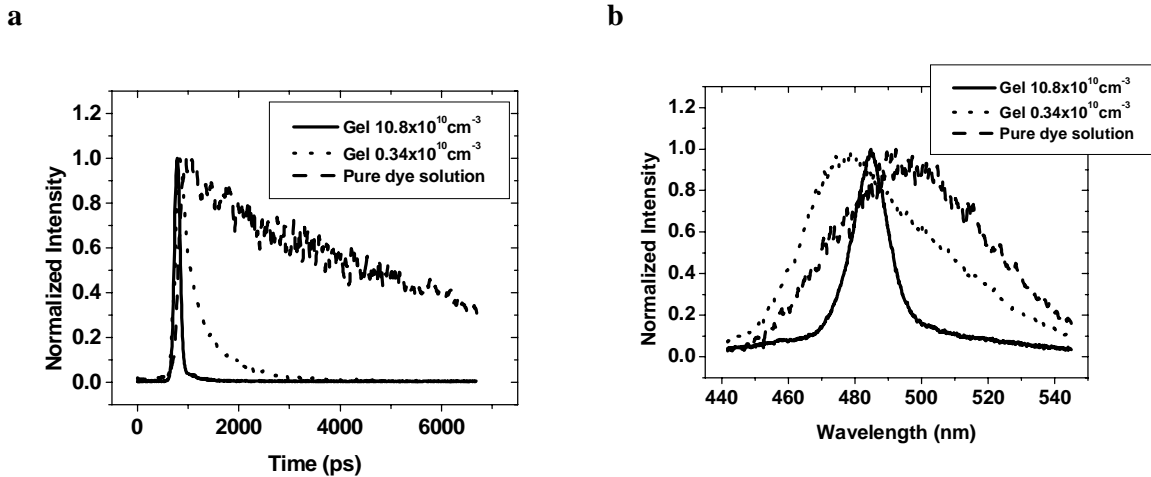
a   **b**

FIG. 4: **a)** *Fluorescence decay curves recorded on pure Coumarin 307 solution (C = 2x10^{-3} M) and on scattering gelatin samples (C = 1.8x10^{-3} M) with two different scatterers concentrations and **b)** the corresponding fluorescence spectra.*

In figure 4b the corresponding spectral distribution curves for the solution and the gel samples under various pumping intensities are depicted. The FWHM of the curve corresponding to the sample with the highest concentration of scatterers (10.8×10^{10} cm^{-3}) is calculated with a Gaussian fitting to be 8 nm. It's worth noticing that the FWHM of the pump laser spectrum is about 10 nm. The width for the pure dye solution is 53 nm. These results are in good agreement with previously published work, concerning both liquid and solid (i.e. polymer) samples, which underwent one-photon excitation [6-9].

The observed response, which is believed to be similar to lasing action, can be interpreted in terms of the increased photons' path length inside the medium as they undergo multiple scattering events. Consequently, the contribution of stimulated emission is increased and when the amplification of the fluorescence light overcomes

a critical value, the observed fluorescence signal collapses in both temporal and spectral domains [18].

    The dependence of the temporal and spectral widths on the excitation energy is depicted in figure 5. The points correspond to measurements obtained under varying pumping energies, ranging from 50-150 μJ. By performing a simple sigmoidal fitting, the threshold energy (60 μJ), can be extracted. The higher threshold energy compared to the one-photon case can be attributed to the consequences of the two-photon excitation. The low absorption cross-section as well as the smaller pumping volume can be thought of the reasons for this behavior, since higher energy is required to overcome the losses of the microcavities.
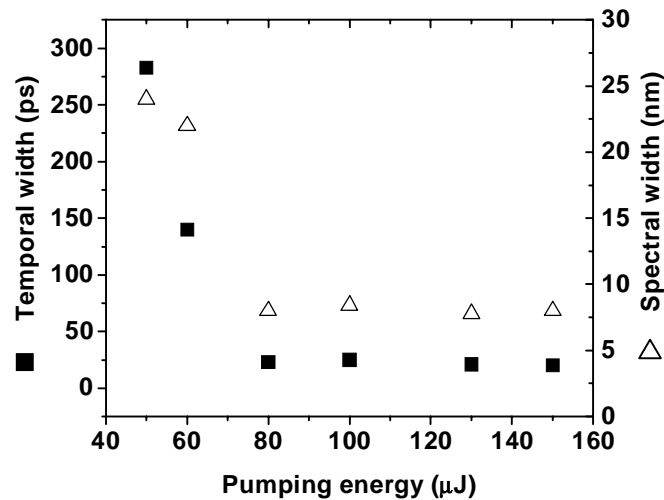
FIG. 5: *The dependence of the temporal and spectral width of the laser-like emission on different excitation intensities. The threshold energy (60 μJ) can be extracted by sigmoidal fitting. The square points correspond to temporal width while triangles to spectral width.*

    Thereafter, the coherent properties of the random lasing action were investigated. To do that, photon counting measurements were performed, exploiting the capabilities of the detection system and photon count distributions were then created [19]. In this case a 50 fs Ti:Sapphire laser system was used. Different distributions are characteristic of different light [19-21]. The Poisson statistics are characteristic of coherent, whereas Bose-Einstein statistics are characteristic of incoherent light. In figure 6 the photon count distribution obtained after two-photon excitation above threshold is depicted. The solid line corresponds to the theoretical

fitting performed by an equation, which linearly combines a Poisson and a Bose-Einstein function:

$$P(n) = a \frac{\langle n \rangle^n e^{-\langle n \rangle}}{n!} + (1-a) \frac{\langle n \rangle^n}{\left[1 + \langle n \rangle\right]^{n+1}} \qquad (4),$$

where n is the photon number and α a constant representing the weight of the coherent component of the fit.
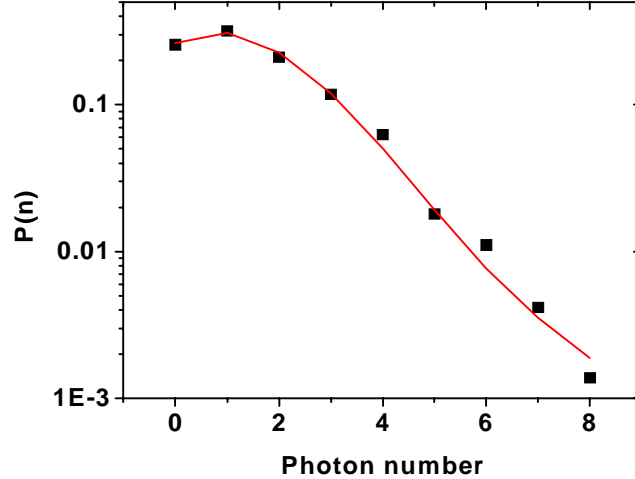

FIG. 6*: Photon statistics of the two-photon excited random lasing above threshold (60 μJ). The square dots correspond to the experimental points and the solid line to the best fit of equation (4) to the experimental data resulting to a 75% contribution of coherent light.*

Thus, the coherent percentage of the recorded light can be obtained. The coherence of the random lasing light is destroyed by the intense scattering undergone by the photons during their propagation outwards from the pumping volume and from the competition of different lasing modes emitted from different microcavities [22]. For zero delay time after the excitation and for a time window of Δt=50 ps, the coherence percentage above the threshold is calculated to be α = 0.75. This value is higher than previously published, because of the two-photon process and the emission of the photons from deeper regions inside the active medium [19]. For longer delay times the coherent percentage is decreased (0.63 for delay time 150 ps). The corresponding coherent percentage below the threshold excitation energy approaches zero, indicating the transition to non-coherent light.

IV. CONCLUSIONS

Random lasing action after two-photon excitation was demonstrated for the first time and the coherent properties of the emitted light have been studied. The need for two-photon excitation of random lasers is raised from the fact that the excitation is made using light with longer wavelength than the emitted one and from the nonlinear (quadratic) dependence of the emitted on the pumping intensity. The use of near infrared wavelength consequently and most importantly provides the necessary penetration inside the strongly scattering media, as well as negligible photobleaching and phototoxication of tissue due to the low energy of the photons. The non-linearity insures that the effect will be confined only on the focal region, thus improving the spatial resolution by minimizing the out of focus fluorescence.

Further experiments are currently underway to complete the study of the possible implementation of two-photon excitation, in reference to the spectrally and temporally narrow fluorophore emission in a highly scattering environment, in a large number of applications. These include imaging of tumors inside biological tissue, two-photon laser scanning microscopy and various applications in photochemistry and photobiology, such as structural mapping of intracellular membranes. Furthermore, it will by far improve the efficiency of the destruction of different types of cancerous cells, based on the localized action of the agents and the deeper penetration of the NIR pump photons in the tissue under treatment.

References

1.   F. Liu, K. M. Yoo, R. R. Alfano, *Opt. Lett.* **19,** 740 (1994)

2.   J. C. Hebden, D. T. Delpy, *Opt. Lett.* **19,** 311 (1994)

3.   M. S. Patterson, B. Chance, B. C. Wilson, *Appl. Opt.* **28**, 2331 (1989)

4.   N. M. Lawandy, R. M. Balachandran, A. S. L. Gomes, E. Sauvain, *Nature* **368**, 436 (1994)

5.   W. Denk, J. H. Strickler, W. W. Webb, *Science* **248**, 73 (1990)

6.   W. L. Sha, C. H. Liu, R. R. Alfano, *Opt. Lett.* **19**, 1922 (1994)

7.   M. Siddique, R. R. Alfano, G. A. Berger, M. Kempe, A. Z. Genack, *Opt. Let.* **21**, 450 (1996)

8.   R. M. Balachandran, N. M. Lawandy, *Opt. Lett.* **20**, 1271 (1995)

9.   G. Zacharakis, G. Heliotis, G. Filippidis, D. Anglos and T. G. Papazoglou, *Appl. Opt.* **38**, 6087 (1999)

10.   H. Cao, Y. G. Zhao, S. T. Ho, E. W. Seelig, Q. H. Wang and R. P. H. Chang, *Phys. Rev. Lett.* **82**, 2278 (1999)

11.   H. Cao, J. Y. Xu, D. Z. Zhang, S. H. Chang, S. T. Ho, E. W. Seelig, X. Liu and R. P. H. Chang, *Phys. Rev. Lett.* **84**, 5584 (2000)

12.   V. S. Letokhov, *Sov. Phys. JEPT* **26**, 835 (1968)

13.   S. John, G. Pang, *Phys. Rev.* **A54**, 3642 (1996)

14.   D. S. Wiersma, A. Lagendijk, *Phys. Rev.* **E54**, 4256 (1996)

15.   Th. M. Nieuwenhuizen, J. M. Luck, *Phys. Rev.* **E48**, 569 (1993)

16.   S. John, *Physics Today* **44**, 32 (1991)

17.   X. Jiang, C. M. Soukoulis, *Phys. Rev. Lett.* **85**, 70 (2000)

18.   Diederick Wiersma, *Nature*, **406**, 132 (2000)

19.   G. Zacharakis, N. A. Papadogiannis, G. Filippidis and T. G. Papazoglou, *Opt. Lett.* **25**, 923 (2000)

20.   R. Loudon*, "The quantum theory of light", Second edition, Oxford Science Publishing, Oxford University Press, Oxford (1983)*

21.   H. Cao, Y. Ling, J. Y. Xu, C. Q. Cao and P. Kumar, *Phys. Rev. Lett.* **86**, 4524 (2001)

22.   Q. Li, K. M. Ho, C. M. Soukoulis, *Physica B* **296**, 78 (2001)

7. Recent developments

7.1 Optical characterization of breast cancer

In Chapter 6.1 the optical properties of different types of female breast tissue were calculated. The tissues under investigation were adipose and fibrous tissues obtained from biopsy operations. However, only very recently was possible to measure the point-spread functions of female breast cancer tissue and calculate the optical properties [see references of Chapter 6.1]. This would complete the study for the mapping of the absorption and scattering coefficients of different types of cancer. The difficulty relies on the fact that it is rather hard to obtain cancer tissue samples since the diagnosis of the patient is based on the histology of the samples. Consequently, the samples, which were possible to obtain from the excision, had a limited size and thus it was very difficult to acquire the appropriate diffusive data, on which the theory is based on for the calculation. In figure 7.1 a typical plot of the intensity versus time of the transmitted laser pulse is depicted along with the theoretical fitting with the Patterson formula (see Section 4 and Chapter 6.1). The study concerned five (5) cases in total, two neoplasms and three tumors. Values for scattering coefficient of 0.55 mm^{-1} and for absorption coefficient of 0.178 mm^{-1} were obtained. However, the calculated values of the coefficients were not reliable since the data were far from being diffusive. Nevertheless, the study is continued concentrated on obtaining as thick samples as possible without risking the patients health and improving the theory used for the fitting of the curves.
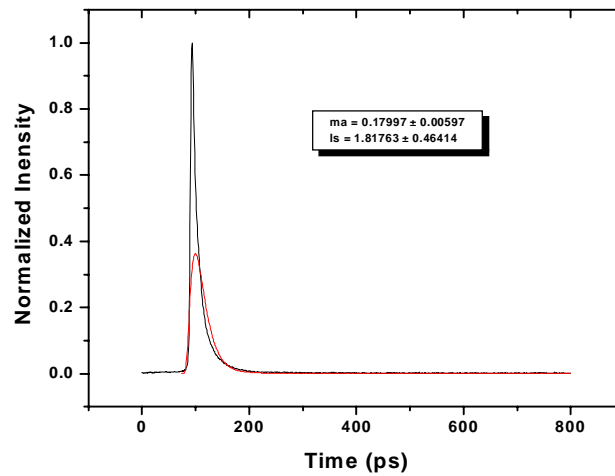
Fig.7.1: The temporal spreading of the transmitted pulse through neoplasm female breast tissue and the theoretical fitting with the Patterson formula, which calculates the absorption and scattering coefficients.

7.2 Random lasing from animal and human tissue

Random lasing in highly scattering gain media has been extensively studied in the contents of this thesis and elsewhere [see references of Chapters 6.3-6.5]. These studies concerned turbid material in which the scattering properties were induced by well-defined particles, such as TiO_2 or ZnO. Yet, what would happen if the scattering originated from physical turbid media, such as biological tissue [1,2]? The temporal and especially the spectral narrowing of the emission would definitely assist the development of both detection and Photodynamic Therapy in combination with biocompatible fluorophores, which are selectively absorbed by cancer tumors. When these fluorophores are injected in the patient's body and if they are excited with the proper laser, a spectral narrow beacon like source is created increasing the contrast of imaging. A more realistic application would be the creation of different types of self-attached patches with different random lasing material for different types of skin cancer or other superficial lesions. Excitation of these materials with the same laser source gives the right radiation for each type of disease.

This was attempted by diffusing standard laser dyes in animal (chicken) and human tissue (adipose and fibrous female breast tissue). The initial results were

encouraging but not satisfactory since only temporal narrowing was observed and not the more important for the medical applications spectral one. In figure 7.2 the decay of the emission of R6G in ethanol is compared with the emission when it is embedded in human adipose breast tissue. Even though the narrowing is evident it is not as dramatic as in the cases discussed in the previous chapters and most importantly it is not accompanied by spectral narrowing.
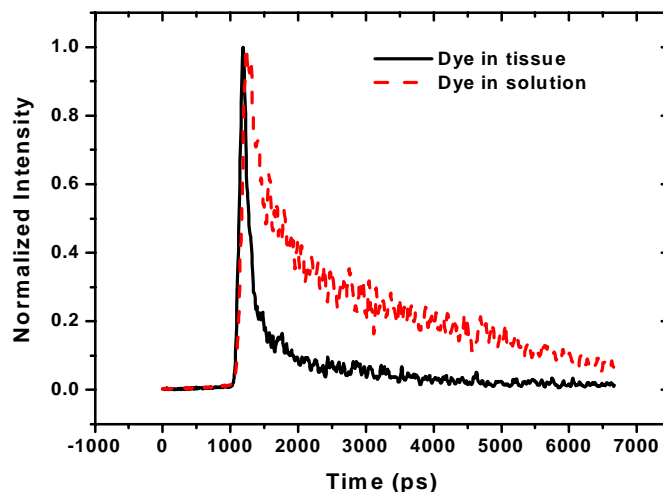
Fig. 7.2: Emission of R6G embedded in human adipose female breast tissue compared with the corresponding emission from R6G ethanol solution.

Results from other research groups report both temporal and spectral narrowing from animal (chicken breast) tissue infused with laser dyes, but there is no complete study related to human tissue with biocompatible fluorophores. With the possible applications being very important the need for an intensive study on random lasing from biological tissue is very demanding.

7.3 Second harmonic generation in random lasers

Random lasing and second harmonic generation after two-photon excitation was observed for the first time, in both scattering and amplifying polymer samples. Pumping was performed with sub-picosecond laser pulses at 830 nm and the emission, was observed with a spectrograph streak camera detection system for

simultaneous recording of spectral and temporal features. SHG was detected at 415 nm and random lasing at 470 nm. The advantages of two photons absorption are discussed because of its enhanced detection efficiency and minimized effects on the irradiated sample (e.g. healthy tissue surrounding tumors) [3-8].

The source of the 200 fsec pulses was a mode-locked Ti:Sapphire laser emitting at 800 nm, pumped by the second harmonic of a Spectra Physics diode pumped Nd:YAG laser operating with a power of 5 W. The repetition rate of the Ti:Sapphire oscillator was 82 MHz with an average power of ~1 W. The pulses were amplified with a regenerative amplifier system with a repetition rate of 1 KHz. This beam was focused on the samples forming a spot size of 0.15 mm^2. The average power was controlled by a neutral density filter wheel and varied from 10 to 150 mW. The resulting fluorescence signal was collected by appropriate optics and focused on the entrance of a 0.10 m spectrograph. The spectrally resolved signal was focused on the entrance slit of a Hamamatsu C 5680 Streak Camera, with a maximum temporal resolution of 2 psec. The effective width of the photocathode (6 mm) resulted to a spectral observation window of approximately 100 nm, with a spectral resolution of the order of 1 nm.

Scattering samples containing Coumarin 307 were made in a form of 1x1x0.1cm PMMA polymer sheets. The particle concentration (0.34x10^{10} cm^{-3} to 10.8x10^{10} cm^{-3}) corresponded to a scattering mean free path of the order of tens of micrometers. The concentration of the dye was varied from 0.6x10^{-3} M to 1.8x10^{-3} M and corresponded to an absorption length of the order of 1 mm (measured in a methanol solution).

Figure 7.3 shows the temporal curves of both the SHG and the fluorescence signal. The fluorescence was recorded at around 470 nm and the second harmonic at 415 nm (fundamental 830 nm). The temporal width of the fluorescence decay was around 1.5 ns and that of the second harmonic 125 ps. The corresponding spectral width was 40 nm and 12 nm respectively. In this case the narrowing of the fluorescence was not dramatic because of the loss of photons in favor of the SHG, which reduced the energy provided for the random lasing. The non-linear dependence of the SHG could be confirmed by recording the signal under different excitation energies and by plotting the integrated (in time and wavelength) intensity versus the excitation intensity. The dependence was quadratic, as expected for the two-photon process, for the low excitation intensities (below 50 mW), but gradually it reached a

plateau. This saturation effect might indicate a compromise between the two processes since the random laser was beginning to exceed the threshold energy (~ 60 mW) for lasing action. However, the above-described proof could not be performed for the fluorescence signal since it was rather difficult to integrate the intensity distribution from the image. However, the spectral region that it was observed (470 nm) confirmed the two-photon absorption.
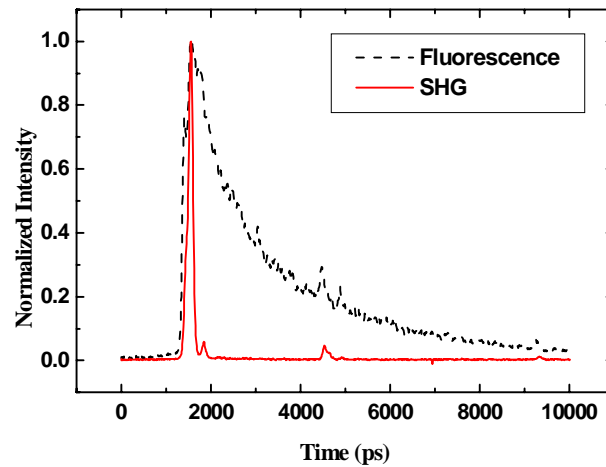
Fig. 7.3: *Temporal curves of SHG and fluorescence signals*

The study of nonlinear properties of random media such as biological tissue is of particular interest in a potential use of light for either detective or therapeutic purposes in various biomedical applications [9-11]. The possibility of generation of UV light after intense laser irradiation of tissue and the risk of malignancies generation is also justifying the extensive study of SHG from random media. Nevertheless, harmonic generation appears to be a potentially new approach for detection of structural differences of biological tissues used for optical histology.

References

1. M. Siddique, L. Yang, Q. Z. Wang, R. R. Alfano, *Opt. Comm.* **117**, 475 (1995)

2. L. Wang, D. Liu, N. He, S. L. Jacques, S. L. Thomsen, *Appl. Opt.* **35**, 1775 (1996)

3. V. E. Kravtsov, V. M. Agranovich and K. I. Grigorishin, *Phys. Rev. B* **44**, 4931 (1991)

4. J. I. Dadap, J. Shan, K. B. Eisenthal and T. F. Heinz, *Phys. Rev. Lett.* **83**, 4045 (1999)

5. M. A. Noginov, S. U. Egarievwe, N. Noginova, J. C. Wang, H. J. Caulfield, *J. Opt. Soc. Am. B* **15**, 2854 (1998)

6. J. Martorell, R. Vilaseca, R. Corbalan, *Phys. Rev. A* **55**, 4520 (1997)

7. N. Yang, W. E. Angerer and A. G. Yodh, *Phys. Rev. Lett.* **87**, 103902-1 (2001)

8. J. F. de Boer, A. Lagendijk and R. Sprik, *Phys. Rev. Lett.* **71**, 3947 (1993)

9. Y. Guo, P. P. Ho, A. Tirksliunas, F. Liu and R. R. Alfano, *Appl. Opt.* **35**, 6810 (1996)

10. Y. Guo, P. P. Ho, H. Savage, D. Harris, P. Sacks, S. Schantz, F. Liu, N. Zhadin and R. R. Alfano, *Opt. Lett.* **22**, 1323 (1997)

11. V. Ying, F. Liu, R. R. Alfano, *Appl. Opt.* **38**, 224 (1999)

8. Conclusions – Future goals

At the end of this thesis the conclusions from the different studies discussed in the preceding chapters will be presented. These results could also be found at the conclusive part of each paper. In the last section some thoughts of the future goals of the study will be brought forward as well as the general trends of the optical tomography and random lasing related research.

Calculation of optical parameters

It was shown that using as criterion the reduced scattering coefficient, the discrimination between lipid and fibrous tissue was possible since a different range of values corresponded to the two types of tissue studied here. For the lipid tissue the values lid in the interval [0.43 - 0.64] mm^{-1} and for the fibrous tissue in the interval [0.71 - 1.1] mm^{-1}. Values, which, were between the two distributions, were assumed to correspond to tissue with different percentage of fat and fiber. This classification was based on the corresponding histologic analysis. The same method could also be used for the discrimination of the other components of the breast. This has been shown in Chapter 7, where the recent measurements and calculations of the optical parameters of cancerous tissue are presented. The study continues with all the types of tissue that the female breast comprises of.

The result was the discrimination between lipid, fibrous and benign tissue with the latter being a sensitive indicator of the presence of a histological deviation (precancerous lesion, benign or malignant tumor). This could lead to a non-invasive technique, which may eventually operate synergistically with biopsy, which requires the extraction of tissue sample from the patient. Optical topography, meaning calculation of the scattering coefficient in specific and very distinct positions of the tissue, could assist in achieving that goal.

A different approach was used for the problem of calculating the optical parameters of biopsy samples with limited size, where the diffusion theory cannot be applied. Ultra-fast laser pulses transmitted through excised human breast tissue have been detected by a streak camera. Experimental data of the temporal spread of the ultra-fast pulse during the transmission through the tissue have been analyzed using the Laguerre expansion technique. This method treats the medium of propagation as a "black box system" and using data sets of incident – transmitted pulse it relates to this system a set of coefficients as well the first order system kernels. The grouping of the corresponding kernels appear to be related to both the different time-spreading of the pulses as they propagate through different tissue and also due to the different time-delay of the laser pulse as it propagated through the two different types of tissue. The main discriminatory feature of the "lipid kernels" is the wider range of their values in both the positive and negative direction of the y-axis. In addition the 0th and 1st order Laguerre expansion coefficients for the two main groups of tissue (lipid vs. fibrous) were calculated to be $c(0) = 0.38 \pm 0.01$, $c(1) = -2.56 \pm 0.24$ for lipid and $c(0) = -0.27 \pm 0.03$, $c(1) = -1.83 \pm 0.14$ for fibrous tissue respectively. In conclusion it has been shown that the Laguerre expansion technique can identify fibrous and lipid tissue from analysis of the temporal point spread functions of the transmitted ultra-fast laser pulse.

One- and two- photon excited random lasing

A significant part of this thesis concerned the new and fascinating field of highly scattering gain media and the study of their behavior. Especially the study of the behavior of the emission of various fluophores embedded in highly scattering matrices. The observed fluorescence signal of the fluophore quenches in both temporal and spectral domains due to the intense scattering that the photons undergo.

This happens when the excitation energy reaches and exceeds a threshold value. Above that value the narrowed fluorescence exhibits the same features as the excitation laser pulse. Lifetime in the order of 50 psec and spectral FWHM in the order of few nanometers were observed. For energies bellow the threshold value the amplification is negligible and the samples behave exactly as those without scatterers. As the excitation energy increases the laser action requirements are fulfilled and the sudden narrowing takes place.

Similar studies are underway when various fluorophores are embedded in biological tissues. The final goal is to take advantage of this effect towards a more spatially and spectrally confined agent in Photodynamic Therapy of target tissue lesions on skin or other types of superficial lesions. Very promising in the field of skin PDT would be thin polymer sheets with various dyes, which could be applied directly on the lesion and allow the selection of different irradiation wavelengths using the same laser as excitation source. Thus, improving by far the efficiency of the destruction of different types of cancerous cells.

The absence of saturation, the very narrow emission spectrum and the instantaneous response of photonic polymers make them very versatile in many applications, in addition to PDT. Some of them are photonic marking for identification purposes (photonic codes, search and rescue missions, military applications, marking of hazardous material), substitution of ordinary lasing media in dye lasers and boosting the emission of LEDs and diode lasers in the blue region of the spectrum (if used with electro luminescent polymers). A lot of effort is also put in the study of dye infiltrated opal photonic crystals and the light emitted from such a simultaneously ordered (crystal structure) and disordered (random photons' path) structure.

Random lasing action after two-photon excitation was also demonstrated for the first time and the coherent properties of the emitted light were studied. The need for two-photon excitation of random lasers is raised from the fact that the excitation is made using light with longer wavelength than the emitted one and from the nonlinear (quadratic) dependence of the emitted on the pumping intensity. The use of near infrared wavelength consequently and most importantly provides the necessary penetration inside the strongly scattering media, as well as negligible photobleaching and phototoxication of tissue due to the low energy of the photons. The non-linearity

insures that the effect will be confined only on the focal region, thus improving the spatial resolution by minimizing the out of focus fluorescence.

Further experiments are currently underway to complete the study of the possible implementation of two-photon excitation, in reference to the spectrally and temporally narrow fluorophore emission in a highly scattering environment, in a large number of applications. These include imaging of tumors inside biological tissue, two-photon laser scanning microscopy and various applications in photochemistry and photobiology, such as structural mapping of intracellular membranes. Furthermore, it will by far improve the efficiency of the destruction of different types of cancerous cells, based on the localized action of the agents and the deeper penetration of the NIR pump photons in the tissue under treatment.

Photon statistics

The next step in the study of random lasing materials was the study of the coherent properties of the emitted light. The excitation source was a frequency doubled 200 femtosecond pulsed laser emitting at 400 nm. Spectral and temporal features were simultaneously recorded using a spectrograph and a streak camera operating on the photon counting mode. Photon number distributions were thus created. The temporal coherence of the laser-like emission above and bellow the excitation energy threshold has been investigated from the photon number distribution obtained. Even though the observed light was not purely coherent but rather a superposition of coherent and incoherent components, further refinements in the preparation procedure of the polymer matrices, with a more controlled construction, will improve also the observed photon statistics. The coherence of the fluorescence has yet to be observed when the host medium is a biological tissue. This will boost the efficiency of both the detection and photodynamic therapy of pathologic conditions at the cellular level.

Acknowledgements

When I started my thesis I thought that it would be fun doing research, setting up experiments and trying to make them work. However, during the course of the thesis I found out that it was much more difficult than I believed in the beginning. In fact to my opinion it must be one of the most frustrating jobs of all. However, there are few exceptions that can make you the happiest person on earth. These are the absolutely thrilling moments of obtaining the results that you have for very long expected. And during these years dedicated to the thesis many people would have helped in completing the projects. So I would like to take this opportunity to express my gratitude and appreciation to them.

Prof. Eugenios Koumantakis for accepting to be my supervisor and his kindness and consideration throughout my thesis whenever I needed his guidance and knowledge.

Prof. Costas Fotakis because I understood in the end that he had believed in me from the first beginning. Or at least this is how I want to believe his sternness and his strictness when dealing with me. I see now that it was him that kept me on the right track, even though some times it was hard to keep up with his demands and his standards.

Dr. Theodore Papazoglou for giving me the opportunity to start and finish this project, his guidance during these years and all the opportunities he gave me to come in contact with the scientific community. I appreciated his calmness even on my most stupid acts. He taught me not only how to address the physical problems we encountered during the experimental work, but also how to cope with the scientific

environment. I consider him to be my mentor and as I would like to believe a very good friend.

Prof. Demetrios Tsiftsis for his really valuable and constructive guidelines on the medical part of my thesis.

Dr. Costas Kalpouzos for asking me the most astonishing question of all. He really gave me a whole new perception of the physical problem I had to deal with. Not to mention his help with almost every problem I encountered during my thesis. I really enjoyed our discussions.

Dr. Nektarios Papadogiannis for his pioneering ideas for new experiments and his help on understanding uncharted physical concepts. A large part of this thesis would not have been completed without his valuable contribution.

Dr. Demetrios Anglos for his help during the experiments and his unique perception on setting up experiments and giving the right solutions in difficult situations.

Dr. George Filippidis for three amazing years and his support inside and outside the lab and for the two even more amazing and thrilling trips to London. The gap during his absence was irreplaceable. I consider him as the soul of our group and a great friend and companion.

Dr. Jorge Ripoll for showing me what research really means and for making me understand how much I enjoy doing that.

Dr. Elias Sanidas for supplying the tissue samples and for the valuable guidance in the clinical part of the project.

Aggeliki Zolindaki for supplying tissue samples but also for many discussions that opened up my eyes on many subjects.

Antonis Mavromanolakis for the photon counting code and many fruitful discussions on Physics and more.

Anna Karaiskou for always trying to wake up my ego and my will to continue and to be more productive. But most of all for not letting me compromise. She was my greatest inspiration and my most exciting adventure. So far…

My friends Anna and Manolis S., Manolis G., Antigoni M., Katerina and Elleni A. for being there for me and for their patients during the long periods of my disappearance.

My mother for her love and support during very hard periods and for always being there for me.

CURICULLUM VITAE

PERSONAL INFORMATION

Given Name:	**Giannis**
Surname:	**Zacharakis**
Date of Birth:	May 3rd 1973
Nationality:	Greek
Home Address:	3rd Kyllinis str., GR-713 05, Heraklion Crete Greece Tel. ++30-81- 252278
Business Address:	Laser and Applications Division Institute of Electronic Structure and Laser Foundation for Research and Technology Hellas P.O. Box 1527, Heraklion 711 10 Tel. ++30-81-391332, 391315 FAX. ++30-81-391318 e-mail : zahari@iesl.forth.gr

EDUCATION

1997	B.Sc. in Physics, Department of Physics, University of Crete
Jun. 1994-Jul. 1994	7th Summer School of Advanced Physics, University of Crete
Jun. 1995-Jul. 1995	8th Summer School of Advanced Physics, University of Crete
Oct. 1994-Oct. 1995	Diploma Thesis, Biomedical Applications Group, IESL - FORTH *"Monte Carlo Modeling of Light Transport through Turbid Media"*
May 1998 – Feb. 2002	Ph.D. Scholar, School of Medical Sciences, Department of Medicine, University of Crete

RESEARCH ACTIVITIES-SCHOLARSHIPS

1992	Undergraduate Scholarship - Hellenic Foundation for Academic Scholarships

Oct. 1995 - Jun.1996	Erasmus Undergraduate Scholarship, Atomic Hydrogen Group, Van der Waals - Zeeman Laboratory, University of Amsterdam
Sept. 1996-Dec. 1996	Laboratory Assistant, Biomedical Applications Group, IESL-FORTH
Jan. 1997 - May 1998	Training Fellowship, Biomedical Applications Group, IESL-FORTH

RESEARCH EXPERIENCE

- Light-Tissue Interaction Modeling (Monte Carlo Method)
- Laser Cooling and Trapping of Atoms
- Laser Induced Fluorescence Spectroscopy (LIFS) for medical diagnostics
- Photodynamic Therapy
- Optical Tomography with Visible and Infrared Laser Light
- Optical characterization of tissue
- Time Resolved Fluorescence Spectroscopy
- Time Resolved Photon Statistics
- Optical Tweezers
- Random Lasers

PUBLICATIONS

The author has published 9 articles in international refereed journals and 15 articles in peer reviewed conference proceedings.

LIST OF PUBLICATIONS

1. G. Filippidis, **G. Zacharakis**, A. Katsamouris, A. Giannoukas, M. Kouktzela, T. G. Papazoglou, "*Effect of liquid nitrogen and formalin -based conservation in the in-vitro measurements of laser-induced fluorescence of peripheral vascular tissue*", J. of Photochem. and Photobiol., Biol. **47**, 109-114 (1998)

2. O. Panou-Diamanti, N. K. Uzunoglou, **G. Zacharakis**, G. Filippidis, T. Papazoglou, D. Koutsouris, "*A one layer tissue fluorescence model based on electromagnetic theory*", J. of Electromagnetic Waves and Applications **12**, 1101-1121, (1998)

3. **G. Zacharakis**, A. Zolindaki, V. Sakkalis, G. Filippidis, E. Koumantakis, and T. G. Papazoglou, "*Nonparametric characterization of human breast tissue by the Laguerre expansion of the kernels technique applied on propagating femtosecond laser pulses through biopsy samples*", Appl. Phys. Lett. **74**, 771-772 (1999)

4. **G. Zacharakis**, G. Heliotis, G. Filippidis, D. Anglos, T.G. Papazoglou, *"Investigation of the laserlike behavior of polymeric scattering gain media under subpicosecond laser excitation"*, App. Opt. **38,** 6087-6092 (1999)

5. G. Filippidis, **G. Zacharakis**, A. Katsamouris, A. Giannoukas, T. G. Papazoglou, *"Single and double wavelength excitation in laser induced fluorescence of normal and atherosclerotic peripheral vascular tissue"*, J. of Photochem. and Photobiol., B. Biol. **56**, 163-171 (2000)

6. **G. Zacharakis**, N. Papadogiannis, G. Filippidis, T.G. Papazoglou, *"Photon statistics of the laser-like emission from polymeric scattering gain media"* Opt. Lett. **25**, 923-925 (2000)

7. G.A. Rovithakis, M. Maniadakis, M. Zervakis, G. Filippidis, **G. Zacharakis**, A. Katsamouris, T.G. Papazoglou, *"Artificial neural networks for discriminating pathologic from normal peripheral vascular tissue"* IEEE Trans. of Biomed. Eng. **10**, 1088-1097 (2001)

8. G. E. Kochiadakis, S. I. Chrysostomakis, M. D, Kalebubas, G, M, Filippidis, **I. G. Zacharakis**, T. G. Papazoglou, P. E. Vardas, *"The role of laser-induced fluorescence in myocardial characterization: An experimental in vitro study"*, Chest **120**, 233-239 (2001)

9. **G. Zacharakis**, A. Zolindaki, V. Sakkalis, G. Filippidis, T.G. Papazoglou, D.D. Tsiftsis, E. Koumantakis, *"In vitro optical characterization and discrimination of female breast tissue during near infrared femtosecond laser pulses propagation"*, J. of Biomed. Opt. **6**, 1-4 (2001)

10. **G. Zacharakis**, N. A. Papadogiannis, A. B. Pravdin, S. P. Chernova, V. V. Tuchin and T. G. Papazoglou, submitted to Phys. Rev. A